NASA/TM—2003–212926

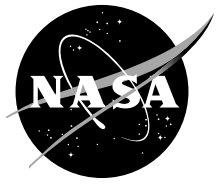

Spray Bar Zero-Gravity Vent System for On-Orbit Liquid Hydrogen Storage

L.J. Hastings
Alpha Technology, Inc., Huntsville, Alabama

R.H. Flachbart, J.J. Martin, A. Hedayat, and M. Fazah
Marshall Space Flight Center, Marshall Space Flight Center, Alabama

T. Lak and H. Nguyen
The Boeing Company, Huntington Beach, California

J.W. Bailey
Sverdrup Technology, Inc., Huntsville, Alabama

October 2003

The NASA STI Program Office…in Profile

Since its founding, NASA has been dedicated to the advancement of aeronautics and space science. The NASA Scientific and Technical Information (STI) Program Office plays a key part in helping NASA maintain this important role.

The NASA STI Program Office is operated by Langley Research Center, the lead center for NASA's scientific and technical information. The NASA STI Program Office provides access to the NASA STI Database, the largest collection of aeronautical and space science STI in the world. The Program Office is also NASA's institutional mechanism for disseminating the results of its research and development activities. These results are published by NASA in the NASA STI Report Series, which includes the following report types:

- TECHNICAL PUBLICATION. Reports of completed research or a major significant phase of research that present the results of NASA programs and include extensive data or theoretical analysis. Includes compilations of significant scientific and technical data and information deemed to be of continuing reference value. NASA's counterpart of peer-reviewed formal professional papers but has less stringent limitations on manuscript length and extent of graphic presentations.

- TECHNICAL MEMORANDUM. Scientific and technical findings that are preliminary or of specialized interest, e.g., quick release reports, working papers, and bibliographies that contain minimal annotation. Does not contain extensive analysis.

- CONTRACTOR REPORT. Scientific and technical findings by NASA-sponsored contractors and grantees.

- CONFERENCE PUBLICATION. Collected papers from scientific and technical conferences, symposia, seminars, or other meetings sponsored or cosponsored by NASA.

- SPECIAL PUBLICATION. Scientific, technical, or historical information from NASA programs, projects, and mission, often concerned with subjects having substantial public interest.

- TECHNICAL TRANSLATION. English-language translations of foreign scientific and technical material pertinent to NASA's mission.

Specialized services that complement the STI Program Office's diverse offerings include creating custom thesauri, building customized databases, organizing and publishing research results…even providing videos.

For more information about the NASA STI Program Office, see the following:

- Access the NASA STI Program Home Page at ***http://www.sti.nasa.gov***

- E-mail your question via the Internet to help@sti.nasa.gov

- Fax your question to the NASA Access Help Desk at (301) 621–0134

- Telephone the NASA Access Help Desk at (301) 621–0390

- Write to:
  NASA Access Help Desk
  NASA Center for AeroSpace Information
  7121 Standard Drive
  Hanover, MD 21076–1320

NASA/TM—2003–212926

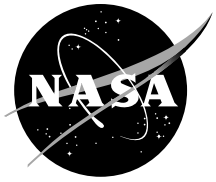

Spray Bar Zero-Gravity Vent System for On-Orbit Liquid Hydrogen Storage

L.J. Hastings
Alpha Technology, Inc., Huntsville, Alabama

R.H. Flachbart, J.J. Martin, A. Hedayat, and M. Fazah
Marshall Space Flight Center, Marshall Space Flight Center, Alabama

T. Lak and H. Nguyen
The Boeing Company, Huntington Beach, California

J.W. Bailey
Sverdrup Technology, Inc., Huntsville, Alabama

National Aeronautics and
Space Administration

Marshall Space Flight Center • MSFC, Alabama 35812

October 2003

TRADEMARKS

Trade names and trademarks are used in this report for identification only. This usage does not constitute an official endorsement, either expressed or implied, by the National Aeronautics and Space Administration.

Available from:

NASA Center for AeroSpace Information
7121 Standard Drive
Hanover, MD 21076–1320
(301) 621–0390

National Technical Information Service
5285 Port Royal Road
Springfield, VA 22161
(703) 487–4650

TABLE OF CONTENTS

TABLE OF CONTENTS (Continued)

LIST OF FIGURES

LIST OF FIGURES (Continued)

LIST OF FIGURES (Continued)

LIST OF FIGURES (Continued)

LIST OF FIGURES (Continued)

LIST OF FIGURES (Continued)

LIST OF TABLES

LIST OF ACRONYMS, SYMBOLS, AND ABBREVIATIONS

ASME	American Society of Mechanical Engineers
CFM	crogenic fluid management
GH_2	gaseous hydrogen
GHe	gaseous helium
GN_2	gaseous nitrogen
GRC	Glenn Research Center
HEX	heat exchanger
J-T	Joule-Thompson
LAD	liquid acquisition device
LH_2	liquid hydrogen
LN_2	liquid nitrogen
MHTB	multipurpose hydrogen test bed
MLI	multilayer insulation
MSFC	Marshall Space Flight Center
RGA	residual gas analyzer
SOFI	spray-on foam insulation
TVS	thermodynamic vent system
TYP	typical

NOMENCLATURE

A	area
A_S/A_T	ratio of the spray orifice to the tank area
A_{SI}	flow area of an injection tube
A_{SM}	flow area of spray manifold
$(A_S)_n$	spray orifice area at node n
$a = \frac{g}{g_c}$	acceleration ratio; ratio of environmental to Earth's gravitational constant
C	specific heat
C_d	discharge coefficient
CdA	effective orifice flow area
C_L	liquid specific heat
c_p	specific heat at constant pressure
c_{pL}	liquid specific heat at constant pressure
c_{pWL}	wall liquid specific heat at constant pressure
c_{VU}	ullage specific heat at constant volume
D	diameter
D_{CHAR}	a characteristic length determined empirically
D_D	droplet diameter
D_m	impeller diameter
D_{SI}	spray injection tube inside diameter
D_{SM}	spray manifold inside diameter

NOMENCLATURE (Continued)

ENTH_U	energy added to ullage
F	Reynolds number factor
f_{SM}	friction coefficient in the spray manifold
G	mass flow rate per unit area
g	acceleration
g_c	Earth's gravitational constant
H	pump head
HP_I	input power to the pump
HP_O	fluid horsepower
h	convection heat transfer coefficient; latent heat of vaporization
h_{FC}	forced convection heat transfer coefficient
h_{NB}	nucleate boiling heat transfer coefficient
h_{fg}	heat of vaporization or condensation
$(h_{fg})_L$	heat of vaporization in liquid
$(h_{fg})_U$	heat of condensation in ullage
h_{gsat}	saturated vapor enthalpy of the ullage
h_I	inlet total enthalpy
h_{in}	TVS inlet enthalpy
$\left(h_L\right)_o$	outlet liquid enthalpy
h_{LS}	heat transfer coefficient between bulk liquid and (submerged) spray bar

NOMENCLATURE (Continued)

$(h_L)_{SM}$	head loss in spray manifold
h_o	outlet total enthalpy
h_{out}	TVS outlet enthalpy
h_{satvap}	saturated vapor enthalpy
h_{UD}	forced convection heat-transfer coefficient between ullage and liquid droplets
h_{UL}	heat transfer coefficient between ullage and bulk liquid
h_{US}	heat transfer coefficient between ullage and (unsubmerged) spray bars
h_{UW}	heat transfer coefficient between ullage and wall
h_{UWL}	heat transfer coefficient between ullage and wall liquid
$(h_V)_O$	outlet vapor enthalpy
h_{vent}	vent gas enthalpy
h_{WL}	heat transfer coefficient between wall and liquid
IC	initial condition
I_p	polar moment of inertia of the pump
i	inlet
J	unit conversion constant
$(K_b)_{SI}$	90° bend resistance
$(K_b)_{SM}$	spray manifold frictional loss coefficient
$(K_c)_{SM}$	spray manifold 90° bend loss coefficient
$(K_f)_{SM}$	spray manifold sudden contraction loss coefficient
K_f	frictional loss coefficient

NOMENCLATURE (Continued)

K_S	loss coefficient of an orifice in duct
K_{SM}	total loss coefficient of an orifice in spray manifold
k	thermal conductivity
k_F	fluid thermal conductivity
k_L	liquid thermal conductivity
L	liquid; length
L_c	characteristic length
L_e	equivalent length of bend
L_{SM}	spray manifold length
M_U	ullage mass
$(M_U)_{IC}$	ullage mass with initial conditions
M_L	liquid mass
$(M_L)_{IC}$	initial liquid mass
M_{WL}	wall liquid mass
$(M_{WL})_{IC}$	initial wall liquid mass
m	mass
$\dot{m}$	mass flow rate
$\dot{m}_{bW}$	mass boiling rate of liquid on tank wall
$\dot{m}_{\mathrm{COND}}$	liquid surface condensation mass flow rate
$\dot{m}_{DU}$	liquid droplet evaporation rate in ullage
$\dot{m}_i$	mass flow rate at inlet

NOMENCLATURE (Continued)

$(\dot{m}_i)_n$	mass flow rate at node *n*
$\dot{m}_{LU}$	liquid boiloff rate
$\left(\dot{m}_o\right)_n$	mass flow rate at node center
$\dot{m}_S$	pump flow rate
$\dot{m}_{SL}$	liquid spray mass flow rate into bulk liquid
$(\dot{m}_S)_n$	spray mass flow rate at node *n*
$\dot{m}_{SU}$	spray flow rate into the ullage
$\left(\dot{m}_{SU}\right)_i$	spray flow rate into the ullage from orifice *i*
$\dot{m}_{SUL}$	liquid spray unevaporated droplet flow rate; liquid spray falling into bulk liquid
$\dot{m}_{SW}$	spray flow rate reaching tank wall
$\dot{m}_{UL}$	ullage condensation flow rate
$\dot{m}_V$	overboard vent flow rate
$\dot{m}_{\text{vent}}$	vent mass flow rate
N	last node; pump rotation speed
N_D	pump design speed
$(N)_{IC}$	initial rotation speed
Nu	Nusselt number
n	node number; node center
n_{drop}	number of droplets

NOMENCLATURE (Continued)

$(n_{\text{drop}})_{\text{i}}$	number of droplets from orifice *i*
o	outlet
$(p_D)_o$	dynamic pressure, outlet
p_o	outlet pressure
$(p_S)_o$	static pressure at outlet
P_T	tank pressure
p	pressure
p_i	inlet pressure
$(p_i)_n$	inlet pressure at node *n*
p_L	liquid vapor pressure
p_n	pressure at node *n*
$(p_o)_n$	outlet pressure at node *n*
p_{sat}	saturation pressure
$(p_{SM})_i$	spray manifold inlet pressure
$(p_{SM})_o$	spray manifold outlet pressure
$(p_T)_n$	tank pressure at node *n*
p_U	ullage pressure
p_{WL}	wall liquid vapor pressure
$\dot{Q}$	total heat-transfer rate
$\dot{Q}_{\text{ave}}$	average value of vent heat extraction
$\dot{Q}_{\text{boiloff}}$	total energy vented as boiloff

NOMENCLATURE (Continued)

$\dot{Q}_{\text{conduction}}$	heat flow through tank support legs, vent assembly, and other fluid lines
Q_D	pump design flow rate
$\dot{Q}_{\text{insulation}}$	heat input through insulation
$\dot{Q}_{\text{vent}}$	energy extraction rate while vent is open
q_{drop}	droplet heat transfer rate
$(q_{drop})_i$	droplet heat transfer rate from orifice i
q_{EL}	heat added to the liquid by environment
q_{EW}	heat input to the wall from environment
q_i	inlet dynamic pressure
$(q_i)_n$	inlet dynamic pressure at node n
q_L	heat transfer rate to the liquid
q_{LS}	heat transfer rate between liquid and (submerged) spray bars
$(q_o)_n$	outlet dynamic pressure
q_{SM}	dynamic pressure in spray manifold
q_U	heat transfer to ullage
q_{UD}	heat transfer rate between the ullage and liquid droplet
p_n	pressure at node n
$(p_o)_n$	node n outlet pressure
p_{sat}	saturation pressure
q_{UL}	heat transfer rate between ullage and liquid
q_{US}	heat transfer rate between ullage and (unsubmerged) spray bar

NOMENCLATURE (Continued)

q_{UWL}	heat transfer rate between ullage and wall liquid
q_{WL}	heat transfer rate between wall and liquid on the wall
q_{WU}	heat transfer rate between tank wall and ullage
Ra	Rayleigh number
Re	Reynolds number
Re_L	liquid Reynolds number
S	suppression factor
$(S_L)_O$	outlet liquid entropy
$(S)_O$	outlet total entropy
$(S_V)_O$	outlet vapor entropy
T	orifice inlet temperature
T_d	droplet temperature
T_f	film temperature
T_L	liquid temperature
$(T_L)_{IC}$	initial liquid temperature
T_S	spray temperature
T_{sat}	saturation temperature
T_{sw}	sprayed wall liquid temperature
T_U	ullage temperature
$(T_U)_{IC}$	initial ullage temperature
T_{Usat}	ullage saturation temperature

NOMENCLATURE (Continued)

T_W	wall temperature
T_{WL}	wall liquid temperature
$(T_{WL})_{IC}$	initial wall liquid temperature
t_{total}	total time
t_{open}	valve open time
U	ullage; tip velocity
V	volume
$(V_D)_i$	droplet volume from orifice i
Vel_D	droplet velocity in ullage
$(Vel_D)_i$	droplet velocity from orifice i
V_L	liquid volume
V_o	outlet fluid velocity
$(V_L)_{IC}$	initial liquid velocity
V_{SM}	velocity in the spray manifold
V_T	tank volume
V_U	ullage volume
V_{WL}	wall liquid volume
$(V_{WL})_{IC}$	initial wall liquid volume
W	tank wall; watts
WL	wall liquid
w_U	work done on the ullage

NOMENCLATURE (Continued)

X	Martinelli parameter
$\overline{Y}$	average total liquid quality between the inlet and outlet
Y_o	outlet fluid quality
z_i, z_o	inlet and outlet elevations
z_n	distance from liquid surface to node n
β	thermal expansion coefficient
ΔH	change in height
ΔP	pressure difference
ΔP_f	pressure loss due to frictional forces
ΔP_m	pressure loss due to momentum change
ΔP_p	pump pressure rise
ΔP_T	total pressure loss
ΔT	temperature difference between heat source and sink
$\frac{\Delta U_{\text{system}}}{\Delta t}$	energy flow rate into or out of test tank wall, insulation, and fluid mass
Δz	nodal length
ε	roughness
η_P	pump mechanical efficiency
λ	latent heat of vaporization
μ	viscosity
μ_L	liquid viscosity

NOMENCLATURE (Continued)

$\overline{\mu}_L$	average liquid viscosity between inlet and outlet
$\overline{\mu}_V$	average vapor viscosity between inlet and outlet
ρ	density
ρ_D	droplet density
ρ_L	liquid density
$\overline{\rho}_L$	average liquid density between inlet and outlet
$(\rho_L)_o$	outlet liquid density
ρ_o	outlet total density
ρ_{sat}	density at saturation conditions
ρ_{satliq}	saturated liquid density
ρ_{satvap}	saturated vapor density
$\overline{\rho}_V$	average vapor density between inlet and outlet
$(\rho_V)_o$	outlet vapor density
ρ_{WL}	wall liquid density
σ	surface tension
Φ_L	Lockhart-Martinelli correlation factor
ϕ	flow coefficient
ψ	head coefficient

TECHNICAL MEMORANDUM

SPRAY BAR ZERO-GRAVITY VENT SYSTEM FOR ON-ORBIT LIQUID HYDROGEN STORAGE

1. INTRODUCTION

1.1 Background

The development of high-energy cryogenic upper stages is necessary for delivery of large payloads to various orbital destinations, such as the geosynchronous orbit and Mars missions. Also, many advanced propulsion systems, including solar thermal and nuclear fission, use hydrogen as the propellant. A key technology challenge for all of these applications is cryogenic fluid management (CFM), including the long-term storage of cryogens in space. In response to this challenge, NASA has initiated an advanced development/technology program to broaden the CFM experience/database. Due to constrained opportunities for orbital experiments, ground testing must be employed to the fullest extent possible. Therefore, a major objective of the NASA technology program has been to perform ground-based advanced development testing on CFM systems for space transportation applications.

A system-level test bed—the multipurpose hydrogen test bed (MHTB)—representative in size and shape of a fully integrated space transportation vehicle liquid hydrogen (LH_2) propellant tank, was established for use at Marshall Space Flight Center (MSFC). The MHTB 18-m^3 (639-ft^3) hydrogen tank was designed to accommodate various CFM concepts as updated or alternative versions become available. The first technology element evaluated with the MHTB was a cryogenic thermal protection concept for ground-based upper stages[1] and the second element addressed the on-orbit control of tank pressure.

Maintaining propellant tank pressure control while minimizing propellant boiloff loss is a significant challenge associated with the storage of cryogens in the near zero-gravity environment of space. Traditionally, auxiliary thrusters are used to settle the propellants in order to accomplish tank venting. However, such systems incur weight penalties associated with the propellant and hardware required to perform the settling burns that increase with the number of settling sequences. In addition, tank venting/resettling may become necessary at inopportune times in a mission timeline, thereby increasing mission complexity. The thermodynamic vent system (TVS) concept enables tank pressure control through venting without resettling. A TVS typically includes a Joule-Thompson (J-T) expansion device, a two-phase heat exchanger, and a mixing pump to destratify and extract thermal energy from the tank contents without significant liquid losses. Implementation of TVSs has been delayed by the lack of opportunities for on-orbit experience, primarily due to funding constraints. Analytical modeling of such systems is difficult due to the complex combination of microgravity heat transfer, thermodynamic, and fluid mechanic phenomena involved. Model correlations are further complicated by the lack of on-orbit data. The TVS design requirements, a description of the concept evaluated, and test program objectives and goals are presented in sections 1.2 through 1.4.

1.2 Requirements

The overall TVS requirement was to maintain the MHTB tank ullage pressure within a 6.9-kPa (1-psi) control band for extended periods of time. The TVS was designed to accommodate tank heat leaks up to 55 W, liquid levels of 10 to 95 percent, and to operate without dependence on a capillary liquid acquisition device (LAD). In addition, there were the general requirements of simplicity, low weight, low power, high efficiency, and mission flexibility.

1.3 Thermodynamic Vent System Spray Bar Concept

The spray bar TVS concept, developed by Rockwell Aerospace (now The Boeing Company), was selected for testing in the MHTB because of some unique features relative to concepts previously tested. This concept is described in reference 2 and is illustrated in figure 1. The major advantage of this concept is that the longitudinal spray bar can be used to thermally destratify both liquid and ullage, independent of liquid-vapor positions in zero gravity. Therefore, the spray bar concept is conducive to verification in normal gravity and minimizes dependence on costly orbital experimentation. A second advantage is that active TVS components; i.e., J-T expansion valve, subsystem pump, and isolation valve, are located outside the tank. Such an approach simplifies component installation and enables modification or change-out of TVS components without entering the tank. Also, this configuration can support feedline and engine thermal conditioning during microgravity coast periods.

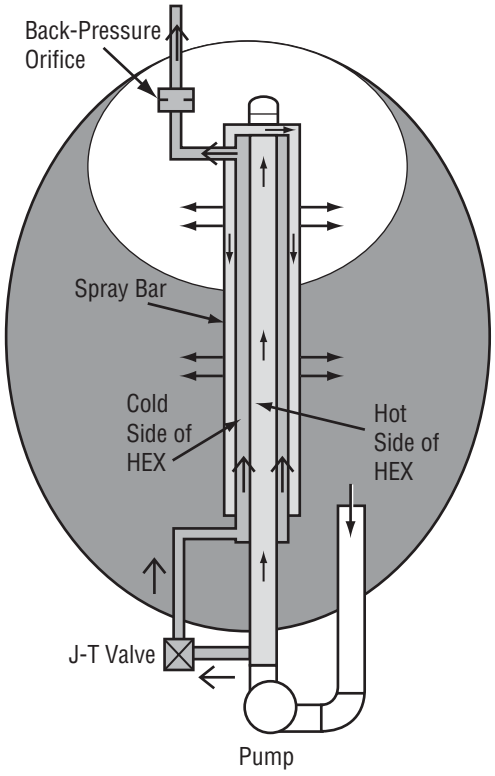

Figure 1. Spray bar TVS schematic.

In the mixing mode, fluid is withdrawn from the tank by the pump and flows back into the tank through the spray bar positioned along or near the tank longitudinal axis. The fluid is expelled radially back into the tank through the spray bar, which forces circulation and mixing of the tank contents regardless of liquid and ullage position, assuring destratification and minimum pressure rise rate. For missions lasting from a few days to weeks, depending on the insulation performance and the degree of bulk liquid subcooling, tank mixing may be sufficient to control the tank pressure with no propellant loss. When pressure control can no longer be achieved with mixing alone (the bulk liquid saturation condition corresponds to the ullage pressure), a portion of the circulated liquid is passed through the J-T valve where it is expanded to a lower temperature and pressure, passed through the heat exchanger element of the spray bar, and finally is vented to space. The vented fluid thereby removes thermal energy from, and thus cools, the bulk fluid circulated through the mixing element of the spray bar. If ullage, instead of liquid, enters the recirculation line in zero gravity, then vapor is vented through the J-T valve and ullage depressurization occurs much as it would in a normal gravity environment.

In an orbital propellant transfer scenario, the spray bar concept can be used to assist tank refill. By filling through the spray bar/heat exchanger, the in-flowing fluid can be cooled and used to mix the tank contents, thus enabling a no-vent fill process with minimal propellant losses. Additionally, if capillary LADs are used for microgravity propellant expulsion, the liquid within the LAD can be conditioned by the spray bar TVS. By withdrawing liquid from the capillary LAD, cooling it through the J-T device, and returning it to the LAD, thermal conditioning of the LAD liquid can be achieved. Thus, the effects of heat entrapment within the LAD can be minimized or perhaps eliminated.

1.4 Objectives

The primary overall objective was to evaluate the effectiveness of a spray bar mixer TVS concept for maintaining ullage pressure control within the MHTB LH_2 tank. Design and test goals included the following:

- Verify that the TVS can maintain the ullage pressure within the 6.9-kPa (1-psi) control band for extended periods of time, independent of fill level.
- Verify that reasonable variations in orbital heat leak can be accommodated with the automated control logic.
- Evaluate the spray bar mixer destratification performance.
- Evaluate the effects of gaseous helium (GHe) pressurant within the ullage.
- Analytically model the spray bar heat exchanger and vent system performance.
- Correlate the measured TVS data with analytical modeling results.

2. TEST ARTICLE ELEMENTS

The major test article elements consist of the test tank with supporting equipment, including an environmental shroud, cryogenic insulation subsystem, and test article instrumentation. Technical descriptions of each of these elements are presented in sections 2.1 through 2.4.

2.1 Multipurpose Hydrogen Test Bed Tank

The MHTB 5083 aluminum tank is cylindrical in shape with a height of 3.05 m (10 ft), a diameter of 3.05 m (10 ft), and 2:1 elliptical domes as shown in figure 2. It has an internal volume of 18.09 m^3 (639 ft^3) and a surface area of 35.74 m^2 (379 ft^2), with a resultant surface area-to-volume ratio of 1.92 1/m (0.58 1/ft) that is reasonably representative of a full-scale vehicle LH_2 tank. The tank is ASME pressure vessel coded for a maximum operational pressure of 344 kPa (50 psid) and was designed to accommodate various CFM technology and advanced concepts as updated versions become available. Major accommodations include a 60.9-cm- (24-in-) diameter manhole, pressurization and vent ports, fill/drain line through tank top, 15.24- and 7.5-cm (6- and 3-in) general purpose penetrations with flanges on top, the zero-gravity pressure control subsystem (thermodynamic vent subsystem) penetration provisions on the tank bottom (one each 5.08-, 3.81-, and 1.27-cm tube) and an enclosure external to the tank, a 7.62-cm- (3-in-) diameter drain at the tank bottom for future growth, a continuous liquid level

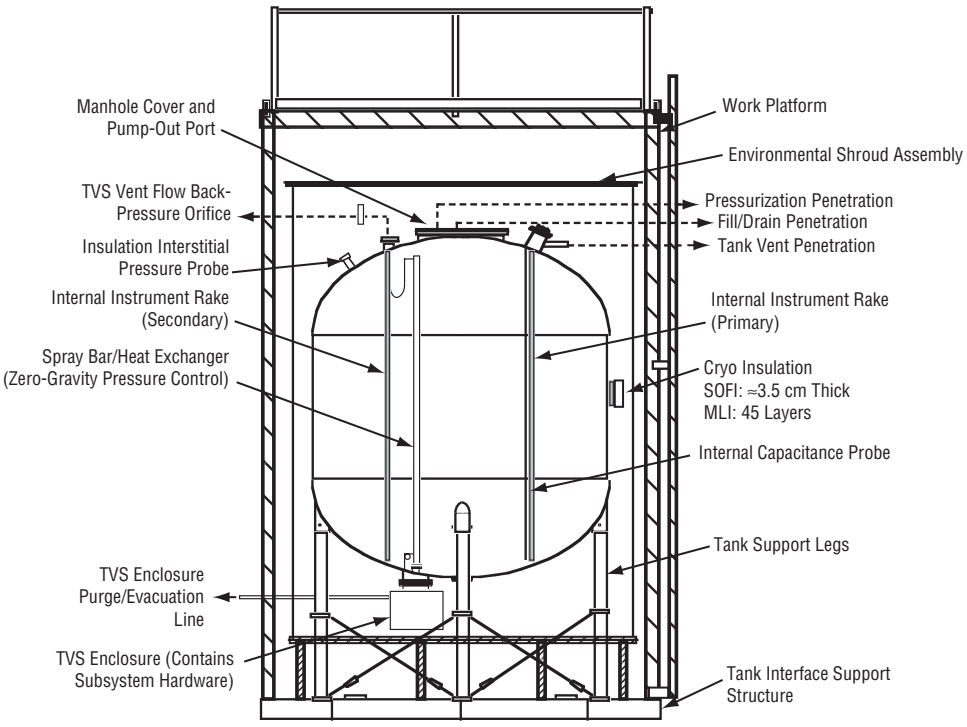

Figure 2. MHTB test tank and supporting hardware schematic.

capacitance probe, two vertical temperature rakes, wall temperature measurements at selected locations, ullage pressure sensors, pressure control/relief safety provisions, internal mounting brackets for future equipment and structural "hard points" for temporary scaffolding and ladder, and low heat leak composite structural supports. Each of the penetrations is equipped with a LH_2 heat guard to intercept heat leak, thereby enabling more accurate measurement of the tank insulation performance as required.

Fluid connections are welded wherever possible and all mechanical seals are the knife-edge/copper gasket (Conflat®) design. The exception is the primary manhole cover design (fig. 3), which incorporates a soft, crushable indium wire as a seal material and Invar® expansion collars on the stainless steel bolts to offset thermal expansion effects. The secondary manhole cover is equipped with a pump-out port so that any primary seal leakage can be intercepted and routed to a facility vacuum pump. Appendix A contains an MHTB tanking table with information regarding fill height, percent liquid/ullage volume, and LH_2 mass.

2.2 Environmental Shroud

The MHTB tank is enclosed within an environmental shroud which enables simulation of a ground hold conditioning purge, similar to that in a payload bay, and the imposition of a range of uniform temperatures on the multilayer insulation (MLI) external surfaces. The shroud (fig. 4) is 4.57 m (15 ft) high by 3.56 m (12 ft) in diameter, and contains a purge ring for distributing dry gaseous nitrogen (GN_2). The shroud heater strips/cooling loops can impose either constant or time-dependent boundary temperatures ranging from 80 K (144 °R) to 320 K (576 °R).

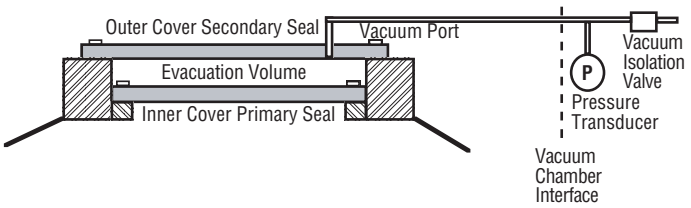

Figure 3. Manhole cover sealing arrangement.

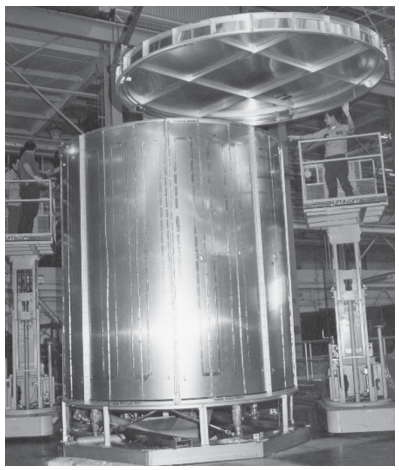

Figure 4. Environmental shroud assembly.

2.3 Cryogenic Insulation Subsystem

The MHTB insulation concept consists of a foam/multilayer combination. The foam element enables the use of a payload bay-type GN_2 purge during ground hold periods. The 45-layer, double-aluminized mylar MLI provides thermal radiation protection while at vacuum conditions on orbit. As reported in reference 1, which describes the insulation in more detail, the combined effects of the MLI variable density, large vent hole pattern, and installation technique resulted in substantial performance improvements over conventional insulation configurations. However, in this application, the insulation system performance was compromised by the thermodynamic vent system hardware installation and by electing, in one series, to not operate the vacuum chamber cold walls.

2.4 Multipurpose Hydrogen Test Bed Instrumentation

The test article and environmental shroud instrumentation details are presented in appendix B; however, the instrumentation arrangement for each primary segment is summarized in this section. The test article instrumentation consists primarily of thermocouple and silicon diodes to measure insulation, fluid, and tank wall temperatures. Typically, silicon diode (Lakeshore type DT–470–11A) temperature transducers are positioned in areas of lowest temperatures, which provide higher accuracy as compared to thermocouples. MLI temperature profiles or gradients are measured at seven positions with one silicon diode and four thermocouples placed at each of the seven measurement positions. The MLI interstitial pressure is measured at the foam/MLI interface and a sampling port for both dewpoint and gas species is provided.

The tank is internally equipped with two instrumentation rakes and a capacitance liquid level probe, all supported from the top of the tank (fig. 5). The rakes, constructed from a fiberglass epoxy channel section, are equipped with silicon diodes attached at 22.9-cm (9-in) intervals using nylon rod offsets and cryogenic compatible epoxy. The instrumentation rakes provide temperature-gradient measurements within both ullage and liquid, and serve as a backup to the continuous liquid level capacitance probe. Two of the four composite legs, vent, fill/drain, pressurization, pressure sensor probe, and manhole pump-out penetrations are instrumented to determine the solid conduction component of heat leak.

During the TVS performance testing, the bulk liquid temperature relative to ullage saturation conditions was monitored using silicon diode TD23 on rake 2 (fig. 5) and ullage pressure sensor P1 (see sec 7.1). TD23 is at the 11.5-percent fill level or 53.3 cm (21 in) above the tank bottom and is considered to be representative of the bulk liquid temperature. As described in section 7.2.3, the TD23 temperature output was converted to an equivalent saturation pressure (termed PSA1) and compared with the ullage pressure (P4). P4 is an MKS Instruments, Inc., Baratron 0–666 kPa (0–96 psia) absolute pressure transducer with an accuracy of ±0.02 percent. TVS-specific instrumentation on the MHTB and test facility is discussed in sections 4.5 and 7.1, respectively.

The environmental shroud is composed of 17 individual panels, each equipped with a minimum of two thermocouples attached to the inner surfaces and placed beneath the electrical heating strips. These thermocouples are used with a closed-loop control system to regulate each shroud panel temperature.

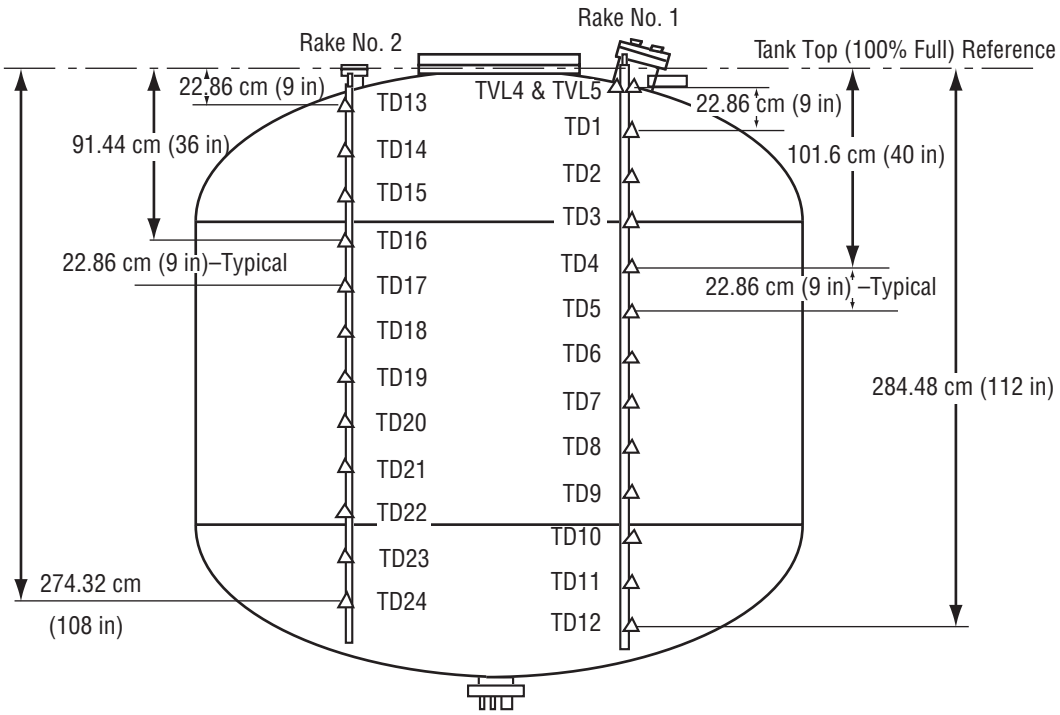

Note: All Diodes Spaced at Intervals of 22.86 cm (9 in)

Figure 5. MHTB internal instrumentation rakes.

3. SPRAY BAR THERMODYNAMIC VENT SYSTEM DESIGN DEFINITION

The TVS was designed to accommodate tank heat leaks up to 55 W and liquid levels ranging from 10 to 95 percent. The four major elements are the heat exchanger, spray injection and recirculation system, controller, and instrumentation. Design selection details regarding each of the TVS elements are presented in reference 2 and are summarized in sections 3.1 through 3.4.

3.1 Heat Exchanger

The heat exchanger is a critical element since its function is to ensure optimal heat transfer between the vented and recirculating fluids. The exchanger design must be capable of rejecting the maximum environmental heat leak rate anticipated and simultaneously reduce the liquid bulk temperature within a reasonable timeframe. To ensure accommodation of a maximum projected heat leak of 55 W without excessive pump and valve operational cycles, the heat exchanger was designed to reject ≈844 W or ≈15 times the maximum heat leak requirement. This reduced the projected vent cycle from a nearly continuous operation to a more reasonable average of ≈5 percent of the total mission time. Additionally, the large heat rejection capability accommodates growth in heat leak, analytical prediction uncertainties, and mission flexibility. Since the TVS is designed to operate in an on-off cycle, the system automatically compensates for environmental and internal performance variations. Three design options were considered in the heat exchanger design trade study:

(1) Coil heat exchanger: Vent tubing is wrapped around the spray injection system.

(2) Concentric single-tube exchanger: Recirculation flow is inside an inner tube with the vent flow in an annulus between the inner and outer tube diameters.

(3) Multitube heat exchanger: Similar to option (2) except repeated vent flow paths are used to increase the total heat exchange area.

Option (1), shown in figure 6, represents the simplest configuration. The vent flow is contained within a small diameter tube wrapped around the outside of the larger liquid recirculation tube. Unfortunately, the heat rejection capability of this configuration is compromised by the reduction in liquid flow that occurs as the recirculating liquid flows from the bottom to the top of the spray bar and the flow regime transitions from highly turbulent conditions at the inlet to laminar at the outlet. To compensate for the reduced heat transfer, the vent tube contact area can be increased by increasing the vent tube length. However, vent flow pressure loss also increases with tube length. Also, the longer vent tube reduces the amount of vent liquid available for phase change and reduces the temperature difference between the vented and recirculated liquid. A sensitivity study was performed to define the heat rejection rate as a function of vent line pressure loss for various tube diameters and the results indicated that the vent line pressure losses increase rapidly with respect to the heat rejection rate. For example, to achieve a heat rejection rate of 422 W, 34.8 m (100 ft) of 0.95-cm tubing is required and incurs a 27.6 kPa (4 psid) pressure loss. However, the vent line pressure loss exceeded the design goal

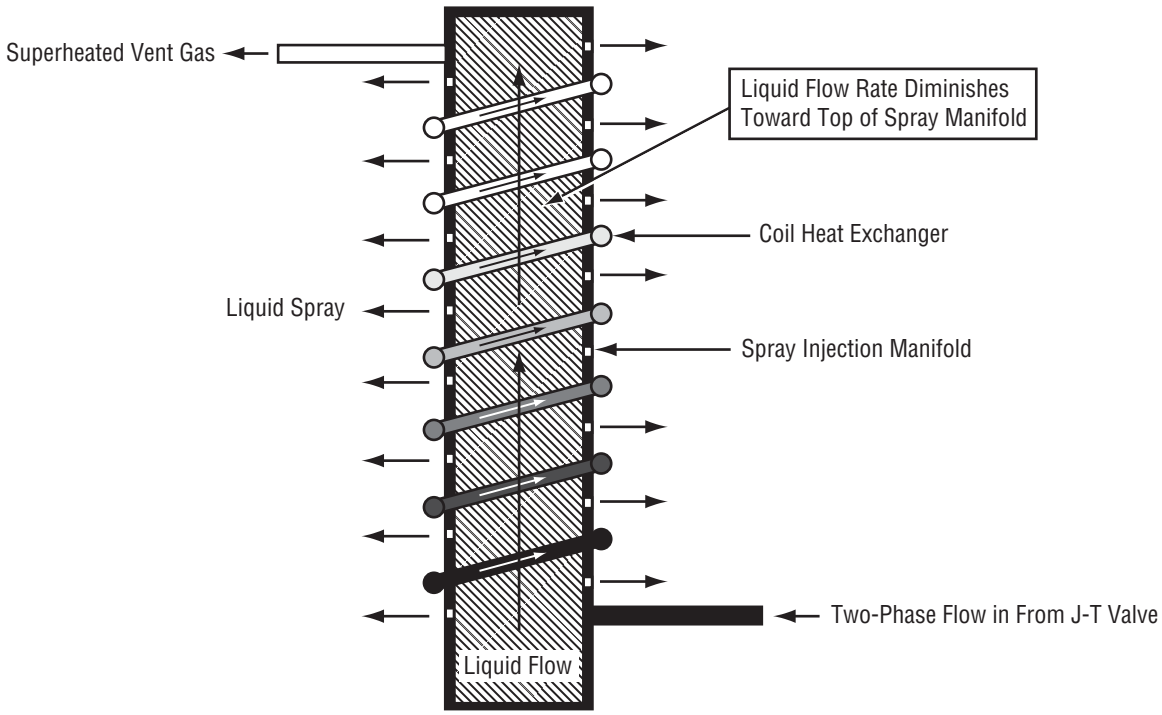

Figure 6. TVS coil heat exchanger—option (1).

of 13.8 kPa (2 psid). Since option (1) did not satisfy the heat rejection design goal of 844 W, resulted in a weight disadvantage, and incurred a risk of vent tube debonding, the concept was not selected.

Option (2), shown in figure 7, consists of two concentric tubes. The inner tube contains the recirculation flow, while the annulus between the inner and outer tubes contains the vent flow. Because the liquid flow rate is constant throughout the heat exchanger length, the hot side (recirculated liquid) heat transfer coefficient exceeds the cold side (vent fluid), unlike the coiled heat exchanger in option (1). Also, the heat transfer area is maximized since the entire length of the inner tube surface area is utilized to transfer heat between the vented and recirculated fluid. Additional energy exchange occurs between the bulk propellants and vented fluid, but was not considered in the analysis. Based on analyses of vent tube diameters ranging from 2.54 to 4.45 cm (1 to 1.75 in) with a fixed spacing of 0.635 cm (0.25 in) between the outside diameters, optimal outside (vent flow) and inside (recirculation flow) tube dimensions of 3.8 cm (1.5 in) outside diameter with a 0.147-cm (0.058-in) wall and 3.175 cm (1.25 in) outside diameter with a 0.089-cm (0.035-in) wall were selected. The design was predicted to reject ≈900 W, which satisfies the design goal of 844 W. Additionally, the 3.175-cm (1.25-in) inner tube diameter resulted in low recirculation flow pressure loss and pump power requirements.

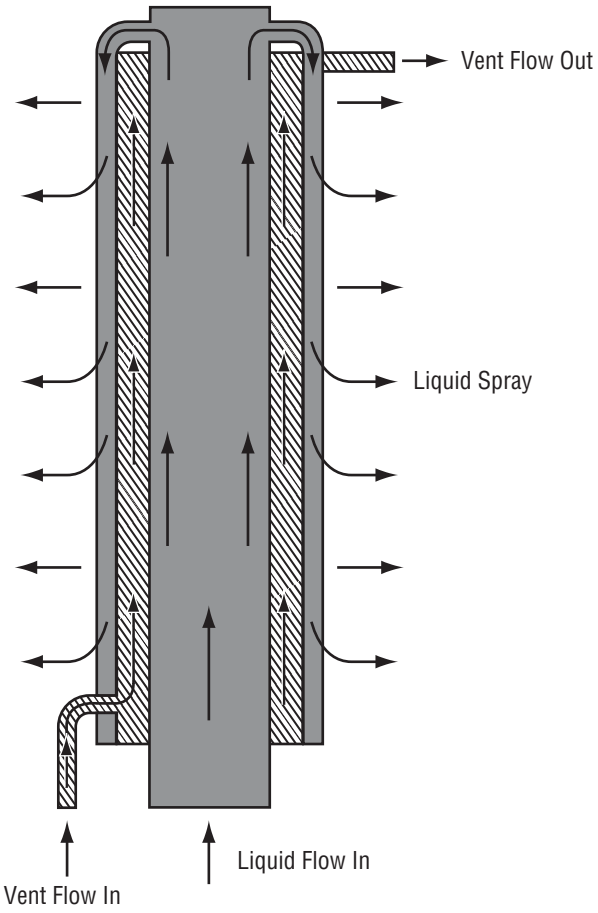

Figure 7. TVS single-tube heat exchanger—option (2).

Option (3), shown in figure 8, is similar to option (2) in that the recirculation flow is contained in the inner tube and the vent flow is in the outer tube. However, the recirculated and vent fluids are divided into a number of smaller tubes to increase both the heat transfer surface area and recirculation fluid heat transfer coefficient relative to the option (2) concept. The sensitivity analyses were based on a 0.953 cm (0.375 in) outside diameter recirculation tube. (Larger tube diameters resulted in low heat transfer coefficients due to large radial clearances on the vent side.) The results indicated that five or more tubes would be required to maintain the pressure losses and pump power below ≈15 percent of the total tank heat leak (8 W). With the five-tube design, a maximum heat rejection of over 2,500 W can be achieved with acceptable pressure losses. However, the multitube option is heavier, more complex to fabricate, and has more flow resistance compared to the single-tube option (option (2)).

In summary, option (2), the single-tube heat exchanger, was selected because of its low weight, fabrication simplicity, low pumping power and pressure losses, and satisfaction of the 844-W heat rejection capability.

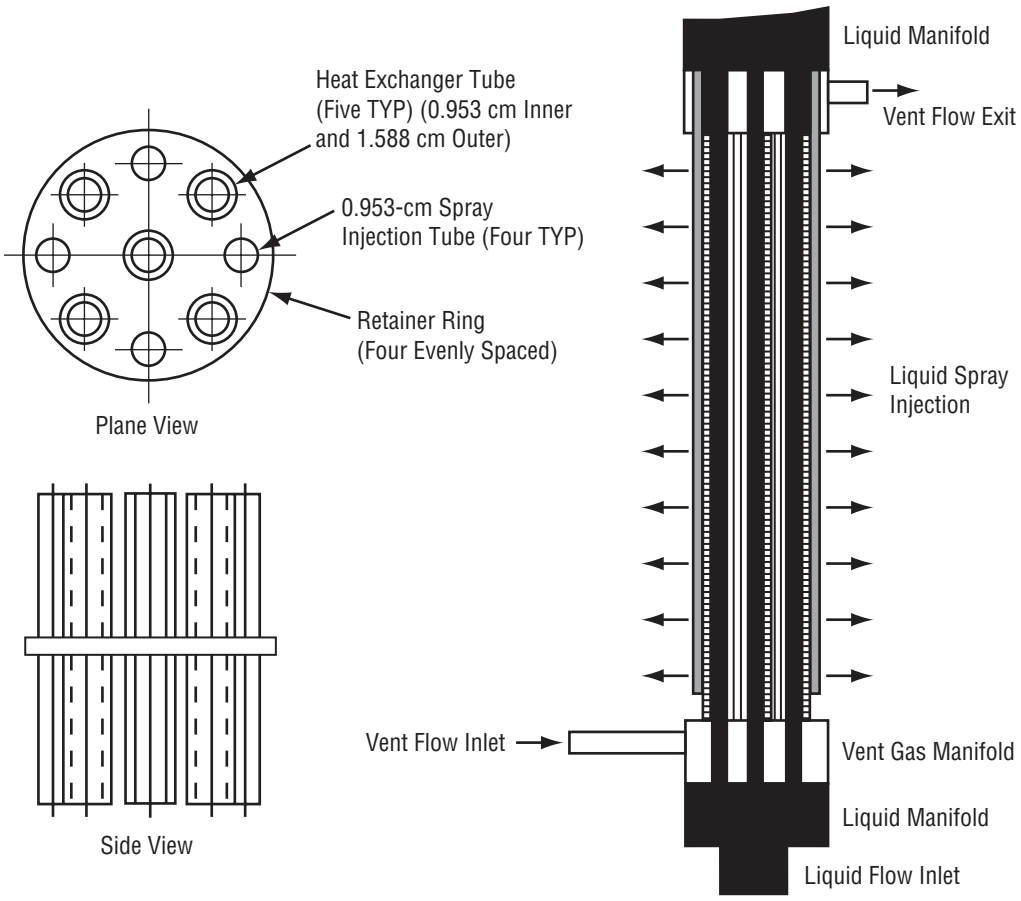

Figure 8. TVS multitube heat exchanger configuration—option (3).

3.2 Operating Pressures

A sensitivity study was performed to define the influence of propellant tank operating pressure and vent system back pressure on the TVS efficiency. The vent fluid heat absorption potential is a combination of heat required to evaporate the two-phase fluid and the sensible heat available for increasing the temperature from the saturation to the superheat condition corresponding to the propellant bulk temperature.

The heat absorbed through evaporation decreases with increasing liquid vapor pressure or tank pressure; however, the net heat absorbed by boiling increases with increasing vent line back pressure due to increasing liquid vapor fractions. The net effect is demonstrated in figure 9 which presents the heat of evaporation versus vent line back pressure for tank vapor pressures ranging from 103 to 241 kPa/m^2 (15 to 35 psia). At a tank pressure of 137.8 kPa/m^2 (20 psia), the heat of evaporation varies from 107 to 115 Whr/kg (166 to 178 Btu/lb) as the back pressure ranges from 6.89 to 34.5 kPa/m^2 (1 to 5 psia). At a back pressure of 34.5 kPa/m^2 (5 psia), the heat of evaporation ranges from 117 to 107 Whr/kg (182 to 166 Btu/lb) as tank pressure varies from 103 to 241 kPa/m^2 (15 to 35 psia).

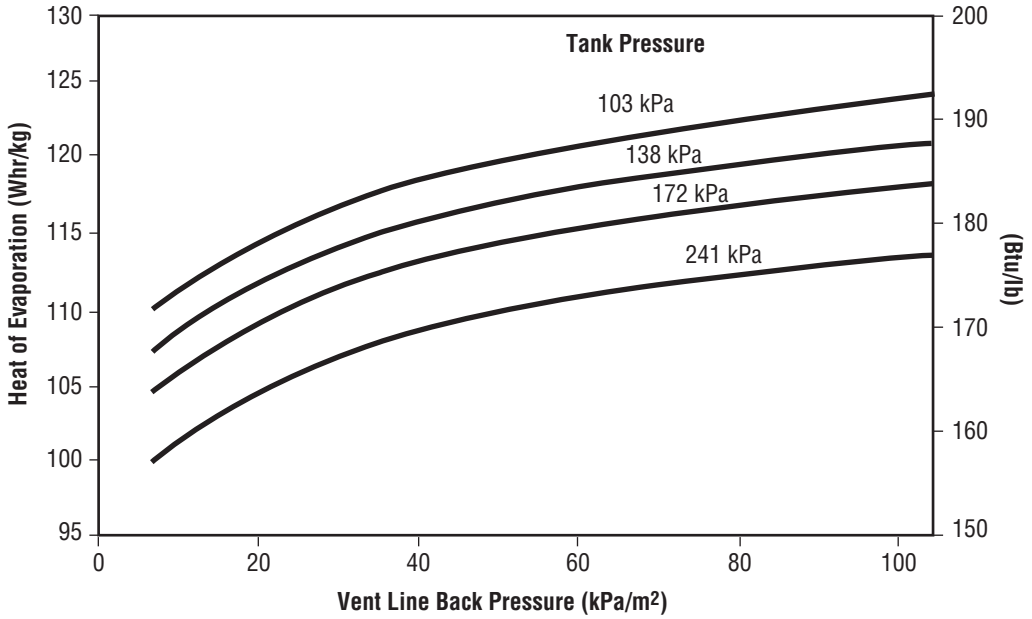

Figure 9. Effects of liquid vapor pressure and vent back pressure on heat absorption.

The effects of vent line and tank pressure on sensible heat capacity are illustrated in figure 10. The sensible heat decreases with increasing vent line back pressure, since the corresponding saturation or boiling point temperatures increase. However, the sensible heat increases as tank pressure increases at a given back pressure due to the increasing tank saturation temperature. At a back pressure of 34.5 kPa/m^2 (5 psia) and a 137.8-kPa/m^2 (20-psia) tank pressure, for example, the sensible heat and heat of evaporation are 12.9 Whr/kg (20 Btu/lb) and 115 Whr/kg (178 Btu/lb), respectively. That is, the sensible heat represents ≈10 percent of the vent fluid total heat absorption capability.

The combined sensible and evaporation energy effects are presented in figure 11 for tank pressures ranging from 103 to 241 kPa/m^2 (15 to 35 psia). The net heat absorption increases with decreasing vent line back pressure; however, a minimum practical limit of 20.7 kPa/m^2 (3 psia) was selected as the baseline back pressure to ensure avoidance of complications with triple-point conditions at 6.9 kPa (1 psia). At a 20.7-kPa/m^2 (3 psia) back pressure, the heat absorption benefits of decreasing tank pressure begin to level off at ≈137.8 kPa/m^2 (20 psia). Therefore, 137.8 kPa (20 psia) was selected as the tank pressure at which venting would be intitiated. Therefore, if tank saturation conditions begin at 103 kPa (15 psia), then ≈4 days can be accommodated without venting due to the heat absorption involved in raising the saturation condition to 137.8 kPa/m^2 (20 psia), assuming a MHTB heat leak of 20 W and a homogeneous bulk liquid.

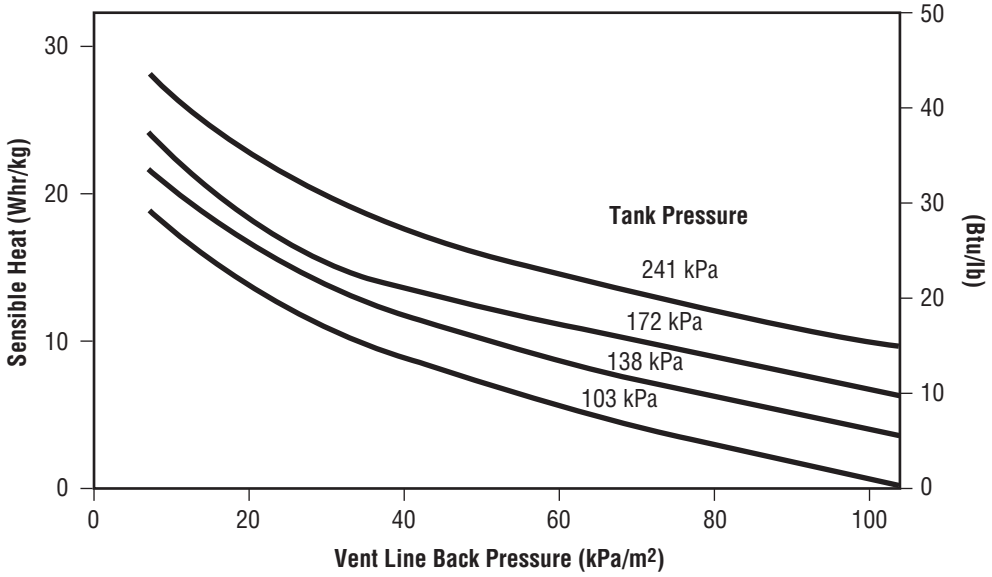

Figure 10. Sensible heat absorption by vent flow versus liquid vapor pressure and vent back pressure.

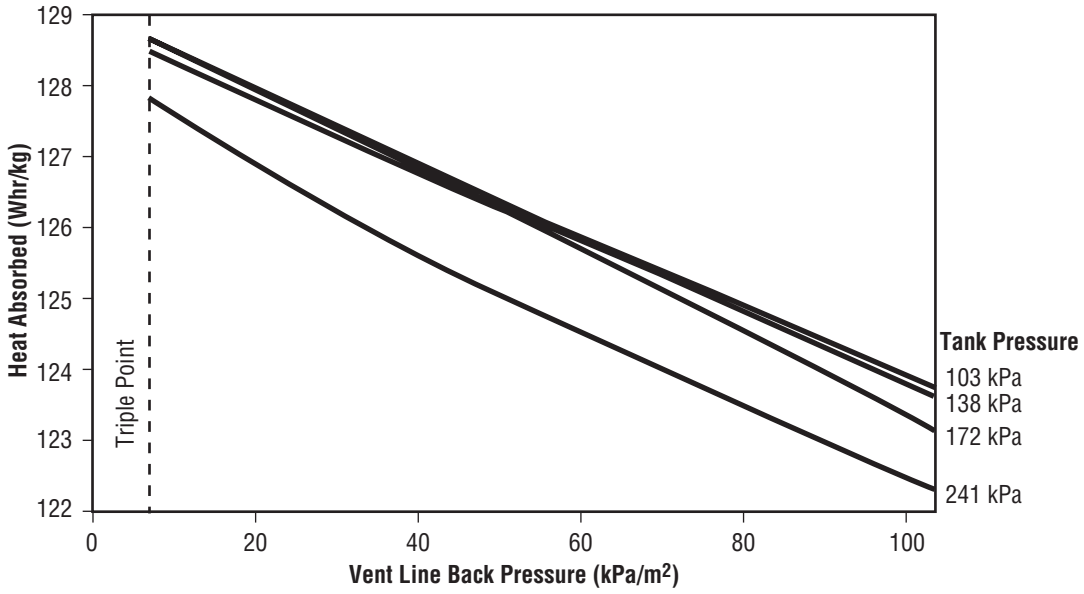

Figure 11. Total heat absorbed by vent flow versus liquid vapor pressure and back pressure.

3.3 Spray Bar Orifice Sizing

Flow from the heat exchanger outlet is manifolded into four 1.27-cm- (0.5-in-) diameter tubes which are aligned along the length of the exchanger, equally spaced radially to provide equal flow in four directions. The goal is to ensure that the spray bar provides relatively uniform flow into the ullage and bulk liquid to achieve destratification through forced convection heat transfer. The spray velocities need to be sufficient to promote good heat transfer, but without excessive pump flow rates and corresponding pressure losses. An ullage pressure decay sensitivity study was performed to guide the selection of spray injection orifice size. Assuming that the liquid droplet was equal to the orifice diameter, the number of droplets and surface area available for heat exchange with the ullage could then be calculated for a given flow rate. The ullage pressure responses computed for a 0.136-kg/s (0.3-lb/s) flow rate into an empty 18-m^3 (639-ft^3) tank with droplet diameters of 0.22, 0.2, and 0.1 cm (0.086, 0.08, and 0.04 in) are depicted in figure 12 and illustrate that the pressure decay rate increases with smaller droplet sizes. Analyses also were conducted to assess the injection flow rate and velocity distributions along the spray bar length. As illustrated in figure 13, 45 orifices with a diameter of 0.17 cm (0.067 in, or a standard 51 drill size) produced relatively uniform injection velocities for the design condition of a half-full tank. The velocity variations are greater with the full and empty tank conditions, but are within an acceptable range; i.e., varied from 5.2 to 7.6 m/s (17 to 25 ft/s). Similiarly, the corresponding mass flow rate variations along the spray bar length were computed to be within 6 percent with the half-full tank.

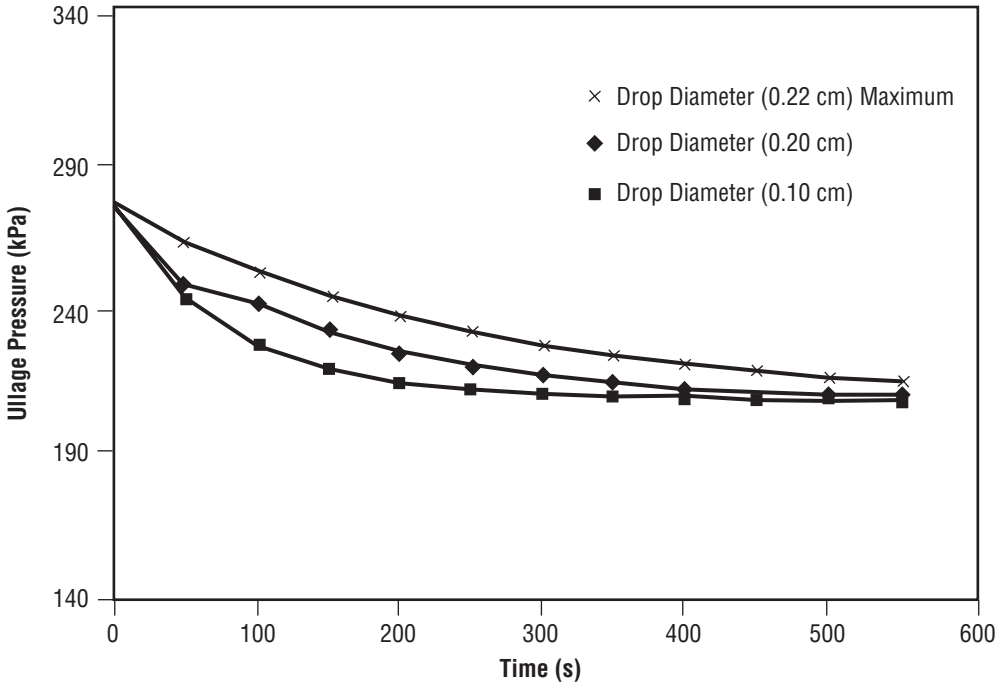

Figure 12. Effects of liquid droplet diameter on ullage pressure decay rate.

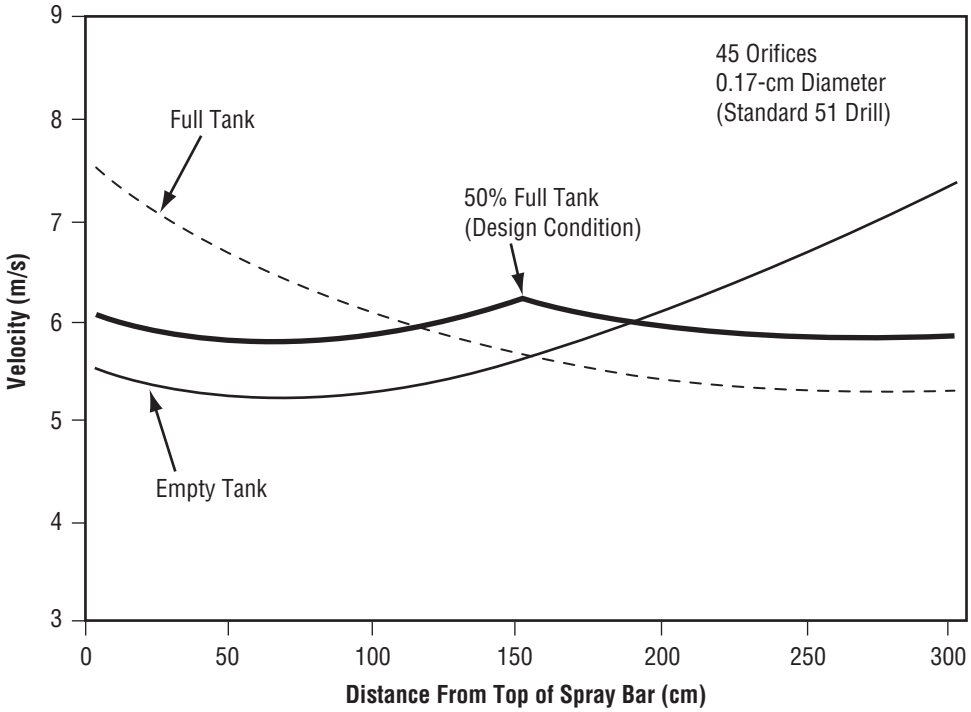

Figure 13. Injection velocity versus distance from spray bar top at 0.136 kg/s flow rate.

3.4 Control Logic

Three pressure control logic options were considered to automate the pump and vent valve operations. One option is to simultaneously activate the pump and vent valve whenever the maximum tank pressure is attained and sustain the operation until the tank pressure drops below the minimum control band level. The disadvantage is that liquid is vented even when pressure control could be achieved with mixing alone (bulk liquid is subcooled relative to the ullage pressure). Also, since bulk liquid cooling occurs with each operation, unacceptably low liquid temperatures could result. A second option is to operate the vent valve and recirculation pump independently based on measured ullage pressure. Again, the pump is activated at the upper control band pressure and is shut down when the minimum level is achieved. This mode is continued until the bulk liquid saturation pressure exceeds the upper control band limit and the vent valve is opened. The vent valve remains open until the bulk liquid saturation conditions are reduced to the minimum control band value. This control logic dictates that the pump continue to operate, adding thermal energy to the liquid, until the lower control band limit is achieved, a process that can require up to 16 hr at the maximum tank fill level. The extended pump operation is inefficient, since the added thermal energy must be removed by venting.

A third option (fig. 14), which was baselined, is to operate the pump and vent valve through separated control logic paths. The pump operation starts when the upper ullage pressure limit is reached and ceases when the lower control limit is reached. In this option, however, the vent valve control logic is based on ullage pressure and the measured bulk liquid temperature. The bulk liquid temperature is used to compute the corresponding saturation pressure, which is then compared with the measured ullage pressure. After the computed saturation pressure attains the minimum ullage pressure control band level, the vent valve is opened and closed with each subsequent recirculation pump operation cycle. The baselined option minimizes vent losses, since venting does not begin until the bulk liquid subcooling is removed; i.e., mixing cycles alone will control ullage pressure until the subcooling is removed. A minor disadvantage is that both a liquid temperature and tank ullage pressure are required, and a computation is required to convert the measured bulk liquid temperature to a corresponding vapor or saturation pressure.

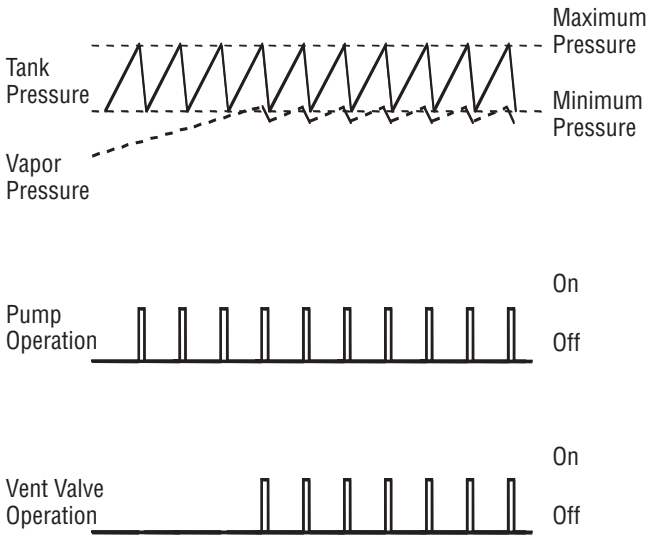

Figure 14. TVS baseline pressure control concept.

4. THERMODYNAMIC VENT SYSTEM DESIGN AND HARDWARE SELECTION

Following definition of TVS hardware design requirements, a survey of available hardware components within NASA and industry inventories was made. The design and selection processes for the recirculation pump, vent valve, heat exchanger assembly, TVS instrumentation, component box assembly, and spray bar support ring are described in detail in reference 2 and are summarized in sections 4.1 through 4.7.

4.1 Recirculation Pump

The design definition phase resulted in a 113.5-L/min (30-gal/min) nominal recirculation flow rate, with a pressure rise between 2.76 and 4.13 kPa/m^2 (0.4 to 0.6 psid), which represents the range corresponding to a full and empty tank. Because the TVS must operate with saturated liquid, the minimum net positive suction pressure is zero. No suitable off-the-shelf pump existed and Barber-Nichols, Inc., was selected to develop the pump. The selected pump, BNHP–08, is based on a previous Barber-Nichols design used with slush hydrogen. The centrifugal pump is powered with an electric motor (variable frequency drive) that is submerged and cooled with LH_2. As indicated in table 1, the pump motor input power require-ment ranges from 0.44 to 37 W with flow rates of 18.9 and 151.4 L/min (1.3 and 40 gal/min), respectively.

Table 1. Barber-Nichols pump (BNHP–08) operating characteristics.

Flow (L/min)	Frequency (Hz)	Pump Power (W)	Motor Input Power (W)	ΔP (mBar)
18.9	18	0.04	0.44	0.9
37.8	37	0.33	1.77	3.9
56.8	55	1.10	3.47	8.6
75.7	73	2.70	6.51	15.2
113.5	110	9.00	16.75	34.5
151.4	147	21.00	37.30	61.3

4.2 Joule-Thompson Vent Valve

To assist in the vent valve selection, a two-phase pressure drop analysis was performed to determine the flow capacity of four candidate valves with orifice diameters ranging from 1.96 to 3.73 mm (0.077 to 0.147 in); the results are presented in figure 15. Although all four valves satisfied the design flow rate goal of 0.1362 kg/min (0.3 lb/min), a valve used in the Space Shuttle power reactant storage distribution system was selected because of its good working condition and flow rate capability of 0.128 kg/min. The selected Consolidated Controls Corporation valve (part number 74405–4220,

serial number 097906–CRP–0020) has an orifice diameter of 1.96 mm (0.077 in) and a pressure loss of 24 kPa/m^2 (3.5 psid) with GN_2 at 689 kPa/m^2 (100 psi) and 21 °C (70 °F). The valve, described in reference 2, is bidirectional with an electrically actuated solenoid and has a minimum life of 20,000 hr. The operating pressure range is 0.07 to 2,205 kPa/m^2 (0.01 to 320 psig). The effect of the bulk LH_2 subcooling on the valve vent flow rate is presented in figure 16 and indicates that the vent flow rate increases linearly from 0.128 kg/min, with no subcooling, up to 0.169 kg/min with 27.6 kPa/m^2 (4 psi) of subcooling.

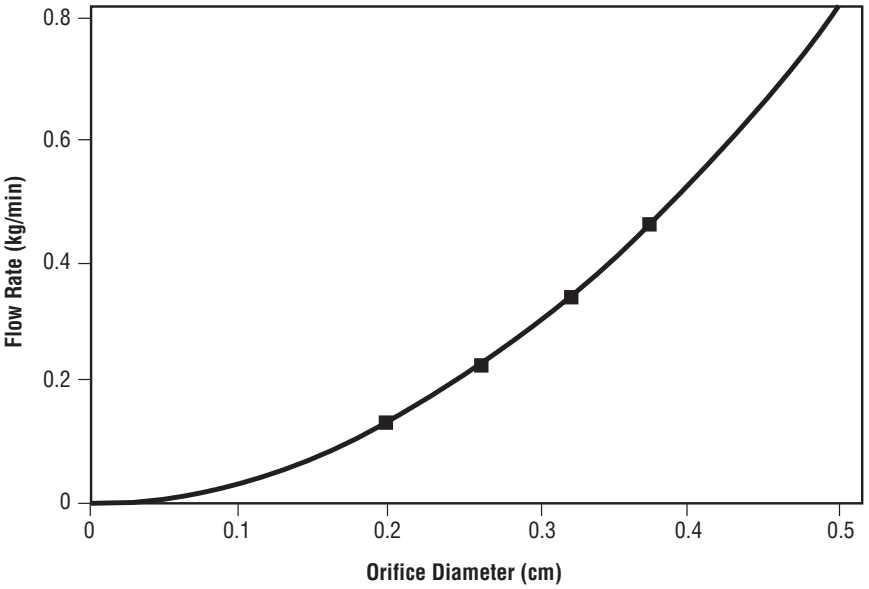

Figure 15. Two-phase flow rate versus J-T vent orifice diameter.

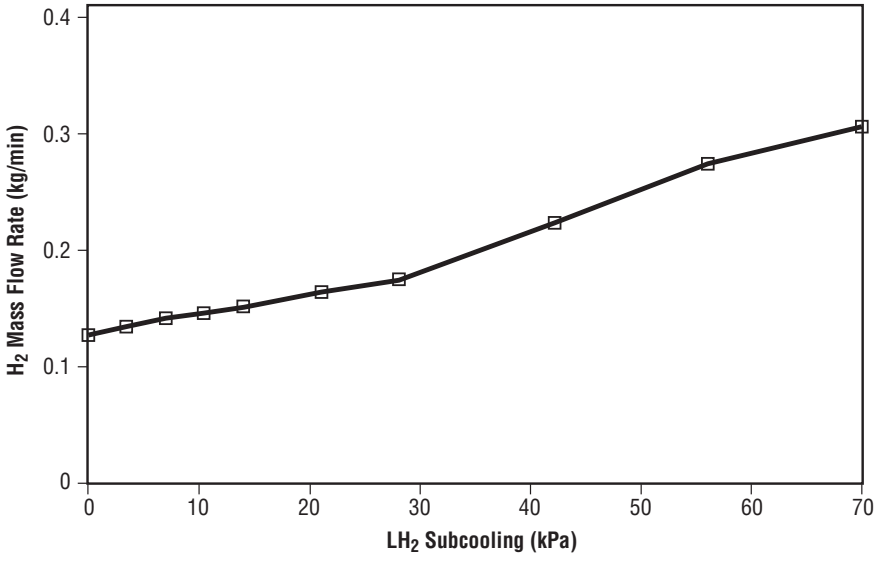

Figure 16. Vent flow rate versus liquid subcooling at 137.8 kPa/m^2 vapor pressure.

4.3 Spray Bar Heat Exchanger Assembly

The spray bar heat exchanger and spray injection assembly schematic is presented in figure 17 and the installation within the MHTB is pictorially presented in figures 18 and 19. The heat exchanger element consists of two concentric stainless steel tubes. The outer and inner tubes have 3.81 and 3.18 cm (1.5 and 1.25 in) outside diameters, respectively, and both have a wall thickness of 0.089 cm (0.035 in). The overall length of the assembly is 2.67 m (105 in) with an area of 0.27 m^2 (2.9 ft^2) for energy exchange between the recirculated and vented fluids. The external area available for energy exchange between the vented and tank or bulk fluids is 0.287 m^2 (3.1 ft^2).

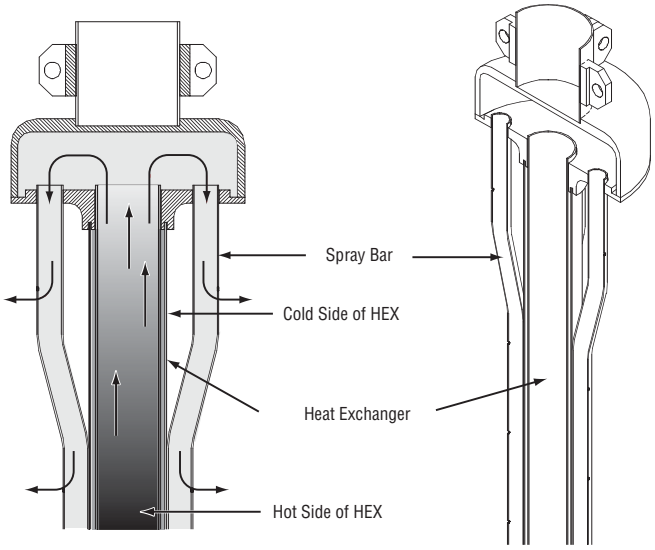

Figure 17. TVS heat exchanger and spray injection assembly.

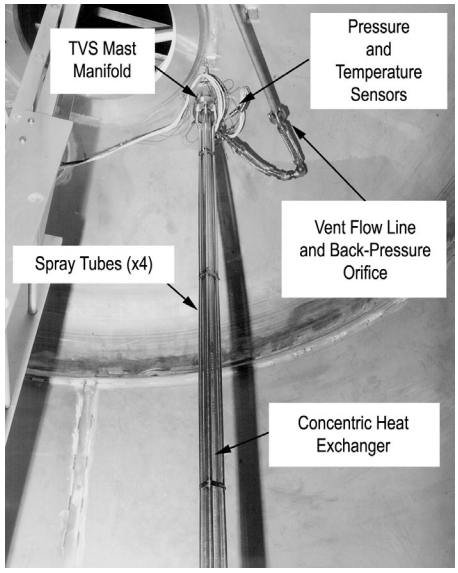

Figure 18. TVS spray bar assembly MHTB installation—top.

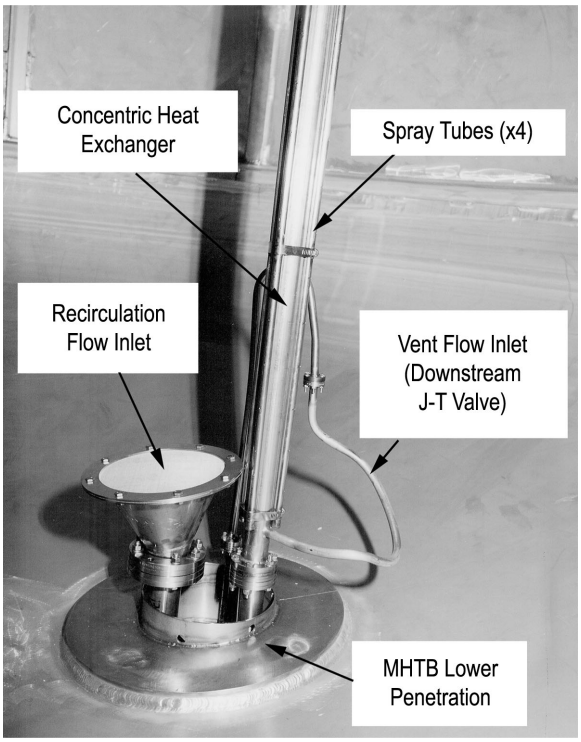

Figure 19. TVS spray bar assembly MHTB installation—bottom.

The spray injection design consists of four 1.27 cm (0.5 in) outside diameter tubes manifolded together at the heat exchanger outlet. Each tube contains 43 orifices equally spaced ≈6.1 cm (2.4 in) apart and enable spray injection in four directions. Additionally, eight orifices (two per axis) were included in the area above the heat exchanger outlet to increase injection cooling in the upper tank dome area.

Because the MHTB 3.2-cm- (1.25-in-) diameter interfacing line flange is 2° from vertical, the spray bar interfacing flange was adjusted to accommodate the misalignment. Additionally, the 1.27-cm (0.5-in) vent line at the top of the spray bar assembly included a 6.35-cm (2.5-in) loop to allow correction for any misalignment during installation (see ref. 2 for details).

4.4 Recirculation and Vent System Assembly

The recirculation and vent system assembly, shown in figures 20 and 21, contains the active components of the TVS; i.e., the pump, vent valve, and turbine flowmeter. As with the spray bar heat exchanger assembly, provisions were made to accommodate misalignments with the MHTB interfaces. A large U-shaped bend was included in the vent tube segment and provisions were made to add a bellows assembly downstream of the recirculation pump, subsequently deemed unnecessary. The assembly was designed to minimize intrusion in the space between the tank bottom and vacuum chamber cold walls on the floor. Additionally, the assembly had to be configured to minimize flow resistance and vapor accumulation in the recirculation pump and line. Therefore, the pump was positioned as close as possible to the tank outlet. Instrumentation provisions are described in section 4.5.

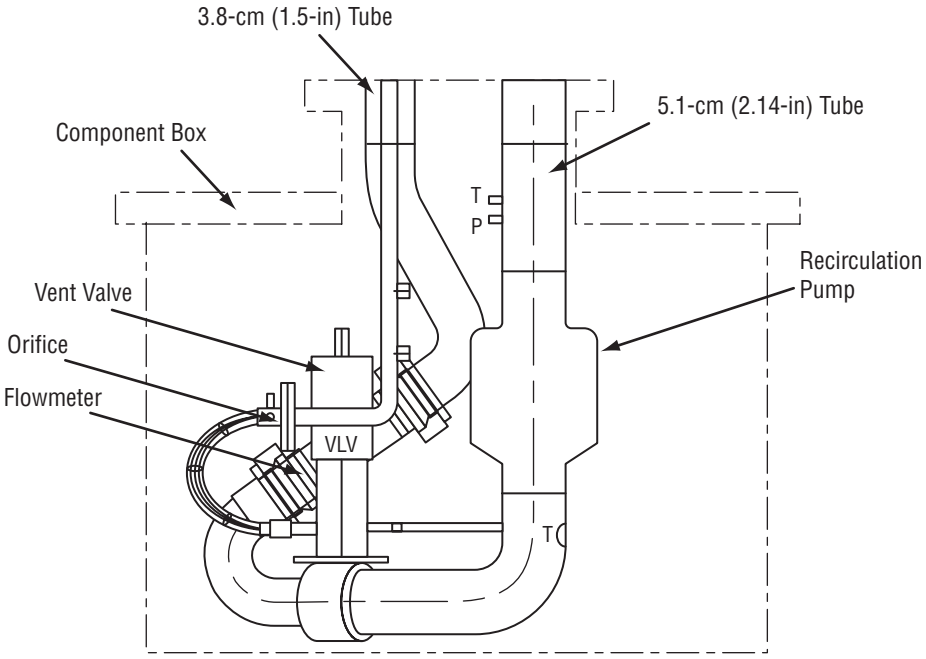

Figure 20. Recirculation pump and vent assembly.

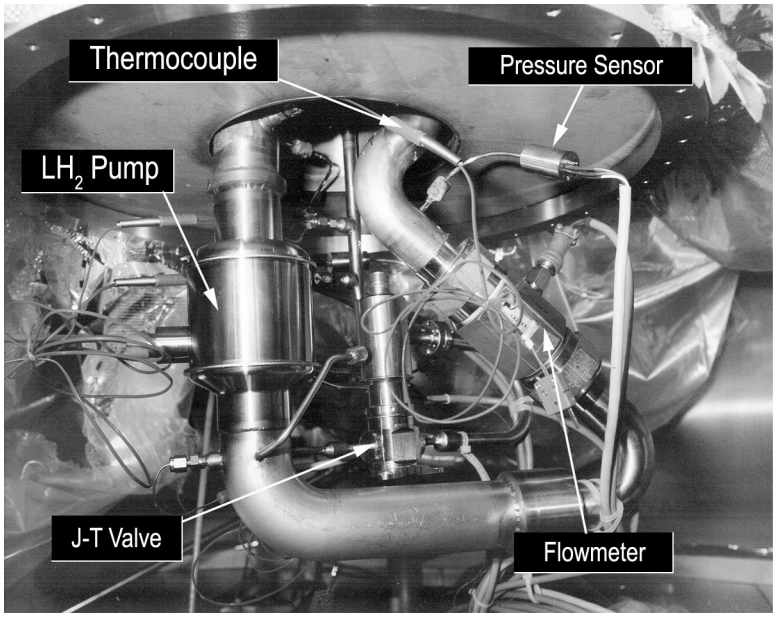

Figure 21. Recirculation pump and vent assembly—MHTB installation.

4.5 Thermodynamic Vent System Instrumentation

The TVS instrumentation presented in figure 22 is arranged to provide input to the controller and to define the TVS performance characteristics. As described in section 2.4, a bulk temperature measurement is used to monitor the bulk liquid saturation conditions relative to the measured ullage pressure and as inputs to the TVS controller. The sensor, TD23, is at the 11.5-percent fill level or 53.3 cm (21 in) above the tank bottom and is considered to be representative of the bulk liquid temperature. The TD23 temperature output is corrected to account for hydrostatic pressure, converted to a corresponding saturation pressure (termed PSA1), and compared with the ullage pressure, P4. As previously described in section 3.4, once PSA1 becomes equal to the minimum pressure control setpoint, the J-T vent valve is thereafter opened each time the mixer is activated.

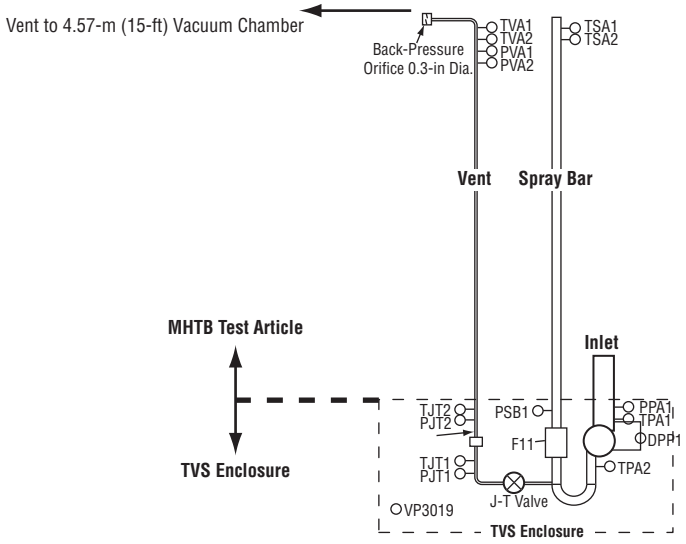

TVS Enclosure		MHTB Test Article	
PPA1	Pump inlet pressure (kPa/m^2)	TSA1	Spray bar liquid temperature (K)
TPA1	Pump inlet temperature (K)	TSA2	Spray bar liquid temperature (K)
DPP1	Pump delta pressure (kPa/m^2)	TVA1	Vent line exit temperature (K)
TPA2	Pump outlet temperature (K)	TVA2	Vent line exit temperature (K)
PSB1	Flowmeter pressure (kPa/m^2)	PVA1	Vent line exit pressure (kPa/m^2)
F11	Flowmeter (L/min)	PVA2	Vent line exit pressure (kPa/m^2)
TJT1	Vent line temperature (K)	P4	Tank ullage pressure (kPa/m^2)
TJT2	Vent line temperature (K)	P1	Tank ullage pressure (kPa/m^2)
PJT1	Vent line pressure (kPa/m^2)	TD23	Tank fluid temperature at 11% fill
PJT2	Vent line pressure (kPa/m^2)	PSA1	Calculated tank saturation pressure based on TD23
VP3019	Enclosure pressure (torr)		
PUP1	Pump on/off (high/low)		
VAV1	Valve open/closed (high/low)		

Figure 22. TVS instrumentation schematic.

The TVS performance characterization includes definition of the vent flow rate, heat exchanger performance, and recirculation spray injection flow rate. The vent flow rate is determined from choked flow calculations based on the calibrated back-pressure orifice discharge coefficient-area product, inlet pressure, and temperature measurement. Two MHTB pressure transducers are positioned upstream of the back-pressure orifice, and three temperatures are provided—two upstream and one downstream. These thermodynamic measurements provide redundancy and definition of the heat exchanger performance.

The heat exchanger performance estimate is based on the vent flow calculation (discussed above), along with the temperature measurements at the inlet and outlet of the vent side of the heat exchanger. The heat exchanger inlet temperature, along with the pump discharge pressure and vent valve inlet pressure, are used to define the heat exchanger inlet fluid two-phase quality and total enthalpy. The change in inlet to outlet enthalpy times the vent flow rate level is used to define the heat exchanger performance and the total MHTB heat extraction rate.

To define spray injection flow rate, a turbine flowmeter is positioned at the heat exchanger inlet. The recirculation flow can also be calculated based on the pump speed indication and the pump delta pressure (ΔP) measurement. The spray injection temperature exiting the heat exchanger is measured through use of the two silicone diode transducers located at the inlet to the four spray tubes. These spray injection temperature measurements can be used in the tank thermodynamic reconstruction analysis to update the liquid spray heat transfer characteristics.

4.6 Component Box Assembly

The component box function is to enclose the recirculation and vent system assembly components so that any leakage can be entrapped and pumped out without compromising the chamber vacuum levels. The cylindrical stainless steel box is 55.9 cm (22 in) in diameter by 45.7 cm (18 in) high. The pump-out or vent line has a 3.81-cm (1.5-in) diameter that is connected to a facility vacuum pump, thereby eliminating the effects of any small leaks on vacuum chamber conditions. The cylindrical section has a 0.32-cm (0.125-in) wall thickness and the top flange is 2.54 cm (1 in) thick. The top flange, used for connecting with the MHTB tank interface, contains a Conflat seal, whereas a 0.159-cm (0.0625-in) indium wire seal is used on the top and bottom box sections. The box was designed to withstand a 275.6-kPa/m^2 (40-psid) burst and 103.3-kPa (15-psid) crushing pressures. The ac and dc power for the pump and valve, respectively, is routed through the box pump-out line.

4.7 Support Ring Assembly

A support ring assembly is provided for horizontal support and alignment of the spray injection and heat exchanger assembly at the upper end. The support ring has three adjustable set screws, three struts, and a strut bracket. The ring assembly is attached to the three brackets inside the upper dome of the MHTB.

5. SUBSYSTEM AND COMPONENT TESTING

Component and subsystem testing of the TVS hardware was performed to verify functionality and integrity, and to anchor analytical modeling. Acceptance testing was conducted, in some cases, with simulant fluids to keep costs within funding constraints.

5.1 Liquid Hydrogen Spray Injection

Liquid hydrogen spray injection tests were performed (ref. 2) at Glenn Research Center (GRC) to verify pressure collapse analytical modeling. The test configuration (fig. 23) consisted of a 63.5-cm- (25-in-) long spray bar segment with 0.14-cm (0.055-in) orifices spaced 6.35 cm (2.5 in) apart along the spray bar length. The spray bar was mounted inside a dewar with an inside diameter of 55.9 cm (22 in), a height of 71 cm (28 in), and an internal volume of 0.178 m^3 (6.3 ft^3). Due to pump performance limitations, the flow rates were limited to 11.35 L/min (3 gal/min), as opposed to the 18.9 L/min (5 gal/min) desired, and to a 20-s steady-state flow duration. However, the testing provided valuable insight and was effectively utilized to anchor analytical modeling. The measured data are presented in figures 24 and 25 for the ullage temperature and wall temperature, respectively. The correlation between the predicted and measured ullage pressure, presented in figure 26, indicated that the appropriate parameters were modeled and that the spray bar would provide good pressure control during the MHTB TVS testing.

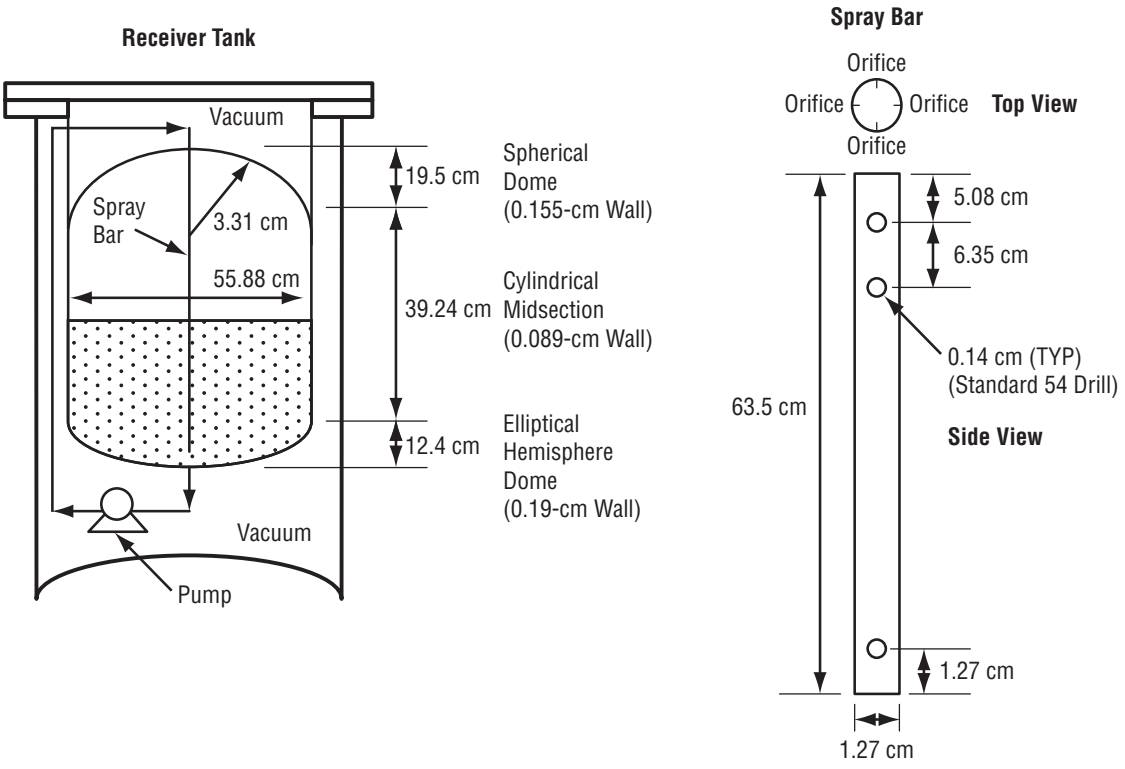

Figure 23. GRC ullage pressure collapse test setup.

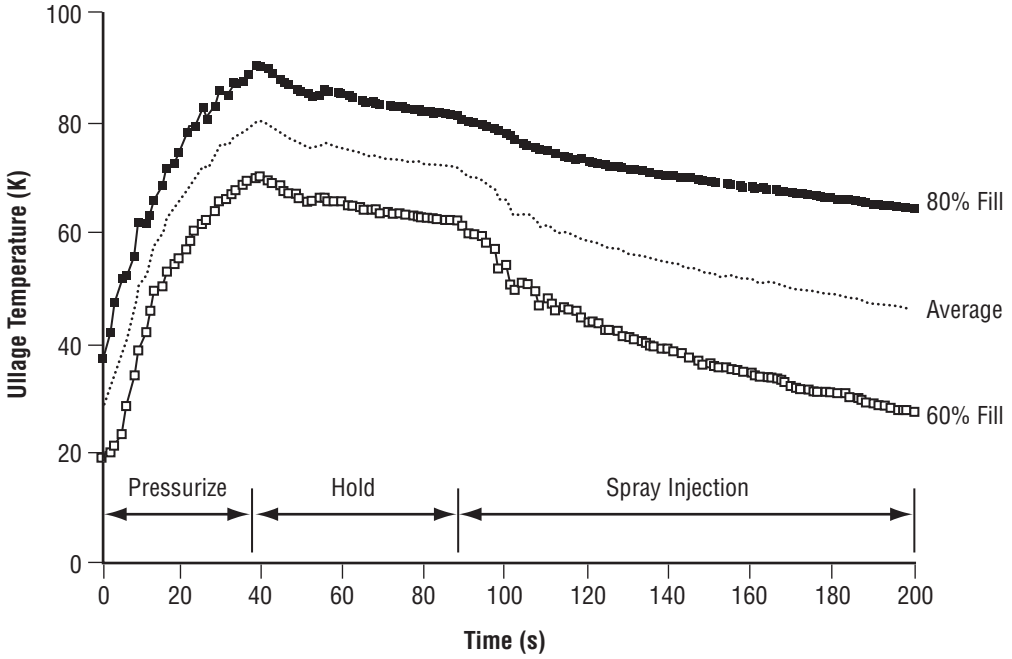

Figure 24. GRC test data for ullage temperature.

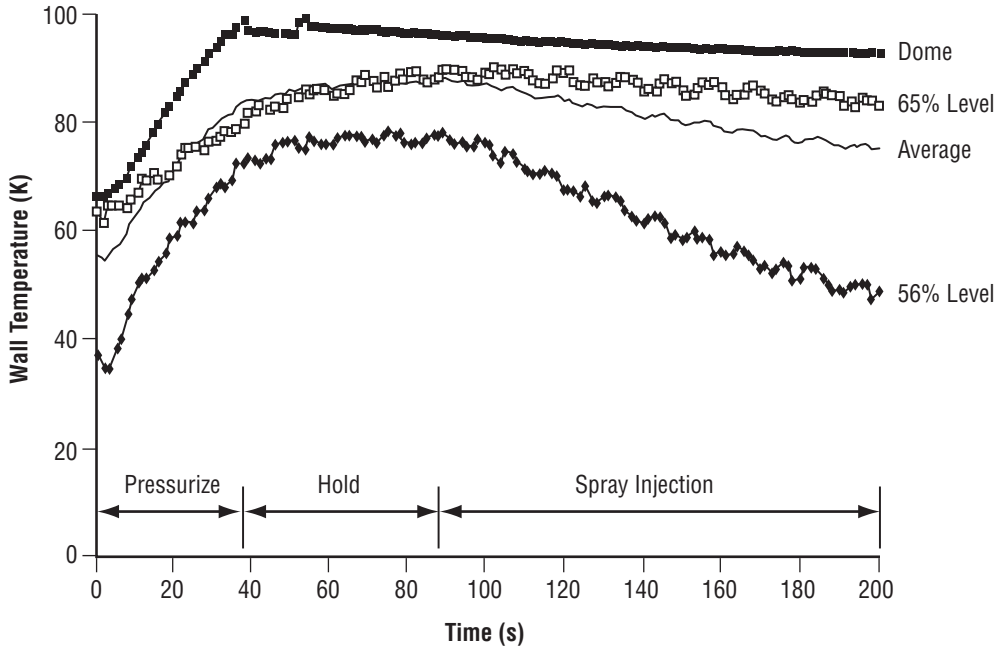

Figure 25. GRC test data for tank wall temperature.

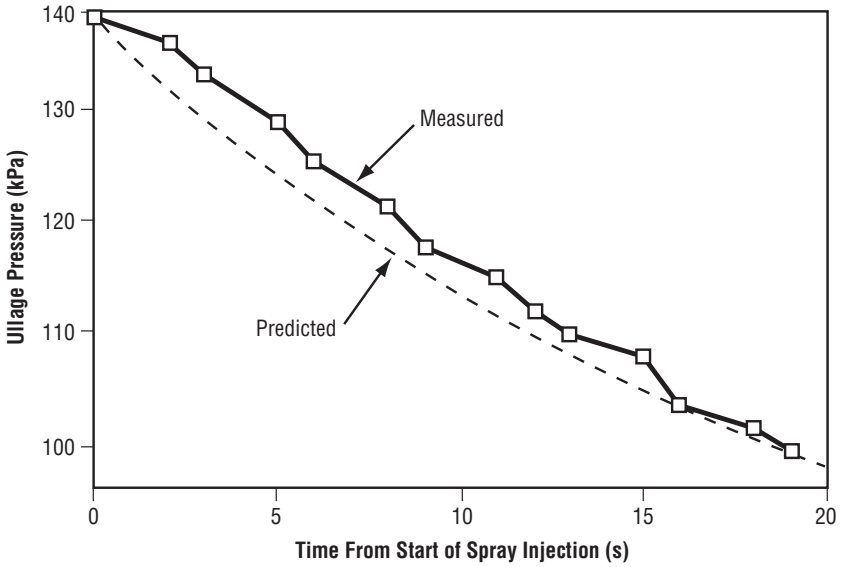

Figure 26. Comparison of predicted ullage pressure and GRC test results.

5.2 Recirculation Pump

The recirculation pump tests, performed at Barber-Nichols, measured the pump head rise versus flow rate for various operating speeds. The testing was conducted with methanol to simulate the low hydrogen density. The pump head and flow coefficients were derived from flow and delta pressure measurements, which were then used in the performance predictions. The predicted and measured flow rates versus head rise data are presented in figure 27 and indicate that the pump produces 113.5 L/min (30 gal/min) with a head rise of 3.3 kPa/m^2 (0.48 psid) and 6.89 kPa/m^2 (1 psid) at 3,134 rpm and 4,158 rpm, respectively. The pump was also operated at low speed (1,000 to 2,000 rpm) submerged in liquid nitrogen (LN_2) to verify functionality at cryogenic temperatures.

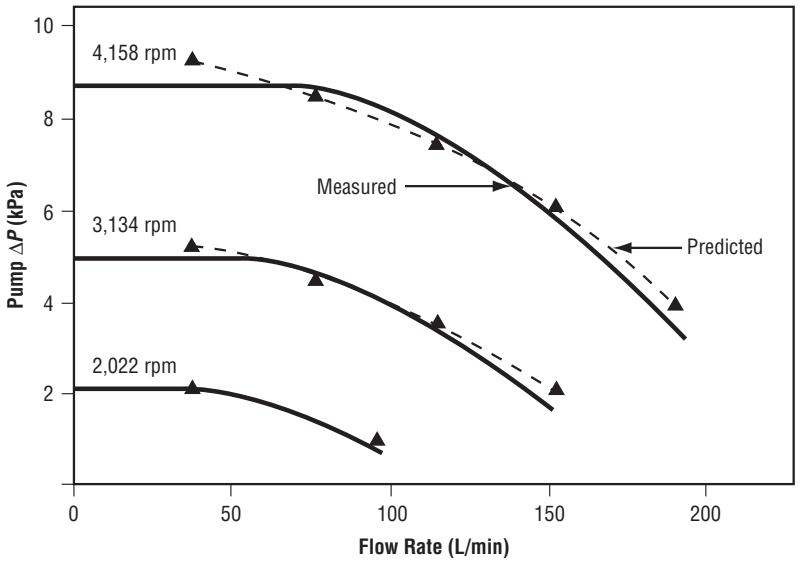

Figure 27. LH_2 recirculation pump predicted and measured performance.

5.3 Other Component and Subsystem Testing

Additional TVS component and subsystem testing included system pressure drop, flowmeter calibration, cryogenic shock, proof pressure, and leakage tests.

The spray injection tubes were individually flow tested in a horizontal position with water to measure spray orifice pressure drop. The test-derived pressure loss coefficients were compared to verify that the orifices had been uniformly drilled and deburred. The measured pressure losses and derived flow coefficients for each of the four tubes are presented in figures 28 and 29, respectively. The pressure losses ranged from about 20.67 to 227.4 kPa/m^2 (3 to 33 psi) with flow rates from 24.6 to 68.1 L/min (6.5 to 18 gal/min). The tube-to-tube loss coefficient variations were within 16 percent, indicating that uniform flow distributions should result.

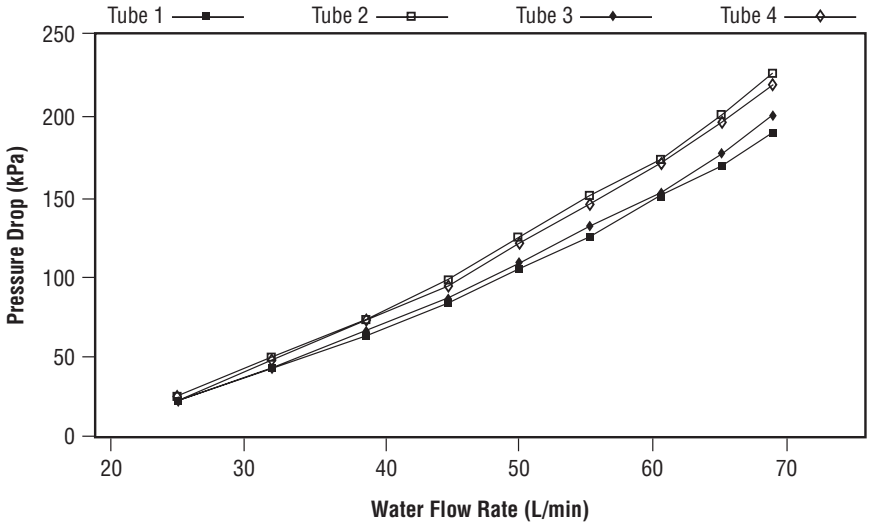

Figure 28. Spray injection tube water flow pressure drop test results.

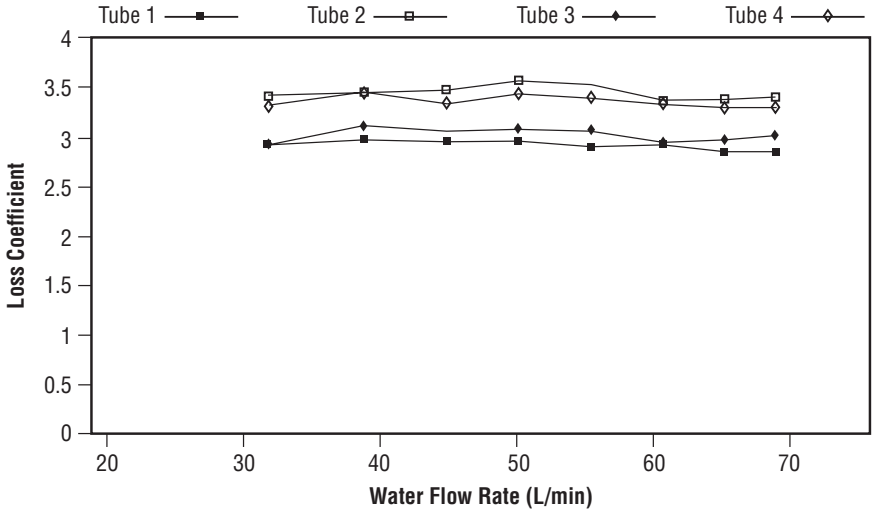

Figure 29. Spray injection tube measured water flow loss coefficients.

The spray tube and heat exchanger assembly was also tested vertically with water. The integrated spray bar and heat exchanger (hot side) pressure loss was defined, minus the hydrostatic pressure; results are presented in figure 30 and, as expected, the total pressure drop was higher than the individual tube losses due to the manifold loss effects. The water pressure loss data for the assembly was then extrapolated to LH_2 and the results are presented in figure 31. With an empty tank (worst case), the pump pressure rise is greater than the TVS pressure loss prediction based on the water data until ≈150 L/min (≈40 gal/min). For example, at 113.55 L/min (30 gal/min) and with an empty tank, the pump pressure rise is 4.134 kPa/m^2 (0.6 psi) and the TVS pressure loss is ≈3.24 kPa/m^2 (≈0.47 psi), indicating that the system should perform well. Additionally, photographic data indicated that the spray pattern exceeded 3.05 m (10 ft), assuring that the MHTB ullage will certainly be penetrated and mixed.

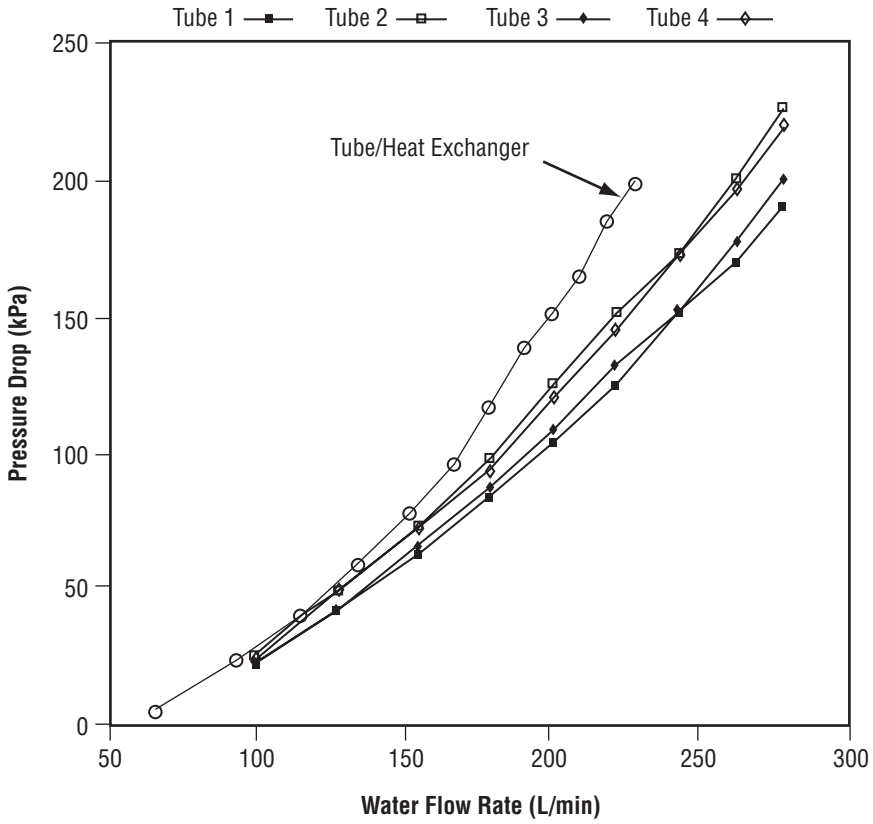

Figure 30. Water flow pressure drop in spray tubes and heat exchanger assembly.

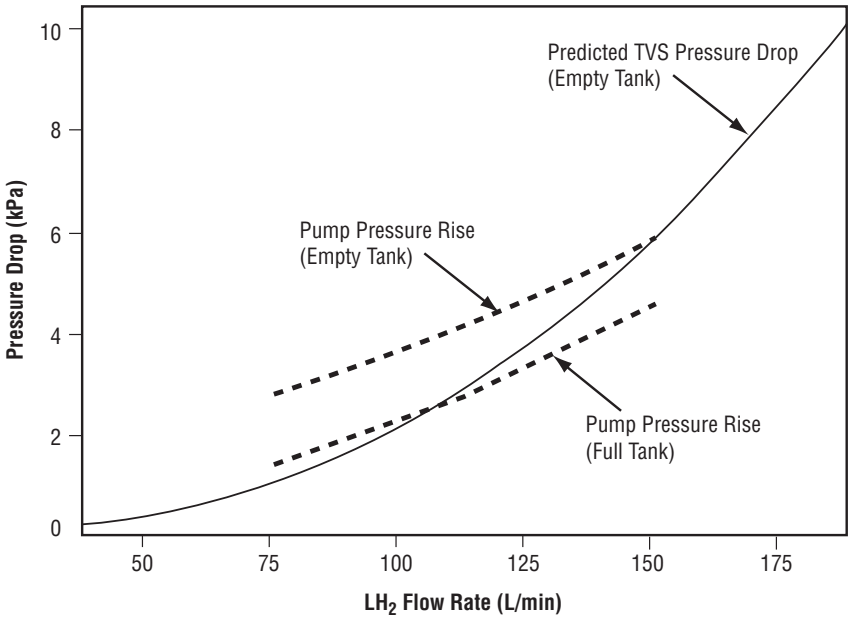

Figure 31. Predicted and measured LH_2 spray injection system pressure loss based on water flow test results.

The pressure drop on the cold side of the heat exchanger was evaluated during the cold shock testing with LN_2 (fig. 32). As LN_2 chilled the heat exchanger and spray bar (hot side), GHe was flowed through the vent or cold side and the pressure drop measured. The loss coefficient was defined based on the test data and is compared with the analytical prediction in figure 33. The measured data are 15 to 25 percent higher than predicted, probably due to entrance and exit losses not accounted for in the analytical model. There was no evidence of leakage; however, the spray tubes were displaced from the original positions due to thermal contraction. The tubing was subsequently spot welded to exisiting metal retainer straps to prevent further displacement.

Figure 32. Spray bar LN_2 test.

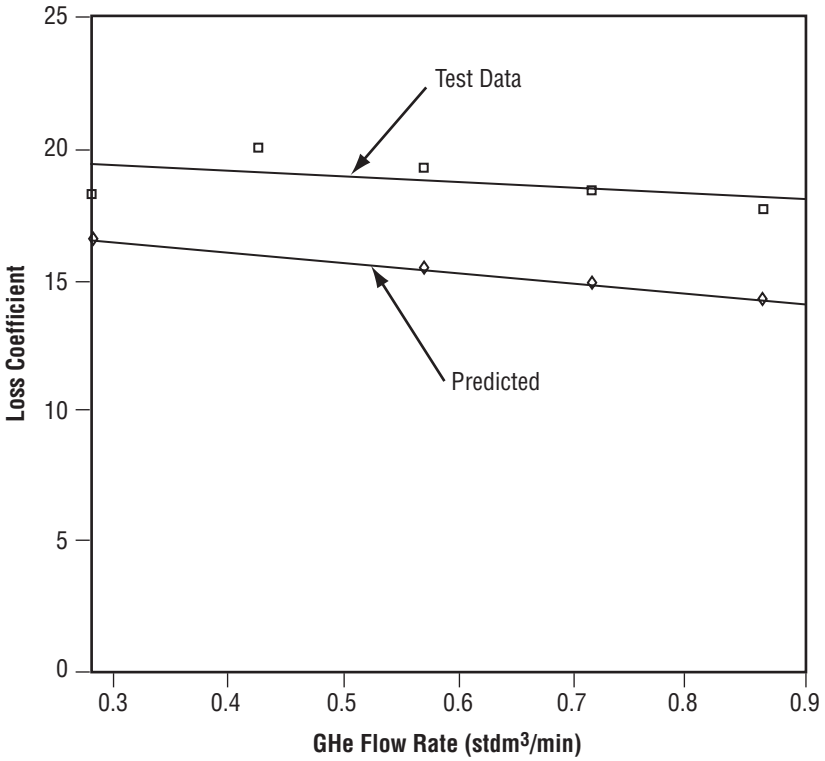

Figure 33. Vent tube loss coefficient prediction and test comparison.

Cryogenic shock and leak tests were performed on the component box assembly. The component box was filled with LN_2 and the assembly then pressurized to 413.4 kPa/m^2 (60 psig) proof pressure. The LN_2 was then drained; the box was returned to ambient temperature and pressurized to 275.6 kPa/m^2 (40 psig) with helium to measure leakage across the welds, Deutsch connectors, pipe plugs, and flange seals. No leakage was indicated by a mass spectrometer. Furthermore, no leakage into the box was observed after the internal pressure was reduced to 0.138 kPa/m^2 (0.02 psia).

The only instrumentation component test activity involved calibration of the recirculation line turbine flowmeter (see sec. 4.5) with water. The flowmeter testing was performed with the actual line inlet and outlet geometries (diameter, bend radii, and angle) and indicated ≈3.785 L/min (1 gal/min) per 4.45-Hz signal output.

6. SPRAY BAR THERMODYNAMIC VENT SYSTEM PERFORMANCE ANALYTICAL MODELING

A transient analytical model of the TVS within the MHTB LH_2 tank was formulated to characterize performance. The model, written in FORTRAN 77 programming language, can be run on various platforms with a FORTRAN compiler. The model is described herein; however, further details, example results, and the computer program listing are presented in reference 3. Individual thermal-fluid models of the heat exchanger, spray manifold and injection tubes, recirculation pump, and tank were developed and verified independently before being integrated into the transient TVS model. Each thermal-fluid model input is described in sections 6.1 through 6.4.

6.1 Heat Exchanger

The heat exchanger model is based on a generalized two-phase cryogenic propellant dump model developed to evaluate the Space Shuttle main propulsion system cryogenic propellant dump/vacuum inerting operations performance.[4] It is a multinode finite difference model that simulates two-phase flow in a quasi-steady-state mode. The model uses the fluid properties at the spray manifold inlet, including total enthalpy, as the input to the first node. The total enthalpy at the exit can then be calculated based on the First Law of Thermodynamics. The total enthalpy at the exit and an assumed mass flow rate are used to determine the exit static pressure which is determined by an iterative process. With the flow assumed choked at the exit, the exit static pressure is increased incrementally until the maximum entropy is achieved (sonic flow), or until it becomes greater than the back pressure (subsonic flow). From the calculated exit pressure, the other exit fluid properties of the last node and the total pressure loss between the heat exchanger inlet and outlet can then be calculated and the inlet fluid properties determined.

Sections 6.1.1 through 6.1.3 provide the equations used in the heat exchanger model.

6.1.1 Fluid Quality at Heat Exchanger Outlet

The outlet static pressure is calculated, assuming choked or sonic flow (maximum entropy). Equations (1)–(4) are solved simultaneously for the liquid quality of the fluid at the outlet:

$$h_o = h_i + \frac{\dot{Q}}{\dot{m}} + \Delta Ha \tag{1}$$

$$V_o = \frac{\dot{m}}{\rho_o A} \tag{2}$$

$$\rho_o = \frac{1}{\frac{1}{(\rho_L)_o} + Y_o\left[\frac{1}{(\rho_V)_o} - \frac{1}{(\rho_L)_o}\right]} \tag{3}$$

$$h_o = (1 - Y_o)(h_L)_o + Y_o(h_V)_o + \frac{{V_o}^2}{2 g_c J} \ , \tag{4}$$

where the following fluid properties are based on the outlet static pressure:

$(h_L)_o$ = outlet liquid enthalpy
$(h_V)_o$ = outlet vapor enthalpy
$(\rho_L)_o$ = outlet liquid density
$(\rho_V)_o$ = outlet vapor density
$\dot{Q}$ = total heat transfer rate to a specific node
ΔH = change in height of the line between inlet and outlet
$a = \frac{g}{g_c}$ = ratio of environmental acceleration to Earth's gravitational constant
$\dot{m}$ = mass flow rate
A = cross-section flow area
J = unit conversion constant
h_I = inlet total enthalpy
h_o = outlet total enthalpy
ρ_o = outlet total density
V_o = outlet fluid velocity
Y_o = outlet fluid quality.

With the outlet quality, the total entropy can then be calculated using the following equation:

$$\left\{(S)_o = (1 - Y_o)(S_L)_o + Y_o(S_V)_o\right\}_{\max} \ , \tag{5}$$

where

$(S_L)_o$ = outlet liquid entropy
$(S_V)_o$ = outlet vapor entropy.

Iteration of the above outlet equations can be performed to obtain the maximum entropy and the outlet static pressure.

6.1.2 Two-Phase Pressure Loss in Heat Exchanger

To calculate the two-phase pressure loss (momentum and friction) between the heat exchanger inlet and outlet, the Lockhart-Martinelli correlation is used. The outlet pressure is

$$p_o = \left(p_S\right)_o + \left(p_D\right)_o \ . \tag{6}$$

The total pressure loss term is further defined as

$$\Delta p_T = \Delta p_m + \Delta p_f \ , \tag{7}$$

where

Δp_m = pressure loss due to momentum change
Δp_f = pressure loss due to frictional forces.

The momentum pressure loss is defined as

$$\Delta p_m = \frac{\dot{m}}{g_c A}\left(V_o - V_i\right) \ . \tag{8}$$

The frictional pressure loss is defined as

$$\Delta p_f = \frac{144K}{2\overline{\rho}_L g_c}\left[\frac{\dot{m}\left(1-\overline{Y}\right)}{A}\right]^2 \Phi_L{}^2 \ , \tag{9}$$

where

$K = \left(f\dfrac{L}{D}\right)$ = line loss coefficient
$\overline{\rho}_L$ = average liquid density between the inlet and outlet
$\overline{Y}$ = average total liquid quality between the inlet and outlet
$\Phi_L = f(X)$ = Lockhart-Martinelli correlation factor.

The Lockhart-Martinelli correlation is approximately defined as

$$\Phi_L{}^2 = 1 + \frac{1}{X} + \frac{1}{X^2} \quad . \tag{10}$$

X is defined as

$$X = \left(\frac{\overline{\mu}_L}{\overline{\mu}_V}\right)^{0.1} \left(\frac{1-\overline{Y}}{\overline{Y}}\right)^{0.9} \left(\frac{\overline{\rho}_V}{\overline{\rho}_L}\right)^{0.5} \quad , \tag{11}$$

where

$\overline{\rho}_V$ = average vapor density between the inlet and outlet
$\overline{\mu}_L$ = average liquid viscosity between the inlet and outlet
$\overline{\mu}_V$ = average vapor viscosity between the inlet and outlet.

6.1.3 Forced Convection Heat Transfer

The heat transfer equations used in the steady-state model are given in equations (12)–(18). Two-phase heat transfer is defined with the correlation proposed by John C. Chen:[5]

$$\frac{\dot{Q}}{A} = \left[h_{FC}F + h_{NB}S\right]\Delta T \quad , \tag{12}$$

where

$$h_{FC} = 0.023\left(\frac{DG}{\mu_L}\right)^{0.8}\left(\frac{\mu_L C_L}{k_L}\right)^{0.4}\left(\frac{k_L}{D}\right) \tag{13}$$

$$h_{FZ} = 0.00122\frac{k_L{}^{0.79} C_L{}^{0.45} \rho_L{}^{0.49} g_c{}^{0.25} \Delta T^{0.24} \Delta P^{0.75}}{\sigma^{0.5} \mu_L{}^{0.29} \lambda^{0.24} \rho v^{0.24}} \tag{14}$$

$$F = f(X) \tag{15}$$

$$Re_L = \frac{DG(1-Y)}{\mu_L} \tag{16}$$

$$\Delta T = T_W - T_S \tag{17}$$

$$\Delta p = \frac{\Delta T \rho_V \lambda}{T_S} \quad , \tag{18}$$

where

μ = viscosity
G = mass flow rate per unit area
C = specific heat
Re = Reynolds number
λ = latent heat of vaporization
σ = surface tension
k = thermal conductivity
A = area
$\dot{Q}$ = total heat transfer rate
F = Reynolds number factor
h_{FC} = forced convection heat transfer coefficient
h_{NB} = nucleate boiling heat transfer coefficient
S = suppression factor
X = Martinelli parameter
T_W = wall temperature
T_S = spray temperature
D = line diameter.

The single-phase heat-transfer correlation used in the model (liquid and superheated gas) is

$$\frac{\dot{Q}}{A} = h\Delta T \tag{19}$$

$$h = 0.023\left(\frac{DG}{\mu_L}\right)^{0.8}\left(\frac{\mu_L C_L}{k_L}\right)^{0.4}\left(\frac{k_L}{D}\right). \tag{20}$$

6.2 Spray Manifold and Injection Tube

Fluid is recirculated from the MHTB tank to the spray manifold and injection tubes that spray it back into the tank ullage and liquid. A one-dimensional, incompressible fluid dynamic model was developed to determine the pressures in the spray manifold and injection tubes, and the spray flow rates and velocities exiting the injection orifices. The manifold model is described below.

6.2.1 Spray Manifold

The spray manifold model calculates the manifold pressure drop and determines the pressure at the spray injection tube inlets (fig. 34). The model accounts for the frictional pressure drop in the manifold, and pressure losses resulting from flow turning and contraction at the manifold exit. From the Bernoulli equation:

$$\frac{(p_{SM})_i}{\rho} + \frac{{V_{SM}}^2}{2g_c} + az_i = \frac{(p_{SM})_o}{\rho} + \frac{{V_{SM}}^2}{2g_c} + az_o + (h_L)_{SM}\ , \tag{21}$$

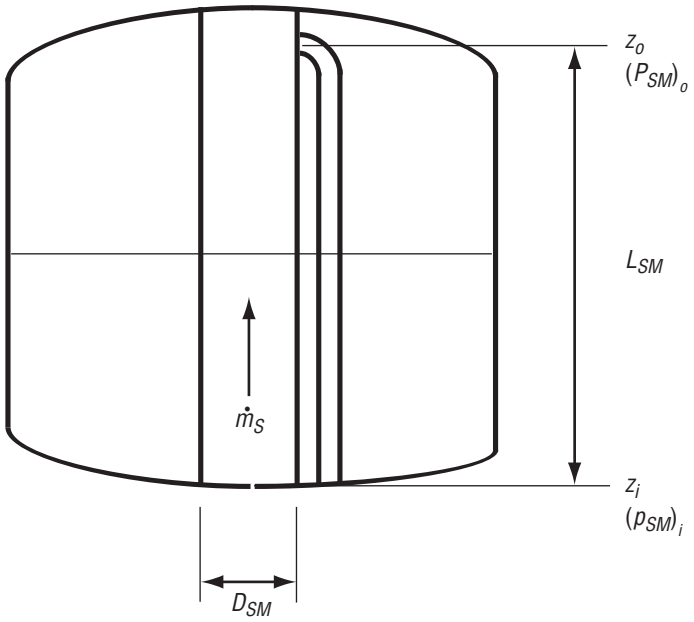

Figure 34. Spray manifold analytical model.

where

$(p_{SM})_i$ = spray manifold inlet pressure

$(p_{SM})_o$ = spray manifold outlet pressure

V_{SM} = velocity in the spray manifold

z_i, z_o = inlet and outlet elevations

$a = \frac{g}{g_c}$ = acceleration ratio.

The total head loss is defined as

$$h_{L_{SM}} = K_{SM} \frac{V_{SM}^2}{2g_c} \quad . \tag{22}$$

The total loss coefficient, K_{SM}, is given by

$$K_{SM} = \left(K_f\right)_{SM} + \left(K_b\right)_{SM} + \left(K_c\right)_{SM} \tag{23}$$

and includes

$$\left(K_f\right)_{SM} = f_{SM}\left(\frac{L}{D}\right)_{SM} \quad \text{(spray manifold frictional loss coefficient)} \tag{24a}$$

$$\left(K_b\right)_{SM} = f_{SM}\left(\frac{L_e}{D}\right) \quad (90° \text{ bend resistance at manifold exit}) \tag{24b}$$

$$\left(K_c\right)_{SM} = 0.5\left[1-\left(\frac{D_{SI}}{D_{SM}}\right)^2\right] \quad \text{(sudden contraction at manifold exit),} \tag{24c}$$

where

$L_{SM} = z_o - z_i$ = spray manifold length
L_e = bend equivalent length
D_{SI} = spray injection tube ID
D_{SM} = spray manifold ID
f_{SM} = friction coefficient in spray manifold is obtained from

$$f_{SM} = \frac{1}{4\left\{\log_{10}\left[\frac{\varepsilon / D}{3.7} + \frac{2.51}{Re\sqrt{0.0056 + \frac{0.5}{\left(Re\right)^{0.32}}}}\right]\right\}^2}, \quad Re > 3{,}000$$

$$f_{SM} = \frac{64}{Re}, \quad Re \le 3{,}000 \ . \tag{25}$$

Equation (21) can be solved for the spray manifold outlet pressure:

$$\left(p_{SM}\right)_o = \left(p_{SM}\right)_i - K_{SM} q_{SM} - \rho a L_{SM} \ , \tag{26}$$

where the dynamic pressure in the spray manifold, q_{SM}, is given by

$$q_{SM} = \rho \frac{V_{SM}{}^2}{2g_c} = \frac{1}{2\rho g_c}\left(\frac{\dot{m}_S}{A_{SM}}\right)^2 \quad . \tag{27}$$

6.2.2 Spray Injection Tube

The spray injection tube model is multinode, which assigns a node to each orifice (fig. 35). The Bernoulli equation is first applied to determine the pressure downstream of the 90° inlet bend (at the straight section inlet):

$$p_i = \left(p_{SM}\right)_o - q_i \left(K_b\right)_{SI} \quad . \tag{28}$$

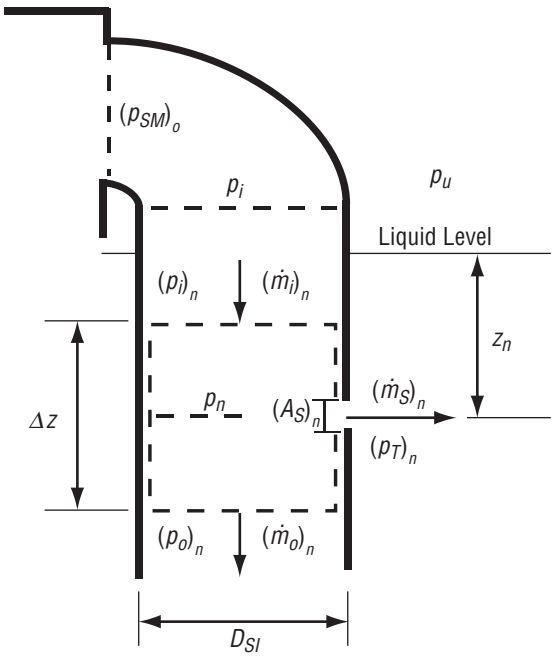

Figure 35. Spray injection tube analytical model.

In equation (28), $(K_b)_{SI}$ is the 90° bend resistance and q_i is the inlet dynamic pressure given by

$$q_i = \frac{1}{2\rho g_c}\left(\frac{\dot{m}_i}{A_{SI}}\right)^2 \quad , \tag{29}$$

where

A_{SI} = flow area of an injection tube
$\dot{m}_i$ = mass flow rate in each tube (equal to the flow rate in the manifold divided by the number of tubes).

The spray injection tube straight section is divided into 45 equal nodes corresponding to the 45 spray orifices. Each node has a pressure and a mass flow rate at the inlet (i), center (n), and outlet (o) of the node. The outlet pressure and mass flow rate of one node is therefore the inlet pressure and mass flow rate from the preceding node:

$$(p_i)_n = (p_o)_{n-1} \tag{29a}$$

$$(\dot{m}_i)_n = (\dot{m}_o)_{n-1} \ . \tag{29b}$$

The Bernoulli equation is applied successively from inlet to center and from center to outlet to determine the pressure at the center and outlet of a node n.

From inlet to center,

$$p_n = (p_i)_n + \rho a \frac{\Delta z}{2} - K_f (q_i)_n \ , \tag{30}$$

where

Δz = nodal length
K_f = frictional loss coefficient.

From center to outlet,

$$(p_o)_n = p_n + \rho a \frac{\Delta z}{2} - K_f (q_o)_n \ , \tag{31}$$

where the outlet dynamic pressure $(q_o)_n$ of node n is given by

$$(q_o)_n = \frac{1}{2\rho g_c} \left[\frac{(\dot{m}_o)_n}{A_{SI}} \right]^2 \ . \tag{32}$$

The mass flow rate at node n outlet, $(\dot{m}_o)_n$, is obtained from

$$(\dot{m}_o)_n = (\dot{m}_i)_n - (\dot{m}_S)_n \quad . \tag{33}$$

$(\dot{m}_S)_n$ in equation (33) is the spray flow rate calculated from an incompressible flow relation

$$(\dot{m}_S)_n = (A_S)_n \sqrt{\frac{2\rho g_c \left[p_n - (p_T)_n \right]}{K_S}} \quad . \tag{34}$$

In equation (34), K_S is the loss coefficient of an orifice in a duct given by

$$K_S = \left[\frac{1}{C_d} - \frac{A_S}{A_T} \right]^2 \quad , \tag{35}$$

where

C_d = discharge coefficient ($C_d = 0.8$)
A_S/A_T = ratio of the orifice to the tank area ($A_S/A_T = 0$).

Thus, K_S is determined to be 1.56.

The tank pressure $(p_T)_n$ at node n is calculated as

$$\begin{aligned} (p_T)_n &= p_U \qquad \text{(ullage nodes)} \\ &= p_U + p_L g z_n, \text{(liquid nodes)} \quad , \end{aligned} \tag{36}$$

where

z_n = distance from the liquid surface to node n.

6.2.3 Spray Manifold and Injection Tube Model Algorithm

The computer model flow chart of the spray manifold and injection tube is given in section 3.2.2 of reference 3. The model is initiated with an estimated pump flow rate and then calculates the pressures and mass flow rates at each node. Using the computed pressure and spray flow rate of the last node N, the model then calculates the tank pressure corresponding to that last node by solving the incompressible flow relation of equation (34):

$$\left(p_T\right)_{N,\,calc} = p_N - \frac{K_S}{2\rho g_c}\left(\frac{\dot{m}_s}{A_s}\right)_N^2 \quad . \tag{37}$$

Next, $(p_T)_{N,calc}$ is compared with $(p_T)_N$ obtained from the ullage pressure and hydrostatic head (eq. (36)). If the pressures are not equal within a specified tolerance (0.00689 kPa or 0.001 psi), a new pump flow rate is estimated and the process repeated until convergence on $(p_T)_N$ is achieved.

6.3 Recirculation Pump

The TVS LH_2 recirculation is provided by a centrifugal pump that is a constant output pressure device since it imparts kinetic pressure to the fluid due to rotation. Consequently, the pump pressure rise (Δp_p) is only a function of rotation speed (N) and tip velocity (U):

$$U = \frac{\pi D_m N}{720} \quad , \tag{38}$$

where

D_m = impeller diameter.

The fluid horsepower required by the pump flow $(\dot{m})$, raised to Δp_p pressure, is

$$HP_o = \frac{\dot{m}\Delta p_P}{\eta_P \rho} \quad , \tag{39}$$

where

η_P = pump mechanical efficiency.

The pump operating speed then changes as a result of the energy absorbed by the fluid and the power supplied to the pump through a power source. The instantaneous rate of change in pump operating speed is

$$\frac{dN}{dt} = \left(\frac{HP_I - HP_O}{I_P N}\right) 6.0185 \times 10^5 \quad , \tag{40}$$

where

I_p = polar moment of inertia of the pump
HP_I = input power to the pump.

Integration of the pump acceleration results in the pump speed at any given time:

$$N = (N)_{IC} + \int \left(\frac{dN}{dt} \right) dt \quad . \tag{41}$$

By specifying the initial pump speed at zero, a pump-start transient can be simulated.

The pump head versus flow rate data presented in figure 36 were provided by the pump manufacturer, Barber-Nichols. The curve was fitted with a polynomial function to provide the head coefficient (ψ) as a function of the flow coefficient (ϕ):

$$\psi = 0.52889 - 1.4956\phi + 47.819\phi^2 - 485.93\phi^3 + 1{,}633.9\phi^4 - 1{,}833.5\phi^5 \quad . \tag{42}$$

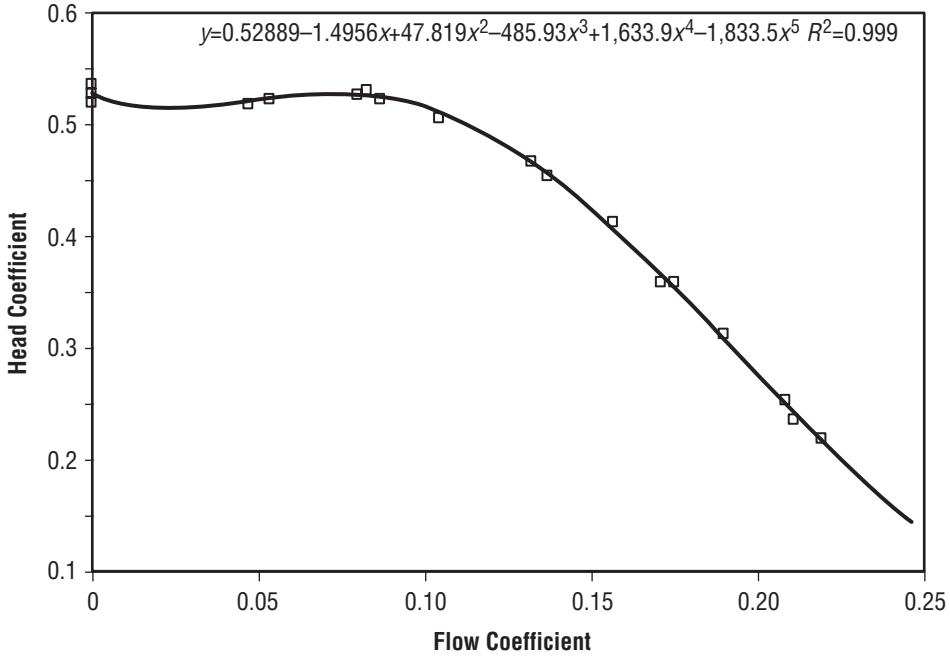

Figure 36. LH_2 recirculation pump head-flow curve.

The flow coefficient (ϕ) is obtained from test data in terms of the flow rate (in gallons per minute) and the pump speed as

$$\phi = \frac{\text{gal/min}}{0.0531N} \quad . \tag{43}$$

The pump head is calculated from the pump speed and head coefficient:

$$H = 4.507 \times 10^{-6} N^2 \psi \ . \tag{44}$$

The pump pressure rise is then obtained as

$$\Delta p_p = \frac{\rho H}{144} \ . \tag{45}$$

The integrated pump model requires the pump design flow rate (Q_D) and speed (N_D) in order to define the other operating characteristics (HP_I, I_p) required by the model.

6.4 Tank Thermodynamics

The tank model is a lumped model consisting of four control volumes (fig. 37): (1) Ullage, (2) tank wall, (3) liquid on the tank wall, and (4) bulk liquid. The thermal model of each control volume is described in sections 6.4.1 through 6.4.4.

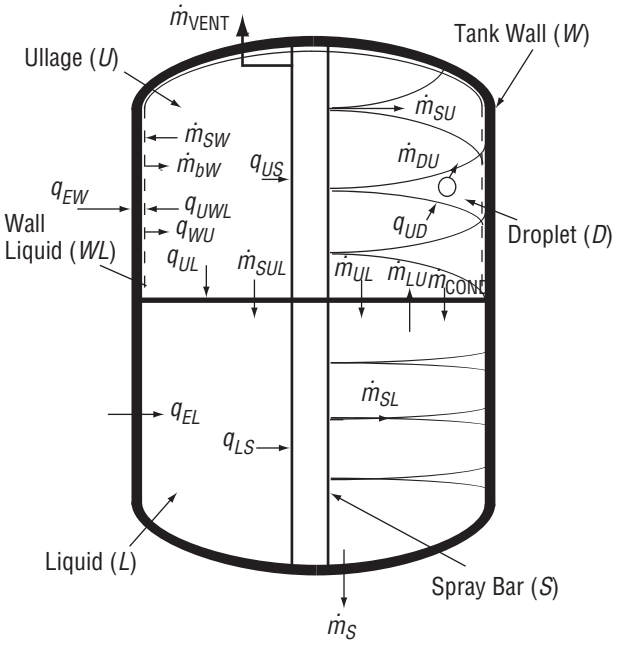

Figure 37. Tank thermal analytical model.

6.4.1 Ullage

The ullage thermal model applies conservation of mass and energy to determine the ullage pressure, temperature, and mass (fig. 38). From conservation of mass, the change in the ullage mass (M_U) is due to all masses entering and leaving the ullage control volume:

(1) Droplet evaporation rate in the ullage ($\dot{m}_{DU}$)
(2) Boiling rate of the liquid on the tank wall ($\dot{m}_{bW}$)
(3) Bulk liquid boiling rate ($\dot{m}_{LU}$), or ullage condensation ($\dot{m}_{UL}$)
(4) Liquid surface condensation ($\dot{m}_{\mathrm{COND}}$):

$$\frac{dM_U}{dt} = \dot{m}_{DU} + \dot{m}_{bW} + \dot{m}_{LU} - \dot{m}_{UL} - \dot{m}_{\mathrm{COND}} \ . \tag{46}$$

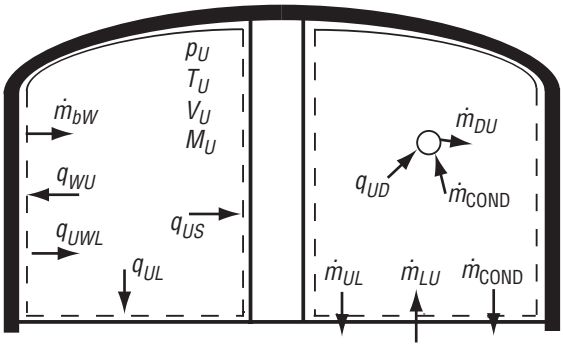

Figure 38. Ullage thermal analytical model.

These mass flow rates are defined in section 6.4.6. The ullage mass is obtained by integrating its time rate of change with respect to time:

$$M_U = \left(M_U\right)_{IC} + \int\left(\frac{dM_U}{dt}\right)dt \ . \tag{47}$$

From conservation of energy, the change in the ullage temperature (T_U) is the result of

(1) Heat transfer to the ullage (q_U)
(2) Work done on the ullage (w_U)
(3) Energy added to the ullage by incoming and leaving masses (ENTH_U):

$$\frac{dT_U}{dt} = \frac{q_U - w_U - \mathrm{ENTH}_U - c_{VU}T_U\dfrac{dM_U}{dt}}{M_U c_{VU}} \ . \tag{48}$$

The terms in equation (48) are defined as follows:

(1) $q_U = q_{WU} - q_{UWL} - q_{UL} - q_{UD} - q_{US}$ (heat transfer to ullage),

where

q_{WU} = heat transfer rate between the tank wall and ullage:

$|q_{WU}| > 0$ for a dry wall
$= 0$ for a wet wall

q_{UWL} = heat transfer rate between the ullage and wall liquid:

$|q_{UWL}| = 0$ for a dry wall
> 0 for a wet wall

q_{UL} = heat transfer rate between the ullage and bulk liquid
q_{UD} = heat transfer rate between the ullage and liquid droplet
q_{US} = heat transfer rate between the ullage and (unsubmerged) spray bar.

The above heat transfer rates are defined in section 6.4.5.

(2) $w_U = p_U \frac{dV_U}{dt}$ (work done on ullage),

where the change in the ullage volume $\left(\frac{dV_U}{dt}\right)$ is equal and opposite to the change in the liquid and wall liquid volumes:

$$\frac{dV_U}{dt} = -\frac{dV_L}{dt} - \frac{dV_{WL}}{dt} \quad . \tag{49}$$

(3) $\text{ENTH}_U = \left(\frac{dM_U}{dt}\right) h_{gsat}$,

where

$h_{gsat} = h_{sat}(p_U)$ = saturated vapor enthalpy of the ullage.

The ullage volume is obtained as the difference between the tank volume and the bulk liquid and wall liquid volumes:

$$V_U = V_T V_L - V_{WL} \quad . \tag{50}$$

Equation (48) is integrated with respect to time to obtain the ullage temperature:

$$T_U = \left(T_U\right)_{IC} + \int \left(\frac{dT_U}{dt} \right) dt \quad . \tag{51}$$

With the ullage mass, temperature, and volume determined, the ullage pressure is calculated from the equation of state:

$$p_U = \frac{M_U R_U T_U}{V_U} \quad . \tag{52}$$

6.4.2 Ullage Tank Wall

The tank wall is divided into two sections—one submerged under the liquid and the other facing the ullage. The tank wall facing the bulk liquid is assumed to be at the same temperature as the liquid. Thus, the tank wall thermal model described herein applies to the dry wall section facing the ullage (fig. 39). Since liquid can form on the tank wall as a result of spraying, the model must account for both

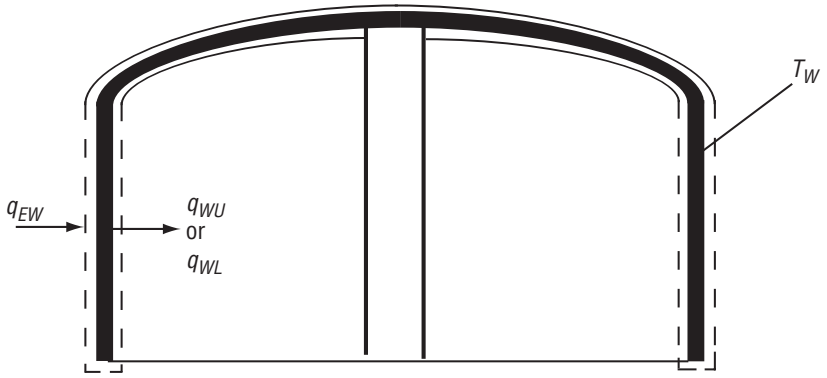

Figure 39. Tank wall thermal analytical model.

dry and wet wall cases.

From conservation of energy, the change in the tank wall temperature is due to:

(1) Heat input to the wall from the environment (q_{EW})

(2) Heat transfer rate between the wall and ullage (q_{WU})
$|q_{WU}| > 0$ for a dry wall
$= 0$ for a wet wall

(3) Heat transfer rate between the wall and liquid on the wall (q_{WL}),

$|q_{WL}| = 0$ for a dry wall

> 0 for a wet wall

$$\frac{dT_W}{dt} = \frac{q_{EW} - q_{WU} - q_{WL}}{M_W c_{pW}} \quad . \tag{53}$$

Section 6.4.5 defines the heat transfer rate computations. Equation (53) can be integrated with respect to time to obtain the tank wall temperature:

$$T_W = \left(T_W\right)_{IC} + \int\left(\frac{dT_W}{dt}\right) \quad . \tag{54}$$

6.4.3 Wetted Wall Liquid

The wetted wall liquid thermal model is also governed by the laws of conservation of mass and energy (fig. 40). From conservation of mass, the change in the wall liquid mass (M_{WL}) is equal to the difference between the liquid mass reaching the wall and the liquid mass boiled off from the wall:

$$\frac{dM_{WL}}{dt} = \dot{m}_{SW} - \dot{m}_{bW} \quad , \tag{55}$$

where

$\dot{m}_{SW}$ = spray flow rate reaching the wall

$\dot{m}_{bW}$ = liquid boiloff rate from the wall.

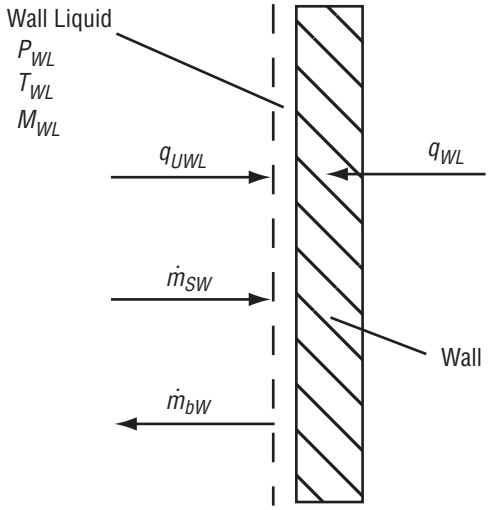

Figure 40. Tank wall liquid thermal analytical model.

These mass flow rate computations are defined in section 6.4.6. Equation (55) can be integrated to obtain the wall liquid mass:

$$M_{WL} = \left(M_{WL}\right)_{IC} + \int\left(\frac{dM_{WL}}{dt}\right) . \tag{56}$$

From conservation of energy, the change in the wall liquid temperature (T_{WL}) is the result of heat transfer to the wall liquid and sensible energy added to the spray to raise its temperature (T_{SW}) to the wall liquid temperature. Heat transfer to the wall liquid includes the heat transfer rate between the wall and wall liquid (q_{WL}), and heat transfer rate between the ullage and wall liquid (q_{UWL}):

$$\frac{dT_{WL}}{dt} = \frac{q_{WL} + q_{UWL} - \dot{m}_{SW} c_{pL}\left(T_{WL} - T_{SW}\right)}{M_{WL} c_{pWL}} . \tag{57}$$

These heat transfer rates are defined in section 6.4.5. Equation (57) can be integrated to obtain the wall liquid temperature:

$$T_{WL} = \left(T_{WL}\right)_{IC} + \int\left(\frac{dT_{WL}}{dt}\right) dt . \tag{58}$$

The wall liquid vapor pressure is then obtained from the thermodynamic database as

$$p_{WL} = p_{sat}\left(T_{WL}\right) . \tag{59}$$

The volume rate of change of the wall liquid is determined from equation (55) as

$$\frac{dV_{WL}}{dt} = \frac{1}{\rho_{WL}} \frac{dM_{WL}}{dt} , \tag{60}$$

where

ρ_{WL}=ρ_{sat}(T_{WL}) = wall liquid density.

Equation (60) is integrated to obtain the wall liquid volume

$$V_{WL} = \left(V_{WL}\right)_{IC} + \int\left(\frac{dV_{WL}}{dt}\right) dt . \tag{61}$$

6.4.4 Bulk Liquid

The bulk liquid thermal model is a single node, as opposed to a multinode model, since (1) mixing will destratify the liquid and create a uniform bulk, and (2) the uncertainties in heat transfer modeling do not seem to justify the added complexities of a multinode model. Like the previously described modeling, the liquid thermal model is based on the laws of conservation of mass and energy. From conservation of mass, the change in the liquid mass must be balanced by a change in the ullage mass and any mass vented overboard (fig. 41):

$$\frac{dM_L}{dt} = \dot{m}_{SL} + \dot{m}_{SUL} + \dot{m}_{COND} + \dot{m}_{UL} - \dot{m}_{LU} - \dot{m}_S - \dot{m}_V \quad , \tag{62}$$

where

$\dot{m}_{SL}$ = liquid spray flow rate into the bulk liquid
$\dot{m}_{SUL}$ = liquid spray unevaporated droplet flow rate
$\dot{m}_{\mathrm{COND}}$ = liquid surface condensation flow rate
$\dot{m}_{UL}$ = ullage condensation flow rate
$\dot{m}_{LU}$ = liquid boiloff rate
$\dot{m}_S$ = pump flow rate
$\dot{m}_V$ = overboard vent flow rate.

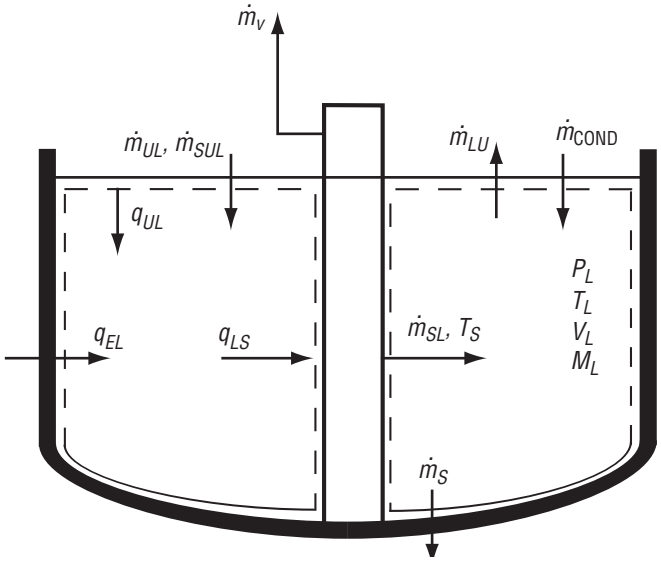

Figure 41. Bulk liquid thermal analytical model.

The liquid mass is obtained by integrating its time rate of change:

$$M_L = (M_L)_{IC} + \int \left(\frac{dM_L}{dt} \right) . \tag{63}$$

From conservation of energy, the change in liquid temperature is caused by

(1) Heat transfer to the liquid

(2) Heat added by the unevaporated droplets

(3) Sensible energy added to the liquid spray to raise its temperature (T_S) to the liquid temperature

(4) Latent heat of vaporization of the liquid:

$$\frac{dT_L}{dt} = \frac{q_L + \dot{m}_{SUL} c_{pL} (T_d - T_L) - \dot{m}_{LU} \left(h_{fg} \right)_L - \dot{m}_{SU} c_{pL} (T_L - T_S)}{M_L c_{pL}} . \tag{64}$$

The heat transfer rate to the liquid (q_L) is given by

$$q_L = q_{EL} + q_{UL} - q_{LS} , \tag{65}$$

where

q_{EL} = heat added to the liquid by the environment
q_{UL} = heat transfer rate between the ullage and liquid
q_{LS} = heat transfer rate between the liquid and (submerged) spray bars.

These heat transfer rates are defined by the equations in section 6.4.5. Equation (64) is integrated with respect to time to give the liquid temperature

$$T_L = (T_L)_{IC} + \int \left(\frac{dT_L}{dt} \right) dt . \tag{66}$$

The liquid vapor pressure is obtained from the thermodynamic database as

$$p_L = p_{\text{sat}} @ T_L . \tag{67}$$

The liquid volume rate of change is determined from the rate of change of the liquid mass:

$$\frac{dV_L}{dt} = \frac{1}{\rho_L}\frac{dM_L}{dt} \ , \tag{68}$$

where

$\rho_L = \rho_{\text{sat}} @\ T_L$ = liquid density.

Equation (68) is integrated to give the liquid volume:

$$V_L = \left(V_L\right)_{IC} + \int\left(\frac{dV_L}{dt}\right)dt \ . \tag{69}$$

6.4.5 Heat Transfer

This section defines the heat transfer rates that are determined from the energy balances defined in sections 6.4.1 to 6.4.4. These heat transfer rates can be divided into two groups—free convection and forced convection. Free convection is the dominant heat transfer mode in the ullage and liquid, while forced convection characterizes liquid droplet heat transfer in the ullage.

The convection heat transfer rate is generally defined as

$$q = hA\Delta T \ , \tag{70}$$

where

h = convection heat transfer coefficient
A = heat transfer surface area
ΔT = temperature difference between the heat source and sink.

The heat transfer coefficient is obtained from the Nusselt number (Nu) as

$$h = \left(\frac{k_F}{L_c}\right)Nu \ , \tag{71}$$

where

k_F = fluid thermal conductivity
L_c = surface characteristic length.

The Nusselt number is a function of the Rayleigh number (Ra) defined as

$$Ra = \frac{g\beta\Delta T {L_c}^3 \rho^2 c_p}{\mu k} \quad , \tag{72}$$

where

g = acceleration
β = thermal expansion coefficient

$\beta = \frac{1}{T_f}$ for gas and $\frac{1}{\rho}\left(\frac{\partial \rho}{\partial T}\right)_p$ for liquid
L_c = characteristic length
ρ = density
c_p = specific heat at constant pressure
μ = dynamic viscosity
k = thermal conductivity.

All properties must be evaluated at the film temperature (T_f), which is defined as the average of the fluid and surface temperatures.

6.4.5.1 Free Convection. Two free convection heat transfer correlations are used in the model. The first is a free convection correlation for interior surfaces of vertical ducts, vertical plates and cylinders, and horizontal cylinders:[6]

$$Nu = 0.555 Ra^{0.25} + 0.447 \quad . \tag{73}$$

This correlation is used to calculate the heat transfer coefficients:

(1) Between the ullage and wall (h_{UW})
(2) Between the ullage and bulk liquid (h_{UL})
(3) Between the ullage and wall liquid (h_{UWL})
(4) Between the ullage and (unsubmerged) spray bars (h_{US})
(5) Between the bulk liquid and (submerged) spray bars (h_{LS}).

The characteristic length for h_{UW}, h_{UL}, and h_{UWL} is the internal tank diameter while that of h_{US} and h_{LS} is the spray bar diameter.

The second correlation is the McAdams correlation for free convection of vertical surfaces in the turbulent range:[7]

$$Nu = 0.13 Ra^{1/3} \quad . \tag{74}$$

This correlation is used to calculate the heat transfer coefficient between the wall and liquid (h_{WL}). Because of the one-third power in Ra, h_{WL} can be obtained without defining the characteristic length, thereby removing the uncertainty in determining the wall liquid layer.

6.4.5.2 <u>Forced Convection</u>. The forced convection heat transfer coefficient between the ullage and liquid droplets (h_{UD}) is based on a McAdams recommended correlation for flow over a sphere:[8]

$$Nu = 0.3125\,\mathrm{Re}^{0.602} \quad . \tag{75}$$

The Reynolds number (Re) of the spray flow is defined as

$$Re = \frac{\rho Vel_D D_D}{\mu} \quad , \tag{76}$$

where

Vel_D = droplet velocity in the ullage
D_D = droplet diameter, assumed to be equal to the orifice diameter
ρ = density of the ullage gas
μ = viscosity of the ullage gas.

Since the droplet diameter and velocity vary with the orifice size, the droplet heat transfer coefficient must be determined for each orifice. The total droplet heat transfer rate is obtained by summing the droplet heat transfer rates from each orifice:

$$q_{\mathrm{drop}} = \sum_{i=1}^{n} \left(n_{\mathrm{drop}}\right)_i \left(q_{\mathrm{drop}}\right)_i \quad , \tag{77}$$

where

$(n_{\mathrm{drop}})_i$ = number of droplets sprayed from orifice i into the ullage. This is given by

$$\left(n_{\mathrm{drop}}\right)_i = \frac{\left(\dot{m}_{SU}\right)_i D_{\mathrm{CHAR}}}{2\rho_D \left(V_D\right)_i \left(Vel_D\right)_i} \quad , \tag{78}$$

where

$(\dot{m}_{SU})_i$ = spray flow rate into the ullage from orifice i

$(V_D)_i$ = droplet volume from orifice i

$(Vel_D)_i$ = droplet velocity from orifice i

ρ_D = droplet density

D_{CHAR} = a characteristic length determined empirically.

By correlating the TVS model with the GRC subscale ullage pressure collapse data (see sec. 3.1 of ref. 2), the characteristic length was determined to be one-fourth of the tank diameter.

6.4.6 Mass Transfer

This section defines the mass-transfer rates computed with the mass balance equations of section 6.4.1 through 6.4.4, which includes:

(1) Bulk liquid boiling ($\dot{m}_{LU}$)

(2) Liquid boiling from the tank wall ($\dot{m}_{bW}$)

(3) Liquid droplet evaporation in the ullage ($\dot{m}_{DU}$)

(4) Liquid spray falling into the bulk liquid ($\dot{m}_{SUL}$) or accumulating on the tank wall ($\dot{m}_{SW}$)

(5) Ullage condensation ($\dot{m}_{\mathrm{UL}}$)

(6) Liquid surface condensation ($\dot{m}_{\mathrm{COND}}$).

6.4.6.1 <u>Bulk Liquid Boiling</u>. Bulk liquid boiling occurs when the liquid vapor pressure is equal to the tank ullage pressure. It can be the result of heat transfer to the liquid and/or pressure decay in the ullage. It must also include sensible energy added to the liquid spray to increase its temperature to the liquid temperature.

If $p_L = p_U$,

$$\dot{m}_{LU} = \frac{1}{(h_{fg})_L}\left[q_L - \dot{m}_{SL} c_{pL}(T_L - T_S)\right], \qquad \frac{dp_U}{dt} > 0$$

$$= \frac{1}{(h_{fg})_L}\left[q_L - \dot{m}_{SL} c_{pL}(T_L - T_S) - M_L c_{pL}\left(\frac{\partial T}{\partial p}\right)_{\mathrm{sat}}\left(\frac{dp_U}{dt}\right)\right], \qquad \frac{dp_U}{dt} < 0 \ . \tag{79}$$

A polynomial fit of the LH_2 saturation temperature versus pressure curve was obtained and its derivative taken to give an expression for $\left(\frac{\partial T}{\partial p}\right)_{\mathrm{sat}}$:

$$\left(\frac{\partial T}{\partial p}\right)_{sat} = 0.37781 - 4.9170\times10^{-3} p_L + 21.7623\times10^{-6} {p_L}^2 \ . \tag{80}$$

If the ullage pressure increases above the liquid vapor pressure, boiling stops, $\dot{m}_{LU} = 0$, if $p_L < p_U$.

6.4.6.2 <u>Wall Liquid Boiling</u>. Wall liquid boiling from the tank wall follows the same mechanism as bulk liquid boiling.

If $p_{WL} = p_U$,

$$\dot{m}_{bW} = \frac{1}{\left(h_{fg}\right)_L}\left[q_{WL} + q_{UWL} - \dot{m}_{SW} c_{pL}(T_{WL} - T_{SW})\right], \qquad \frac{dp_U}{dt} > 0$$

$$= \frac{1}{\left(h_{fg}\right)_L}\left[q_{WL} + q_{UWL} - \dot{m}_{SW} c_{pL}(T_{WL} - T_{SW}) - M_{WL} c_{pL}\left(\frac{\partial T}{\partial p}\right)_{sat}\left(\frac{dp_U}{dt}\right)\right], \frac{dp_U}{dt} < 0 \ . \tag{81}$$

where

$$\left(\frac{\partial T}{\partial p}\right)_{sat} = 0.37781 - 4.9170\times10^{-3} p_{WL} + 21.7623\times10^{-6} {p_{WL}}^2 \ . \tag{82}$$

If $p_{WL} < p_U, \dot{m}_{bW} = 0$.

As with bulk boiling, wall liquid boiling includes heat transfer to the wall liquid and sensible energy added to the spray liquid to increase its temperature to the wall liquid temperature.

6.4.6.3 <u>Liquid Droplet Evaporation in the Ullage</u>. Liquid droplets in the ullage start boiling once the subcooled liquid spray attains saturation. From an energy balance on the liquid droplets, an expression for the liquid droplet boiling is obtained:

$$\dot{m}_{DU} = \frac{1}{\left(h_{fg}\right)_U}\left[q_{UD} - \dot{m}_{SU} c_{pL}(T_{Usat} - T_S)\right] \ , \tag{83}$$

where

$T_{Usat} = T_{sat}(p_U)$ = ullage saturation temperature.

6.4.6.4 Liquid Spray Falling Into Bulk Liquid or Accumulating on Tank Wall. The unevaporated sprayed mass in the ullage is assumed to fall into the bulk liquid with normal gravity, or to accumulate on the tank wall with zero gravity (fig. 42); i.e.,

$$\dot{m}_{SUL} = \dot{m}_{SU} - \dot{m}_{DU} \quad \text{(for normal gravity)}$$
$$\dot{m}_{SW} = \dot{m}_{SU} - \dot{m}_{DU} \quad \text{(for zero gravity).} \tag{84}$$

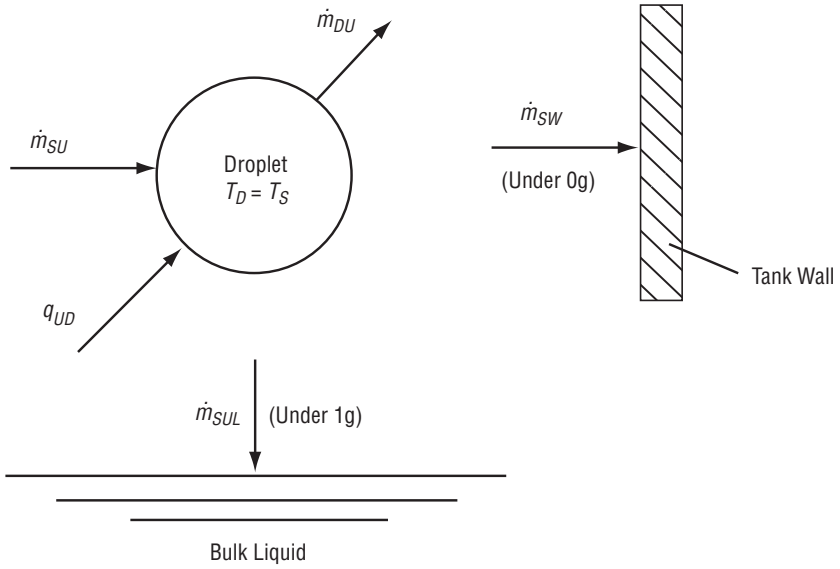

Figure 42. Droplet evaporation analytical model.

6.4.6.5 Ullage Condensation. Ullage condensation occurs whenever the ullage temperature is equal to the saturation temperature corresponding to the ullage pressure. It is the result of ullage heat removal by the liquid droplet, when there is spraying, and by the wall liquid (fig. 43):

$$\dot{m}_{UL} = \frac{q_{UD} + q_{UL} + q_{UWL}}{\left(h_{fg}\right)_U} \qquad T_U = T_{sat}(p_U) \ . \tag{85}$$

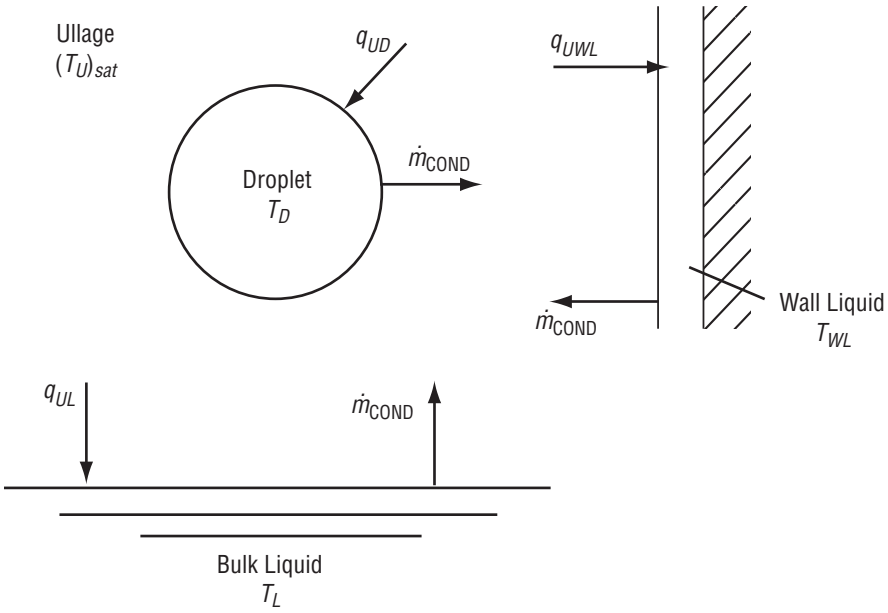

Figure 43. Ullage condensation analytical model.

6.4.6.6 <u>Liquid Surface Condensation</u>. When helium is not present to act as a barrier to mass transfer, bulk liquid mixing during pump operation induces condensation on the liquid surface. This condensation rate is controlled by the heat transfer rate from the ullage to the liquid:

$$\dot{m}_{\mathrm{COND}} = \frac{q_{UL}}{\left(h_{fg}\right)_U} \quad . \tag{86}$$

7. TEST FACILITY AND PROCEDURES

7.1 Facility Description

Testing was performed at the MSFC east test area thermal vacuum facility, test stand 300 (fig. 44). The test article and facility flow schematic is presented in figure 45. The primary vacuum chamber is cylindrical in shape and has usable internal dimensions of 5.5 m (18 ft) in diameter and 7.9 m (26 ft) in height. Personnel access is through a small side-entry door, but the chamber lid is removable for installation of large test articles (fig. 46). The chamber pumping train consists of a single-stage GN_2 ejector, three mechanical roughing pumps (rated at 140 L/s (300 ft^3/min each) with blowers rated at 610 L/s (1,300 ft^3/min each), and two 1.2-m (48-in) oil diffusion pumps rated at 95,000 L/s (200,000 ft^3/min N_2 each). LN_2 cold walls provide cryopumping and thermal conditioning capability and are comprised of five parallel zones, which totally surround the usable chamber volume with a surface emissivity of ≈0.95. The facility systems in combination with the test article shroud enable simulation of orbit environmental conditions by providing vacuum levels of 10^{-8} torr and a temperature range of 80 to 320 K (140 to 576 °R) on test article exterior surfaces.

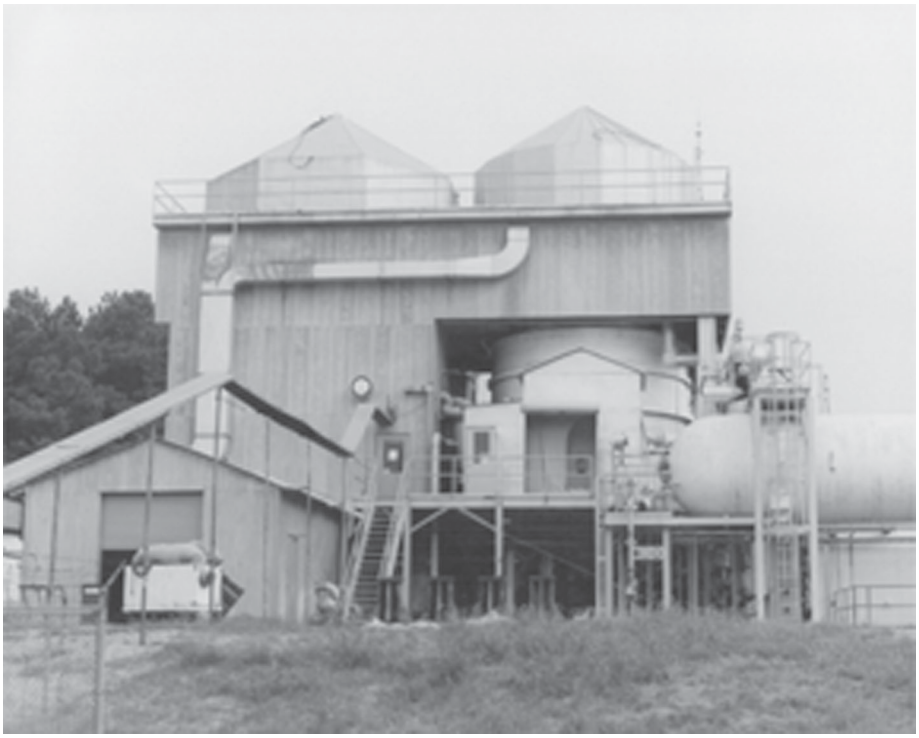

Figure 44. MSFC east test area thermal vacuum facility, test stand 300.

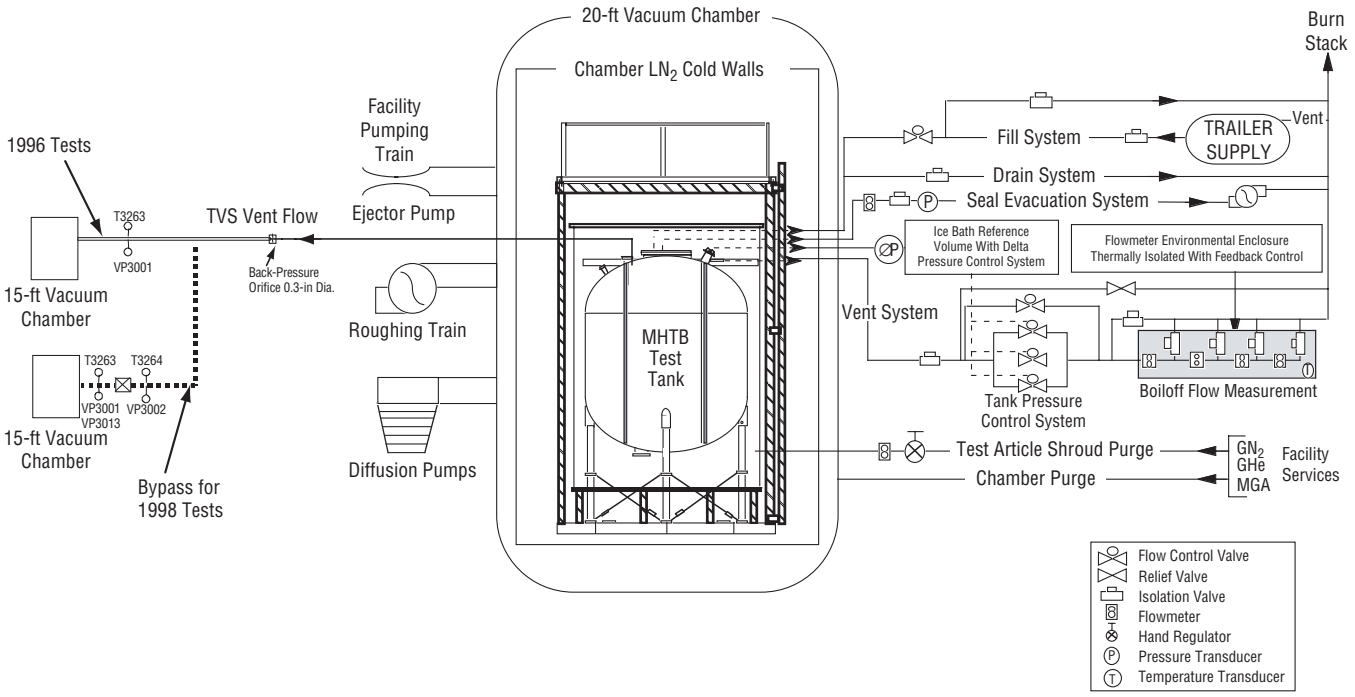

Figure 45. MHTB and test stand 300 simplified flow schematic.

Figure 46. MHTB installation in test stand 300 vacuum chamber.

A vacuum-jacketed fill and drain system provides cryogenic fluid servicing to and from the test article. All facility lines have welded construction to ensure that vacuum conditions are not compromised by leakage. During the heat leak measurement phases of the testing, conditions within the MHTB were controlled utilizing the facility subsystems described below:

- A tank pressure control subsystem maintained the MHTB ullage pressure at the required steady-state conditions. The system was composed of several flow control valves, located in the vent line, each of which was regulated through a closed-loop control system. This control loop manipulated the valve positions based on a comparison of the measured tank ullage pressure and the desired setpoint. An MKS Instruments, Inc., Baratron 0–133 kPa (0–19 psia) absolute pressure transducer (accuracy of ±0.02 percent) and an MKS ΔP transducer (1 torr or 133 Pa head with an accuracy of ±0.04 percent) located outside the vacuum chamber were used to measure ullage pressure. The system can maintain setpoints ranging from 110–124 kPa (16–18 psia) with a tolerance of ±0.00689 kPa (±0.001 psi) for the orbital simulation conditions.

- Hydrogen boiloff flow instrumentation was located in the vent downstream of the flow control valves. During orbit hold simulations, one of three mass flowmeters (MKS model 258C, Hastings model 200, and Hastings model H–3MS) was used. These meters spanned flow ranges of zero to 280 stdL/min, zero to 50 stdL/min, and zero to 1 stdL/min with accuracies of ±0.8, ±1, and ±1 percent of full scale, respectively. To minimize ambient temperature effects on measurement accuracy, the flowmeter system was placed within a containment box and equipped with a temperature-controlled purge, which maintained the box interior at constant temperature, typically 306 K (550 °R).

- A seal evacuation system—MKS model 258 with a range of zero to 1,000 $stdcm^3$/min or zero to 61 $stdcm^3$/min—captured and measured any boiloff gases leaked past the 61-cm (24-in) primary tank seal. This setup was required to prevent degradation of vacuum levels during orbit simulation and ensure boiloff measurement accuracy. The vacuum system, connected to the volume between the tank's primary and secondary seals, maintained a seal volume pressure of 133 Pa (1 torr) or less.

During TVS testing, the hydrogen vented out of the MHTB through the J-T valve and was routed into an adjacent 4.57-m (15-ft) vacuum chamber, which enabled venting into a moderate vacuum (fig. 45). Additionally, the facility and MHTB instrumentation that directly supported the TVS operation is shown in figure 47.

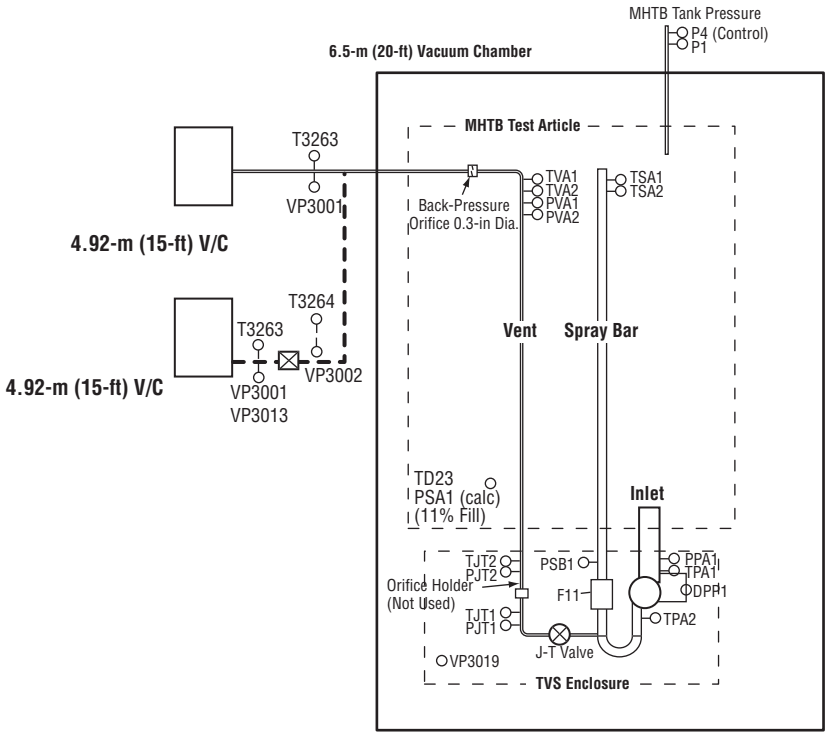

TVS Enclosure

PPA1	Pump inlet pressure (kPa/m^2)
TPA1	Pump inlet temperature (K)
DPP1	Pump delta pressure (kPa/m^2)
TPA2	Pump outlet temperature (K)
PSB1	Flowmeter pressure (kPa/m^2)
F11	Flowmeter (L/min)
TJT1	Vent line temperature (K)
TJT2	Vent line temperature (K)
PJT1	Vent line pressure (kPa/m^2)
PJT2	Vent line pressure (kPa/m^2)
VP3019	Enclosure pressure (torr)
PUP1	Pump on/off (high/low)
VAV1	Valve open/closed (high/low)

MHTB Test Article

TSA1	Spray bar liquid temperature (K)
TSA2	Spray bar liquid temperature (K)
TVA1	Vent line exit temperature (K)
TVA2	Vent line exit temperature (K)
PVA1	Vent line exit pressure (kPa/m^2)
PVA2	Vent line exit pressure (kPa/m^2)
P4	Tank ullage pressured (kPa/m^2)
P1	Tank ullage pressured (kPa/m^2)
TD23	Tank fluid temperature at 11% fill
PSA1	Calculated tank saturation pressure based on TD23

Vent

T3263	Vent line pressure 4.92-m V/C (K)
VP3001	Vent line pressure at T3263(torr); also 4.93 V/C pressure during nonventing periods
HSA17	4.92-m V/C volume temperature (K)

Figure 47. Spray bar TVS instrumentation schematic.

7.2 Test Procedures

The procedures and approaches utilized for test preparations, orbital heat leak measurement, TVS performance evaluation, and posttest operations are summarized in sections 7.2.1 through 7.2.4.

7.2.1 Pretest Operations

Prior to testing, the vacuum chamber and environmental shroud were purged at a trickle rate with dry GN_2 for ≈5 days to reduce the MLI dewpoint to acceptable levels. Prior to tanking, the environmental shroud purge ring was operated at a GN_2 flow rate of 5 kg/min (11.2 lb/min) with a dewpoint not to exceed –54 °C (–65 °F). Also, the seal evacuation system was activated and held steady

at a level of 2×10^{-2} torr or less. Approximately 2 hr prior to tanking, dry GN_2 (followed by gaseous hydrogen (GH_2)) with a dewpoint of –54 °C (–65 °F) was used for the internal purge/conditioning operations of the test tank, fill/drain line, and vent line. This purge and conditioning process was accomplished using charge-vent cycles during which the tank was pressurized to ≈103 kPa (15 psig) with GH_2, held for ≈1 min, and then vented back down to near atmospheric pressure. This sequence was typically repeated 15–20 times prior to loading LH_2 into the MHTB. The test tank is designed to withstand an internal vacuum against external atmospheric pressure enabling vacuum cycling with GH_2 pressurization, a much more efficient method of conditioning. However, the vacuum cycling approach was not implemented during this test program.

The vacuum chamber was pumped down to a steady-state vacuum level (10^{-6} torr or less) and the MLI allowed time to evacuate prior to initiating tank fill. The test article was then filled with LH_2 to the 85-percent level while maintaining the ullage pressure ≈103.4 torr (2 psi) above the required setpoint pressure. Completion of fill to the 95-percent level was then accomplished with the automated pressure control subsystem activated to control the ullage ≈25.8 torr (0.5 psi) above the setpoint. Once filling was completed, the transition to the test setpoint pressure occurred over a period of 10–20 min. Several hours were required to saturate and equilibrate the tanked LH_2 at the setpoint pressure.

7.2.2 Tank Heat Leak Testing

Boiloff testing was conducted to determine the ambient heat leak into the MHTB tank and to set up consistent initial conditions for each of the TVS tests. The first test series (series 1) was conducted with the vacuum chamber LN_2 cold walls operating to produce a minimum heat leak condition. The second series (series 2) was conducted without the LN_2 cold walls, thereby providing a high ambient heat leak condition and reducing test costs. Also, additional hardware (an axial jet mixer/TVS system), was installed, which also added heat leak in the second series. The heat leak test procedures are summarized herein and further details are presented in reference 1.

Steady-state vacuum and thermal conditions, within both the chamber and MLI, were achieved before the on-orbit heat leak test phase. The four criteria that had to occur simultaneously for steady-state thermal conditions were as follows:

(1) Interstitial MLI pressures had to be 10^{-5} torr or less to preclude a transient convective heat transfer effect as the insulation pressure continues to drop. A vacuum chamber pressure of 10^{-6} torr or less was required to ensure an adequate vacuum within the insulation.

(2) Insulation temperatures (MLI and SOFI) had to be in a steady-state condition with the MLI surface temperature at the prescribed setpoint (305 K for the TVS testing) imposed by the environmental shroud. Insulation equilibrium was assumed to exist once temperature transients of no more than 0.55 K in 6 hr are measured in any section of the insulation system.

(3) Thermal equilibrium of the LH_2 had to be maintained through precise ullage pressure control during the low heat leak orbital simulation. Ullage pressure was maintained at a setpoint in the range of 110.316 to 124.106 kPa (16 to 18 psia) with a tolerance of ±0.00689 kPa (±0.001 psi). In the TVS testing, the boiloff rate was recorded for 6 hr after steady state was achieved.

(4) The vented ullage gas temperature had to increase with time (positive slope), indicating that the tank dome was in thermal equilibrium; i.e., the dome was no longer cooling and contributing to the vented gas enthalpy.

When performing the heat leak cryogenic storage testing, either a loss of ullage pressure control or the chamber vacuum can significantly increase unproductive test time. Each 6.89 kPa (1 psi) of LH_2 subcooling, due to a sudden reduction in ullage pressure, requires 30 hr for recovery to saturation, due to the low heat leak conditions. Similarly, a sudden increase in vacuum chamber pressure (10^{-4} torr or above) can dramatically alter the MLI temperatures, necessitating several days to recover the steady-state temperature profile. Therefore, great care was taken to ensure tight control of the tank ullage and vacuum chamber pressures.

An RGA (residual gas analyzer) system was used to record vacuum chamber and MLI interstitial gas composition periodically during steady-state simulated orbit hold periods. RGA sampling intervals varied depending on the vacuum chamber pressure stability and assisted in determining the source of any chamber pressure variations; e.g., test article or chamber leakage, or outgassing. Species possibilities included H_2O, N_2, O_2, CO_2, and the foam-blowing agent CFC–11 (CCL_3F molecular weight of 137.4).

7.2.3 Thermodynamic Vent System Performance Testing

The TVS spray bar was evaluated at MHTB tank fill levels of 90, 50, and 25 percent. As mentioned earlier, two test series were conducted—series 1 with a low heat leak condition and series 2 with an elevated heat leak. For each fill level, after the heat leak testing was completed, the tank was locked up and allowed to self-pressurize until the ullage pressure attained the maximum tank pressure setpoint of 138 kPa (20 psia). Upon reaching this pressure, the recirculation pump was turned on and mixing continued until the ulllage pressure reached 131 kPa (19 psia), the minimum setpoint. After the pump was turned off at the minimum setpoint, the tank was allowed to self-pressurize and the cycle began again. As depicted in figure 14, this automated operation cycle continued until the bulk liquid saturation condition (PSA1) attained the lower setpoint. The J-T vent valve was then opened and the spray bar heat exchanger utilized to extract thermal energy from the tank contents. Thereafter, the J-T valve was opened each time the pump cycled on and the spray bar heat exchanger was used to extract thermal energy from the bulk liquid.

As described in section 2.4, a liquid temperature sensor was used to monitor the bulk liquid saturation conditions relative to the measured ullage pressure and as inputs to the TVS controller. The sensor, TD23, is at the 11.5-percent fill level or 53.3 cm (21 in) above the tank bottom and is considered to be representative of the bulk liquid temperature. The TD23 temperature output was converted to an equivalent saturation pressure (termed PSA1) and compared with the ullage pressure, P4.

Most of the TVS testing was conducted with a GH_2 ullage; however, helium pressurization is frequently considered to provide appropriate conditions for engine restart sequences. Furthermore, the amount of GHe could increase with each pressurization cycle since primarily GH_2 is vented through the TVS in multiple engine restart missions. The partial pressure effects of the GHe would be expected to influence the number and duration of the TVS cycles. Therefore, at the end of the second test series, GHe was injected into the ullage and the effects of a noncondensable gas on TVS performance were evaluated.

7.2.4 Posttest Operations

Chamber repressurization conditions after the TVS tests were selected primarily to protect the test article and facility. Also, following a test, the MHTB was not held under vacuum conditions for needlessly long periods. The chamber and test article were warmed and repressurized within 8–12 hr after testing was concluded. Chamber repressurization occurred slowly (≈30 min) with dry GN_2 (dew-point –54 °C (–65 °F)) in the 4–27 °C (40–80 °F) temperature range. To prevent water condensation, repressurization was initiated only after the vacuum chamber cold walls and all test article insulation (SOFI/MLI) had reached ≈15.5 °C (60 °F). The dry GN_2 was also used to accomplish purge and inerting operations for the test article volume and all service lines. These operations were designed so that the test article was not subjected to a positive differential pressure in excess of 344 kPa (50 psid). Typically, the GN_2 shield purge remained on for 24 hr after completion of testing.

8. TEST RESULTS

8.1 Tank Heat Leak Data Reduction

As mentioned earlier, boiloff testing was conducted to determine the heat leak into the MHTB tank and to establish consistent conditions prior to each of the two TVS test series. During the heat leak test periods, digital data were recorded at sample rates ranging from 1 to 0.017 Hz. These raw data were then time averaged over the steady-state period of interest to obtain measurement values required to calculate thermal performance. The heat input was expressed as an energy balance across the tank boundary by equating the total measured boiloff with the sum of heat flow through the insulation, the penetrations, and the rate of energy storage, if any:

$$\dot{Q}_{\text{boiloff}} = \dot{Q}_{\text{insulation}} + \dot{Q}_{\text{conduction}} + \frac{\Delta U_{\text{system}}}{\Delta t} \quad . \tag{87}$$

The terms $\dot{Q}_{\text{boiloff}}$ and $\dot{Q}_{\text{conduction}}$ were defined using the measured test data. The thermal storage term $\frac{\Delta U_{\text{system}}}{\Delta t}$ (energy flow into or out of the test tank wall, insulation, and fluid mass) is driven by the fluid saturation temperature which varies as ullage pressure fluctuates. The storage term was eliminated since the ullage pressure was maintained within a tight control band about the setpoint ($\pm 9 \times 10^{-4}$ kPa). The insulation performance term, $\dot{Q}_{\text{insulation}}$, could then be determined from the other measured quantities.

The $\dot{Q}_{\text{boiloff}}$ term represents the total energy vented as boiloff and includes both the evaporated fluid latent heat and the sensible heat absorbed while the vented gas passes through the ullage space, also known as ullage superheat:

$$\dot{Q}_{\text{boiloff}} = \dot{m} h_{fg} \left(\frac{\rho_{\text{satliq}}}{\rho_{\text{satliq}} - \rho_{\text{satvap}}} \right) + \dot{m} \left(h_{\text{vent}} - h_{\text{satvap}} \right) \quad . \tag{88}$$

The latent heat term of the above equation contains a density ratio that accounts for the increased volume of gas, and hence remaining energy, resulting from the decrease in liquid volume due to boiloff losses.

The solid conduction term, $\dot{Q}_{\text{conduction}}$, represents the heat flow through the tank support legs, vent assembly, and other fluid lines. Solid conduction was evaluated by using the Fourier heat transfer equation (ref. 8) with known structural geometry, material properties, and a measured temperature difference as follows:

$$\dot{Q}_{\text{conduction}} = \left(\frac{A}{L}\right) \int_{T_{\text{cold}}}^{T_{\text{hot}}} k(T)dT \ . \tag{89}$$

The heat input through the insulation, $\dot{Q}_{\text{insulation}}$, was then assessed using experimental data, fluid properties, and the assumption that energy storage in tank material and fluid are defined as follows:

$$\dot{Q}_{\text{insulation}} = \dot{Q}_{\text{boiloff}} - \dot{Q}_{\text{conduction}} \ . \tag{90}$$

8.2 Tank Heat Leak

The results from the heat leak (boiloff) testing are presented in table 2 for the three fill levels utilized in the TVS testing (90, 50, and 25 percent). As expected, the heat leak was slightly less with reduced fill levels. The high heat leak series 2 testing (51–54 W) was ≈2.7 times greater than in the low heat leak series 1 (19–20 W) due to the installation of additional hardware for testing of an axial jet mixer, and because the vacuum chamber LN_2 cold walls were not operated. As one would expect, increasing the heat leak had a significant influence on the vent cycle operation, which is described in section 8.3.

Table 2. Measured MHTB tank heat leak.

Fill Level (%)	Low Heat Leak Test, Series 1 (W)	High Heat Leak Test, Series 2 (W)
90	20.2	54.1
50	18.7	51.0
25	18.8	–

8.3 Thermodynamic Vent System Performance

The TVS was evaluated at 90-, 50-, and 25-percent fill levels in the first test series with low heat leak and at 90- and 50-percent fill levels in the second series with the high heat leak condition. Test results involving destratification, energy extraction, and the presence of noncondensible gases are discussed in sections 8.3.1 through 8.3.4.

8.3.1 Destratification and Pressure Control

Both the low and high heat leak test data confirmed that the spray bar was effective in destratifying both the ullage and liquid for all conditions. The mixer durations for the entire range of conditions tested are presented in table 3. Generally, the mixing durations were shorter when venting occurred due to the heat extraction effect. Also, the mixing durations clearly increased with decreasing fill level at the low heat leak with venting conditions. However, the data at the high heat leak condition were less consistent, and are believed to be due to sometimes erratic J-T valve operation coupled with limited test durations at given conditions. For all tests, the mixer cycle durations ranged from 43 to 535 s, depending on the test conditions. The mixer durations prior to the initiation of venting gradually

increased with time after lockup due to the increasing saturation pressure/temperature. For example, at the 90-percent fill level, the mixer operation duration per cycle increased from 134 s at the beginning to 535 s at the time just prior to the initiation of venting. Representative times between mixing cycles, with and without venting, are listed in table 4. With the low heat leak, the time interval between cycles increased from 57 min at 90-percent fill level to 173 min at 25-percent fill level; i.e., increased with increasing ullage size. With the high heat leak condition, the time between cycles was 25 and 83 min at 90- and 50-percent fill, respectively. In summary, the trends with the low heat leak condition are more reliable and once the J-T venting began, the average TVS duty cycle ranged from 1.25 percent at 90-percent fill level to 1.5 percent at 25-percent fill level.

Table 3. Representative mixing cycle durations.

Fill Level (%)	Tank Heat Leak (W)	Mixing Duration (s)	
		With Venting	Without Venting
90	20.2	43	134–535
50	18.7	71–89	111*
25	18.8	89–167	–
90	54.1	144**	120–470
50	51.0	97*	42–78

* Limited Data Available
** J-T Valve Operated Intermittently

Table 4. Representative times between mixing cycles.

Fill Level (%)	Tank Heat Leak (W)	Minutes Between Mixing Cycles	
		With Venting	Without Venting
90	20.2	57	80–96
50	18.7	145	158
25	18.8	173	–
90	54.1	25	32
50	51.0	83	70

Example temperature-time stratification data for the 50-percent fill level, low heat leak condition is presented in figure 48. Note that the percentages listed with each silicon diode designation represent the fill level corresponding to that sensor position. As expected, during tank lockup, the ullage became significantly stratified. Upon mixer startup, both the liquid and gas temperatures were reduced to within 0.4 K of each other within 86 s.

The preceding results are significant since buoyancy effects impede mixing in normal gravity. In zero gravity, the spray bar would be an even more efficient ullage mixer since there would be no significant gravitational force to pull the sprayed fluid out of the ullage. Also, due to the absence of buoyancy forces within the liquid, liquid mixing would be more effective. The spray bar is also effective in chilling down warm tank walls regardless of propellant position, which would be beneficial in tank fill operations. For example, during the 50-percent fill test illustrated in figure 48, the tank dome cooled ≈2 K during spray bar operation.

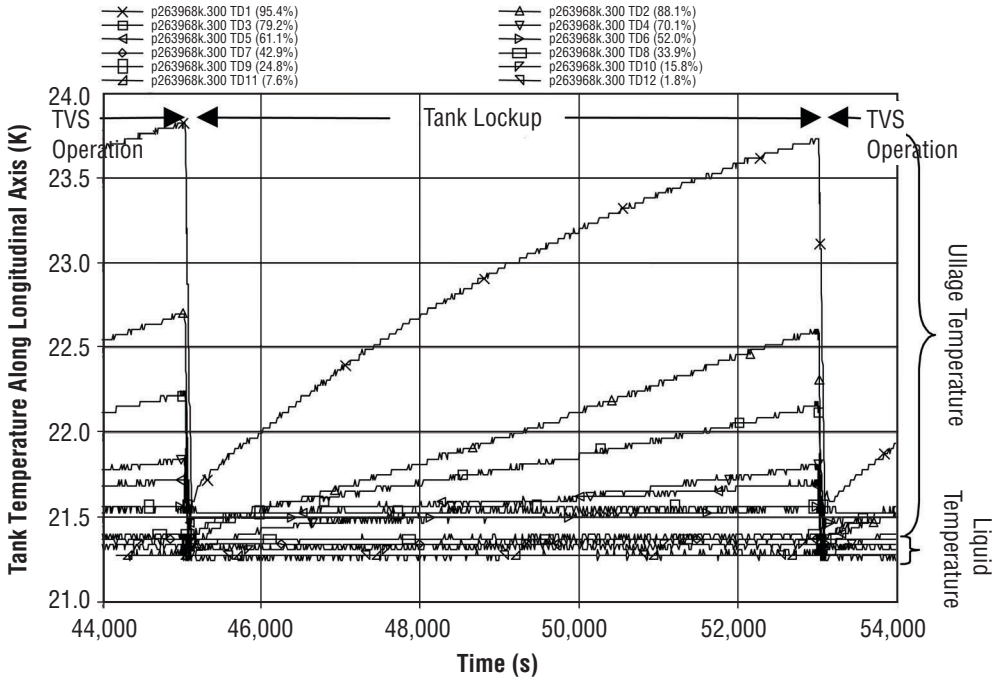

Figure 48. Tank stratification/destratification, 50-percent fill level during series 1.

8.3.2 Liquid Saturation Pressure Rise Rates

As mentioned earlier, tank mixing alone is sufficient to maintain pressure control until the thermal energy absorbed by the propellant increases the saturation pressure to the lower limit of the TVS control band. The rate of increase in liquid saturation pressure is summarized for all test conditions in table 5. This gradual increase in saturation pressure (indicated as PSA1) for the low heat leak series 1 testing is illustrated in figures 49–51 for fill levels of 90, 50, and 25 percent, respectively. For example, in the 90-percent fill test, the propellant was saturated at a pressure level of 112 kPa when the tank was locked up and ≈61 hr or 2.5 days elapsed before the saturation pressure increased to the lower vent control limit of 131 kPa and venting began. In the 50-percent fill test tank, lockup occurred with the tank saturated at 122 kPa and ≈33 hr or 1.4 days elapsed before the lower vent control limit of 131 kPa was reached. At the 25-percent level, the saturation pressure started at 122 kPa, and 19.4 hr or 0.81 days elapsed before the lower limit of 131 kPa was reached. Thus, the low heat leak saturation pressure rise rates were ≈0.3 kPa/hr at the 90- and 50-percent fill levels and ≈0.50 kPa/hr at 25-percent fill. Although the low heat leak magnitude varied only slightly with fill level, the saturation level increased much more rapidly at the 25-percent level due to the relatively low liquid mass available to absorb the thermal energy. Also, as illustrated in figure 51, there apparently is a minimum liquid level below which tank mixing alone will not reduce tank pressure beginning with the first mixing cycle; i.e., both the pump and J-T valve begin operation simultaneously.

The high heat leak effects on pressure rise rates are also shown in table 5. The high heat leak saturation pressure rise rates were 2.9 and 3.1 times as fast as in the low heat leak tests at the 90- and 50-percent fill levels, respectively. Since the high heat leak series was ≈2.7 times that in low heat leak series, the relative pressure rise rates are reasonable.

Table 5. Liquid saturation pressure rise rates after tank lockup.

Fill Level (%)	Tank Heat Leak (W)	Liquid Saturation Pressure Rise Rate (kPa/hr)
90	20.2	0.31
50	18.7	0.29
25	18.8	0.50
90	54.1	0.89
50	51.0	0.96

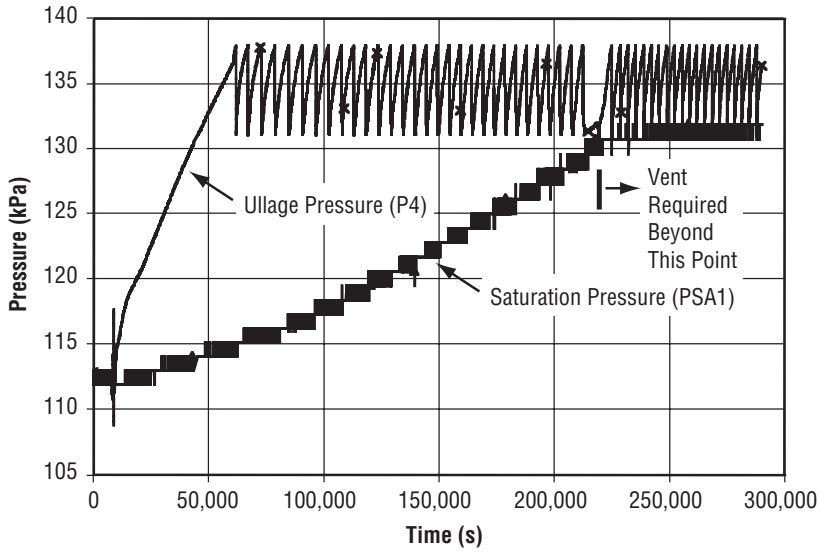

Figure 49. Spray bar performance at 90-percent fill level during series 1.

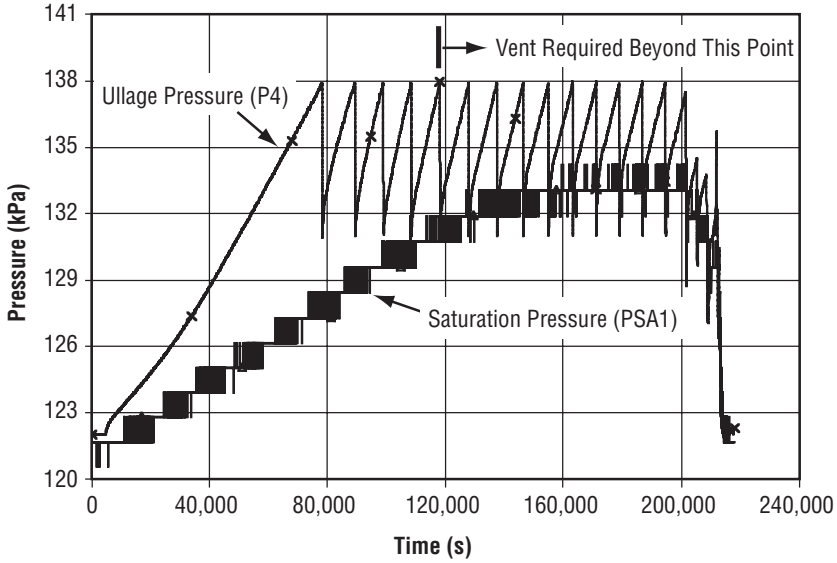

Figure 50. Spray bar performance at 50-percent fill level during series 1.

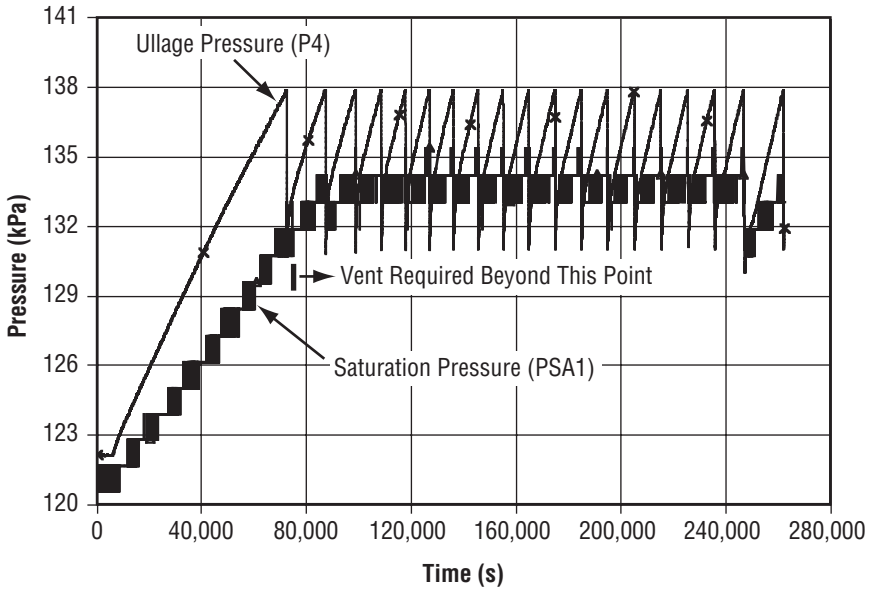

Figure 51. Spray bar performance at 25-percent fill level during series 1.

8.3.3 Heat Energy Extraction

The most important measure of TVS performance is the capability to extract thermal energy from the propellant. Once the propellant is saturated at the lower limit of the TVS pressure control band, the TVS must begin to extract enough energy to offset the tank heat leak into the tank and maintain pressure control. The heat extracted by the vent flow was calculated or derived from the test data using the following equations:

$$\dot{Q}_{\text{vent}} = \dot{m}_{\text{vent}}(h_{\text{out}} - h_{\text{in}})$$

$$\dot{Q}_{\text{ave}} = \dot{Q}_{\text{vent}}\left(\frac{t_{\text{open}}}{t_{\text{total}}}\right), \tag{91}$$

where

$\dot{Q}_{\text{vent}}$ = energy extraction rate while the vent is open
$\dot{m}_{\text{vent}}$ = vent mass flow rate
h_{out} = TVS outlet enthalpies
h_{in} = TVS inlet enthalpies.

Given the TVS duty cycle interval (valve open time, t_{open}, divided by the sum of valve open plus valve closed time or t_{total}) for a particular test, the average value of vent heat extraction ($\dot{Q}_{\text{ave}}$) could be computed for each test and enabled a comparison of TVS performance from test to test. The vent mass

flow rate was calculated using the compressible flow equation for a gas through a sonic orifice (the back-pressure orifice) as follows:

$$\dot{m}_{\text{vent}} \frac{0.14(CdA)p}{\sqrt{T}} \quad , \tag{92}$$

where

T = orifice inlet temperature
p = orifice inlet pressure
CdA = effective orifice flow area.

The assumption that gas was flowing through the back-pressure orifice was verified with the test data which indicated that the heat exchanger completely vaporized the two-phase mixture exiting the J-T valve; i.e., measured inlet temperature at the orifice was always well above tank saturation temperature corresponding to the pressure. Table 6 summarizes the average heat extraction rates for all testing conducted. When comparing the derived heat extraction ($\dot{Q}_{\text{ave}}$) values to the tank heat leak for the same test (table 2), the $\dot{Q}_{\text{ave}}$ value is 7- to 21-percent lower than the corresponding tank heat. In reality, the thermal energy removed by the TVS equaled the heat leak into the tank. Otherwise, the tank pressure would not have remained within the prescribed pressure control band and the liquid saturation pressure would have continued to rise.

Table 6. Derived TVS heat extraction data.

Test Series	Fill Level (%)	$\dot{Q}_{\text{vent}}$ (W)	$\dot{Q}_{\text{ave}}$ (W)	$\dot{m}_{\text{vent}}$ (kg/s)
1	90	1,444	15.9	0.0034
1	50	1,486	16.3	0.0035
1	25	1,507	17.5	0.0036
2	90	*	*	*
2	50	2,108	40.6	0.0048

* Hardware problem; not enough J-T cycles to calculate heat extracted

Potential sources for the difference between the derived TVS heat extraction rate and the measured tank heat leak were investigated. One source considered, but ruled out, was instrumentation uncertainties. The error in measured quantities would have to have been much larger than the instrumentation uncertainties to yield the additional enthalpy necessary to increase the derived heat extraction rate to the measured tank heat leak. The most likely candidate involved the method of calculating vent mass flow rate, $\dot{m}_{\text{vent}}$. As seen from table 6, the vent mass flow rate was extremely small, averaging ≈0.0035 kg/s for the low heat leak series 1 tests; a gain of only ≈0.0009 kg/s would eliminate the delta between the ambient heat leak and the derived TVS heat extraction values. The equation for mass flow rate is extremely sensitive to the magnitude of CdA, and to the coefficient,

C=0.14, which was actually calculated from the ratio of specific heats and other terms in a more general form of the compressible flow equation. Thus, the differences between the tank heat leak and the TVS heat extraction are most likely due to the computational sensitivity of the extremely small mass flow rate.

Propellant conditioning, such as reducing the saturation pressure, could prove useful in increasing propellant storage durations and improving on-orbit propellant transfer efficiencies in future applications. Therefore, an additional test at the 25-percent fill level was conducted to evaluate the ability of the TVS to reduce the saturation conditions of the bulk LH_2 by continually extracting thermal energy. In this case, the J-T valve was allowed to remain open and the mixer operated continuously for 118 min, which reduced the saturation conditions from 133 to 70 kPa (19.3 to 10 psia) in 118 min (fig. 52). About 25.5 kg (56 lb) of vented LH_2 were required to achieve the saturation pressure reduction.

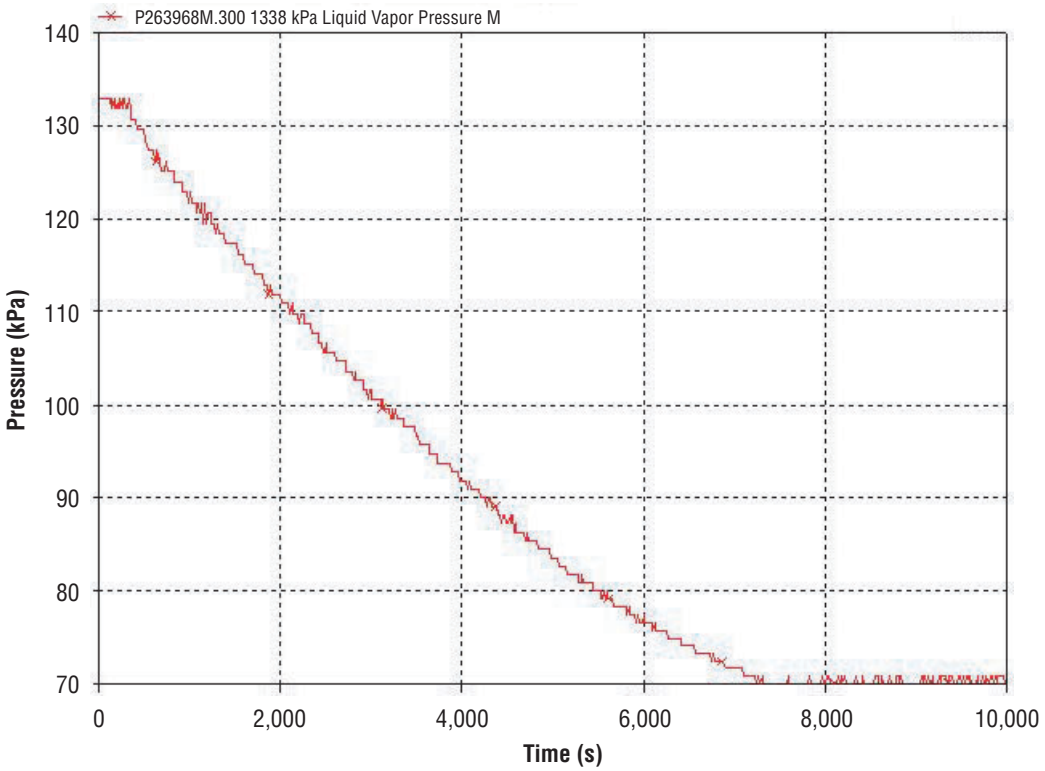

Figure 52. Bulk liquid saturation pressure reduction at 25-percent fill level.

8.3.4 Helium Pressurization Gas Effects

In a multiple engine restart scenario, for example, the GHe quantity in the ullage can increase with the number of prepressurization cycles performed, since only vaporized hydrogen is vented whenever liquid is at the TVS pump inlet. Additionally, GHe is frequently considered for hydrogen expulsion in orbital propellant transfer scenarios. Therefore, limited testing was conducted to evaluate the spray bar TVS performance with a noncondensable gas, GHe, in the ullage. Testing with helium was first attempted during the series 1 low heat leak testing at the 25-percent fill level; however, J-T valve

plugging occurred due to small amounts of moisture within the facility-provided GHe and testing was terminated. Subsequently, the GHe was dryed prior to injection into the MHTB and GHe pressurization testing was repeated during the series 2 testing.

It is estimated that there was ≈9.3 kg (20.5 lbm) of GHe in the ullage during the series 2 test, which was conducted at the 50-percent fill level and with a heat leak of 51 W. The injected GHe initially elevated the ullage pressure to above the upper control limit of 213 kPa. Then the ullage was vented to the lower pressure control limit of 206.84 kPa whereupon the tank was locked up and testing began. At this point, the tank liquid was saturated at ≈165 kPa (24 psia) and the helium partial pressure was ≈43 kPa which resulted in the total pressure of 206.8 kPa. After the tank self-pressurized to an upper setpoint of 213.7 kPa, the mixer cycled on. As can be seen in figure 53, the mixer operated alone until the ullage pressure decay slope became positive, at which point the J-T valve was manually opened to further reduce the tank pressure.

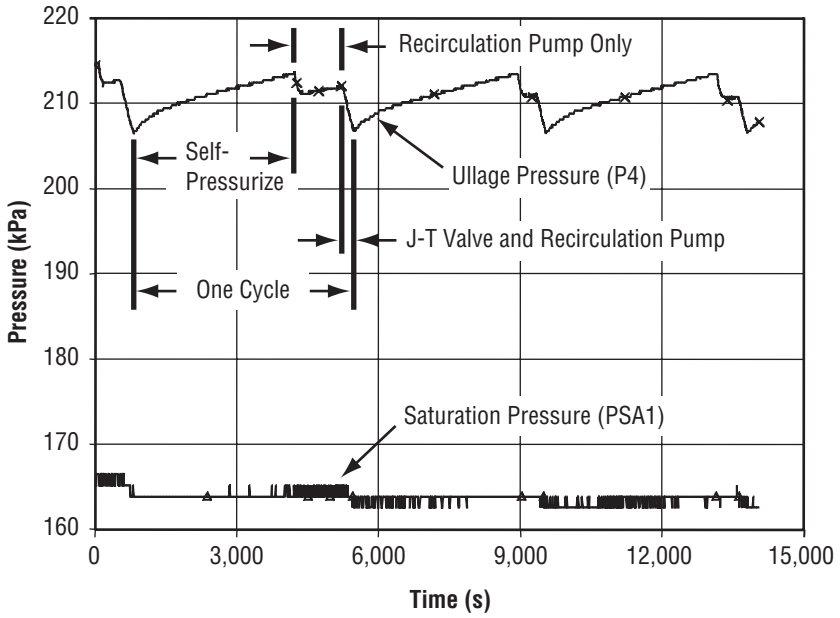

Figure 53. TVS operation cycles with GHe in ullage, 50-percent fill level during series 2.

It was apparent that mixing alone could not reduce the pressure below ≈211 kPa. Since the mass of helium remained constant throughout the vent/mixing cycles, the helium and hydrogen partial pressure to total pressure ratios also remained constant (Dalton's Law). Therefore, an error in injected helium mass or in helium partial pressure could not have been a factor in the incomplete pressure reduction during the mixing-only phase. Thus, it was concluded that the helium presence constrained the energy exchange between the sprayed hydrogen droplets and the ullage, thereby reducing condensation. Furthermore, the density of GHe is about twice that of hydrogen and ≈10 hr were required after initial helium injection to establish the initial conditions. Hence, it is believed that helium, with its larger than hydrogen density (factor of 2 larger), settled on the liquid-vapor interface and significantly reduced the mass and energy exchange between the ullage and bulk LH_2 (see sec. 6.4.6.6). Only when the J-T vent valve was used to inject cooler hydrogen into the ullage did condensation continue and a further

reduction in ullage pressure occurred. Furthermore, it was noted that the pressure reduction magnitude with the mixing-only phase became slightly more effective with each of the subsequent two cycles. Thus, the trend was toward more effective mixing with each succeeding cycle, and it is possible that the pressure leveling-off effect would have eventually disappeared with more mixing cycles. However, since test time was limited for this phase of testing, insufficient data exist to validate definite conclusions.

As expected, the presence of helium increased the mixing duration, but quantitative observations must be qualified due to the limited test duration. The time for TVS one cycle averaged ≈63 min with a self-pressurization time of ≈58 min. The mixer operated an average of 187 s before the pressure reduction leveled off, and then the mixer/J-T combination period averaged 129 s. The leveling-off duration varied since it was manually controlled, and therefore is not included in the total duty cycle time; this would be automated in a flight application. Thus, the mixer duty cycle was ≈9 percent and the J-T duty cycle ≈3.7 percent of the total cycle period.

It can be concluded from the helium testing that the spray bar TVS maintained the tank ullage pressure within a prescribed control band with helium pressurant. However, changes in the automated control system logic would be necessary to accommodate the presence of helium in future testing or applications. Further testing is required to ascertain the effects of helium on TVS performance; however, it is expected that the effects in reduced gravity would be less since helium settling on the liquid-vapor interface would not occur.

8.4 Test Facility and Hardware Performance

Overall, the test facility performed very well, especially during the critical orbital simulations. For the low heat leak series 1 tests, the vacuum chamber pressure was maintained in the low 10^{-6} torr range with LN_2 cold walls engaged. During the high heat leak series 2 testing, the vacuum level was in the low 10^{-5} torr range without the cold walls operating. During each of the two test series, the warm boundary temperatures on the MLI surfaces were successfully controlled to 305 K by the environmental shroud. The facility back-pressure control system was especially effective in maintaining the tight ullage pressure control requirements during the tank heat leak testing and controlled ullage pressures to within ±0.00689 kPa (0.001 psi) of the setpoint. During testing with TVS venting into the adjacent 4.6-m-(15-ft-) diameter vacuum chamber, the 4.6-m chamber maintained pressure levels below 75 torr (1.4 psia).

The MHTB continuous liquid level capacitance probe served as a guide for determining propellant level; however, the silicon diode sensors on the instrumentation rake became the primary means for determining liquid level and ullage volume. Several TVS transducers failed during the second test series and somewhat compromised the data analyses. Specifically, both pressure transducers (PVA1 and PVA2) upstream of the back-pressure orifice, a vent line temperature, TJT2, and PJT1, a vent line pressure, failed. Erratic J-T valve operation compromised test results on two occasions; i.e., stuck open for a few seconds on one test and remained open on another, necessitating test termination. During one test instrumentation noise or false signal spikes on the bulk temperature sensor (TD23) caused the control system to briefly activate the J-T vent valve. A more reliable valve is recommended for future testing and component redundancy would be necessary in an actual flight application.

9. THERMODYNAMIC VENT SYSTEM ANALYTICAL MODEL CORRELATIONS

As mentioned previously, eight TVS tests were performed with various test conditions. Using the previously described analytical model (sec. 6) correlations with the measured ullage pressure and temperature and with the bulk liquid saturation pressure and temperature were developed for the eight test segments presented in table 7. Correlations for seven representative test segments are presented in figures 49 through 73 and discussed below. The remaining test segment is discussed in appendix C. Further details regarding analytical modeling correlations with the test data are reported in reference 9.

Table 7. TVS test conditions compared with analytical model.

Ullage	Fill Level (%)	Heat Leak (W)	Year, Test No.	Discussion
GH_2	90	20.2	1996, P263968E,F	Section 9.1
GH_2	90	20.2	1996, P263968G	Section 9.1
GH_2	50	18.7	1996, P263968K	Section 9.1
GH_2	25	18.8	1998, P263968L	Section 9.1
GH_2	90	54.1	1998, P263981D	Section 9.2
GH_2	50	51.0	1998, P263981T	Section 9.2
GH_2 and GHe	50	51.0	1996, P263981X	Section 9.2
GH_2	90	54.1	1998, P263981E	Appendix C

9.1 Series 1, Low Heat Leak Tests

Analytical correlations for segments from all four of the series 1 tests were performed. Test segments discussed herein include P263968E, P263968F; P263968G; P263968K; and P263968L. In each case the upper and lower tank pressure control limits were 137.9 kPa (20 psia) and 131 kPa (19 psia), respectively, and the vent flow rates ranged from 0.0036 to 0.0034 kg/s. All analytically modeled periods were initialized using measured conditions.

9.1.1 Test Segments P263968E and P263968F—Self-Pressurization and Mixing, 90-Percent Fill Level

Correlations for self-pressurization and mixing were performed using test segments P263968E and P263968F, with a 90-percent fill level and 20.2-W tank heat leak. Results are presented in figures 54–57 for the ullage pressure, ullage temperature, bulk liquid saturation pressure, and bulk liquid saturation temperature, respectively. As illustrated in figure 54, tank lockup occurred at 2.2 hr (8,000 s) and the long-term self-pressurization proceeded until the mixing cycles began and continued throughout the remainder of the test segment without venting. The model is in good agreement with the test data in the early stages of self-pressurization after tank lockup at 111.5 kPa (16.2 psia); however, the analytical pressure begins to deviate after ≈1.7 hr (at 14,000 s) and rises more rapidly than the measured values. The computed and measured ullage pressures reached the upper pressure limit of 137.9 kPa (20 psia)

Test and Model Conditions

- 90% Fill, GH_2 Ullage
- Test and Model: No Venting
- Tank Heat Leak: 20.2 W
- P4 Upper Limit: 137.9 kPa
- P4 Lower Limit: 131.0 kPa

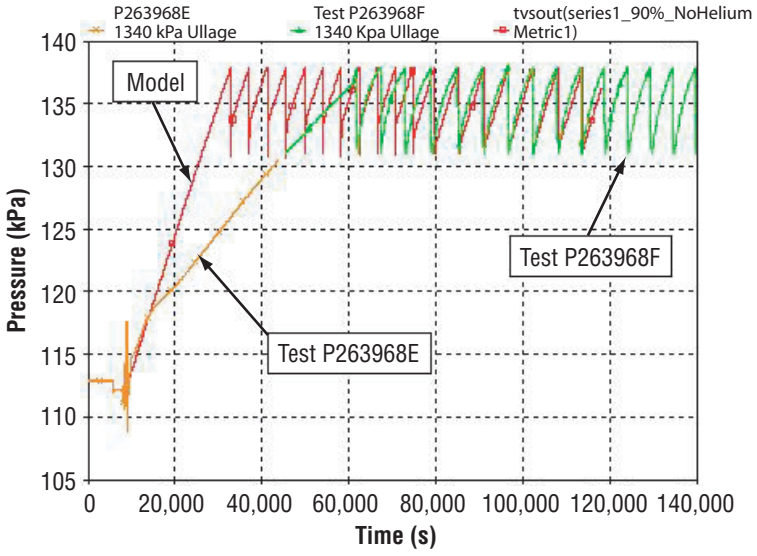

Figure 54. Ullage pressure modeling comparison with 1996 tests P263968E and P263968F—self-pressurization and mixing with 90-percent fill.

after ≈6.8 hr (at 32,500 s) and 14.7 hr (at 61,000 s), respectively. It is believed the analytical modeling, which assumes that the liquid and ullage are each represented by a single node, did not simulate the complex energy exchange that actually occurred at the liquid-vapor interface. Examination of modeled ullage pressure rise rate sensitivity to various parameters suggested that mass was added to the ullage across the liquid-vapor interface beginning at 14,000 s into the test, whereas the model assumed that thermal energy continued to be added at a constant rate with no mass addition. Thus, during the test, the low-temperature mass transfer across the liquid-vapor interface began to suppress the ullage pressure rise rate, whereas the modeled energy transfer and pressure rise rate remained relatively constant. Therefore, the analytical pressure rise rate after tank lockup is conservative relative to the measured data, and the modeled mixing cycles began earlier.

With mixing, the stratification effects are minimized and the energy exchange across the liquid surface is more predictable during the relatively short self-pressurization periods (≈40 min) between mixing cycles. Therefore, once the mixing and pressure rise cycles began, the analytical and measured data closely matched; however, it was noted that the measured pressure rise rates were slightly steeper than analytically modeled, whereas the pressure reduction rates were practically identical. Consequently, the measured cycle rate was ≈11 percent higher; i.e., one cycle per 1.34 hr (0.75 cycles/hr) and 1.49 hr (0.67 cycles/hr) occurred with the test and model data, respectively.

The analytical and measured ullage temperatures are presented in figure 55. Since the mixing cycles began earlier with the analytical model, the test data initially indicates higher ullage temperatures. However, after mixing began in the test, good agreement between the modeled and measured data was achieved. The bulk liquid saturation pressure and temperature correlations, presented in figures 56 and 57, respectively, indicate higher temperatures and pressures with the model. The calculated bulk liquid saturation conditions exceeded the measured pressures and temperatures by up to 15 kPa (2.2 psia) and 0.45 K, respectively. These temperature and pressure differences, however, were not factors in the pressure rise rate correlations.

Test and Model Conditions

- 90% Fill, GH_2 Ullage
- Test and Model: No Venting
- Tank Heat Leak: 20.2 W
- P4 Upper Limit: 137.9 kPa
- P4 Lower Limit: 131.0 kPa

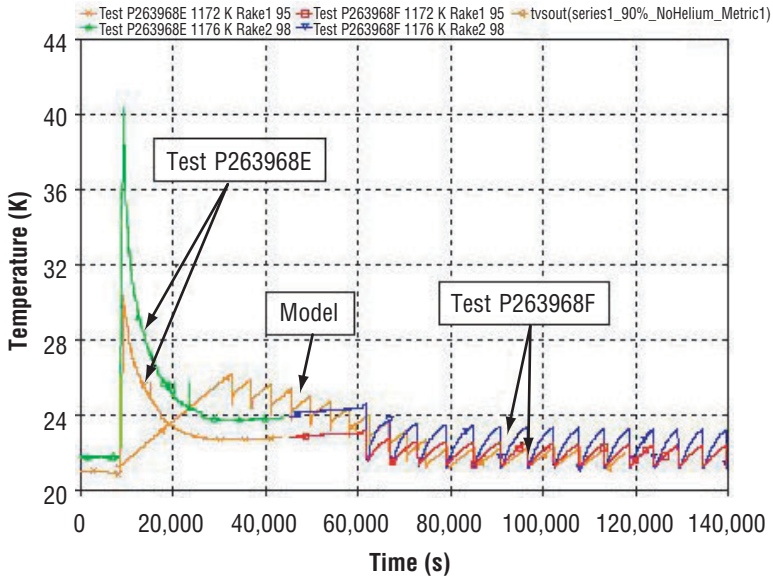

Figure 55. Ullage temperature modeling comparison with 1996 tests P263968E and P263968F—self-pressurization and mixing with 90-percent fill.

Test and Model Conditions

- 90% Fill, GH_2 Ullage
- Test and Model: No Venting
- Tank Heat Leak: 20.2 W
- P4 Upper Limit: 137.9 kPa
- P4 Lower Limit: 131.0 kPa

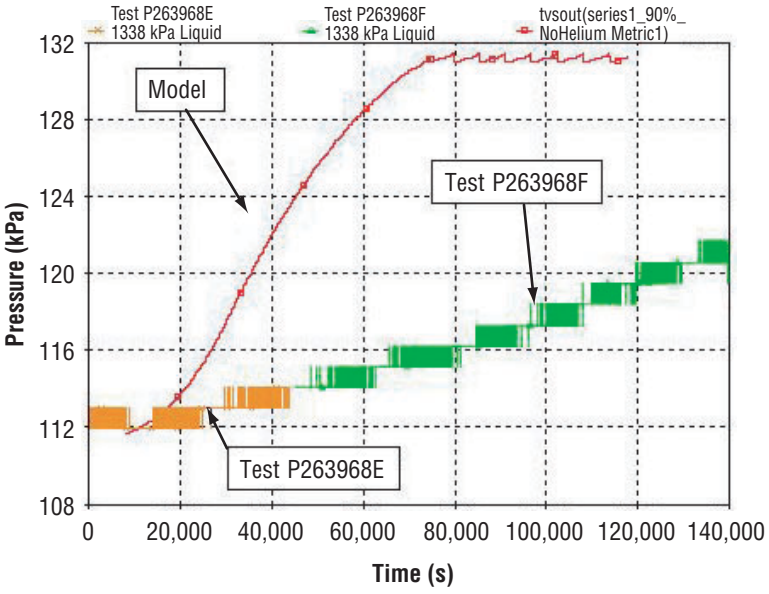

Figure 56. Bulk liquid saturation pressure modeling comparison with 1996 tests P263968E and P263968F—self-pressurization and mixing with 90-percent fill.

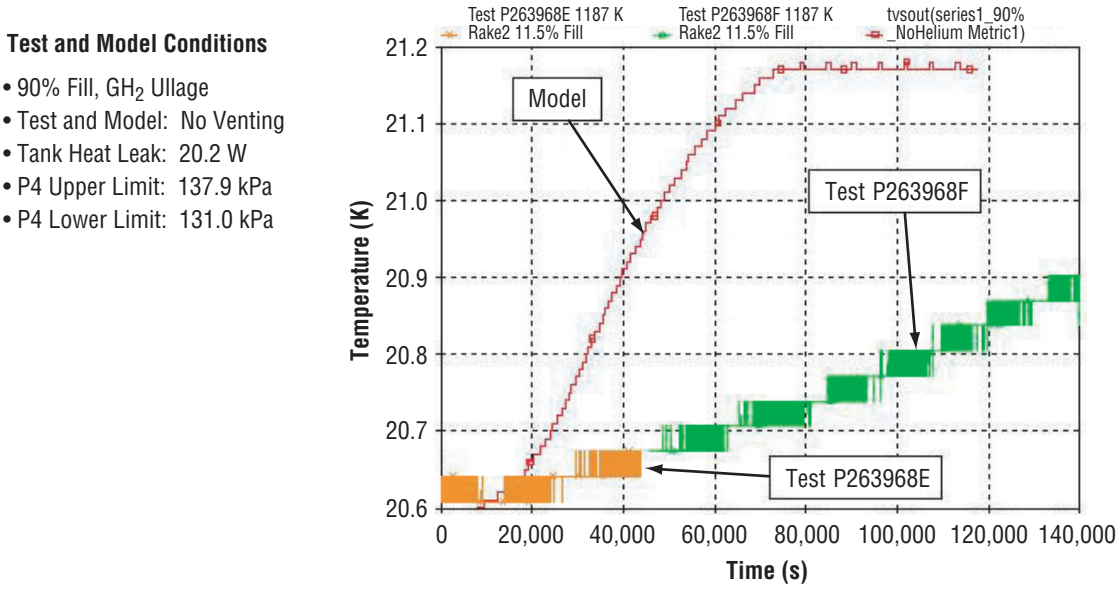

Figure 57. Bulk liquid saturation temperature modeling comparison with 1996 tests P263968E and P263968F—self-pressurization and mixing with 90-percent fill.

9.1.2 Test Segment P263968G—Mixing and Venting, 90-Percent Fill Level

Correlations for the venting and mixing operation were performed using test segment P263968G, with a 90-percent fill level and 20.2-W tank heat leak. The ullage pressure comparison is presented in figure 58. Although the timing of the first J-T valve opening event was somewhat obscured in the test data, the analytical modeling was initialized at 12,829 s and allowed to self-pressurize to the 137.9 kPa (20 psia) upper limit, whereupon the J-T valve (with a vent flow of 0.0034 kg/s) and mixer pump were activated. The data comparison indicates that the analytical model tracks the measured data very well initially; however, the model cycles about once per 1.58 hr (0.63 cycles/hr) compared with1.06 hr (0.94 cycles/hr) in the test (computed rate is ≈33-percent lower). As with the mixing cycles-only data (no venting), the measured pressure rise rates are steeper than the modeled data, whereas the pressure reduction rates again closely match. The ullage temperature comparison in figure 59 indicates that the averaged measured and computed ullage temperatures are 22.15 and 21.75 K, respectively; i.e., deviate by <2 percent. Similarly, the modeled and measured bulk liquid saturation pressure and temperature, presented in figures 60 and 61, respectively, are practically identical. A sensitivity analysis concluded that the differences in the short-term pressure rise rates between cycles are most likely due to errors in modeling the stratification effects on the ullage energy exchange across the liquid-vapor interface.

Test Conditions

- 90% Fill, GH_2 Ullage
- Tank Heat Leak: 20.2 W
- P4 Upper Limit: 137.9 kPa
- P4 Lower Limit: 131.0 kPa
- Vent Flow Rate: 0.0034 kg/s

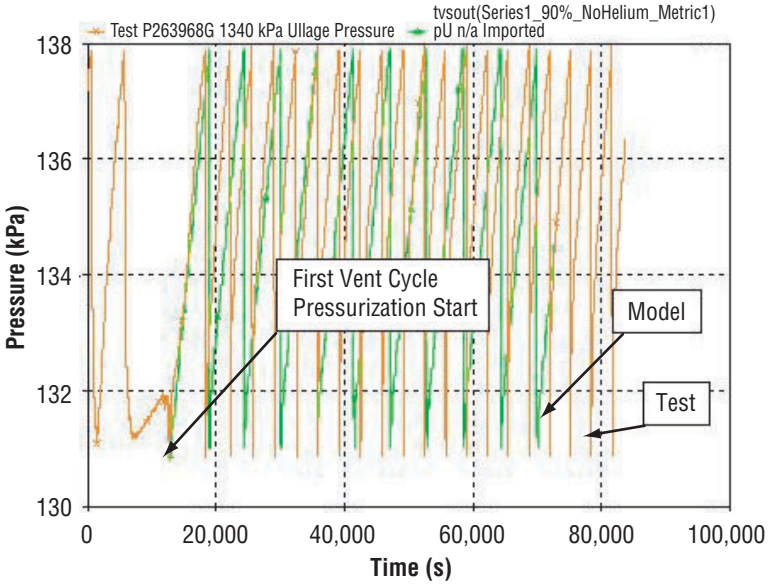

Figure 58. Ullage pressure modeling comparison with 1996 test P263968G—mixing and venting with 90-percent fill.

Test Conditions

- 90% Fill, GH_2 Ullage
- Tank Heat Leak: 20.2 W
- P4 Upper Limit: 137.9 kPa
- P4 Lower Limit: 131.0 kPa
- Vent Flow Rate: 0.0034 kg/s

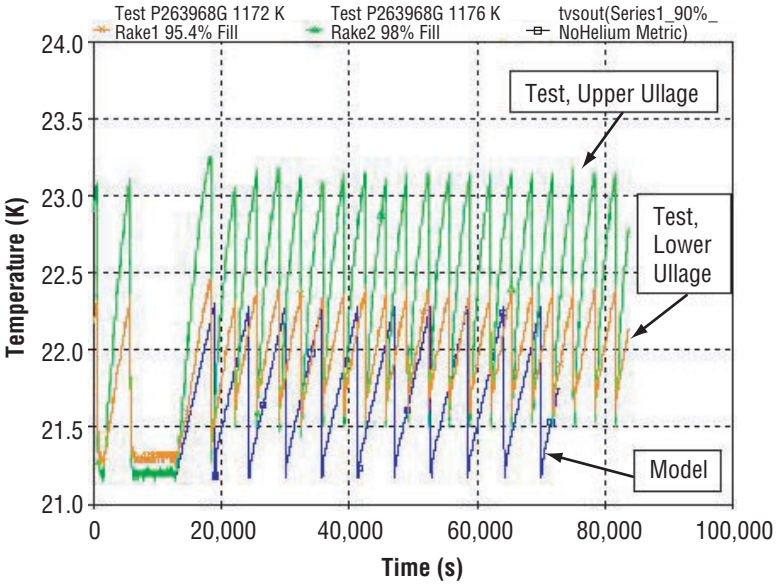

Figure 59. Ullage temperature modeling comparison with 1996 test P263968G—mixing and venting with 90-percent fill.

Test Conditions

- 90% Fill, GH_2 Ullage
- Tank Heat Leak: 20.2 W
- P4 Upper Limit: 137.9 kPa
- P4 Lower Limit: 131.0 kPa
- Vent Flow Rate: 0.0034 kg/s

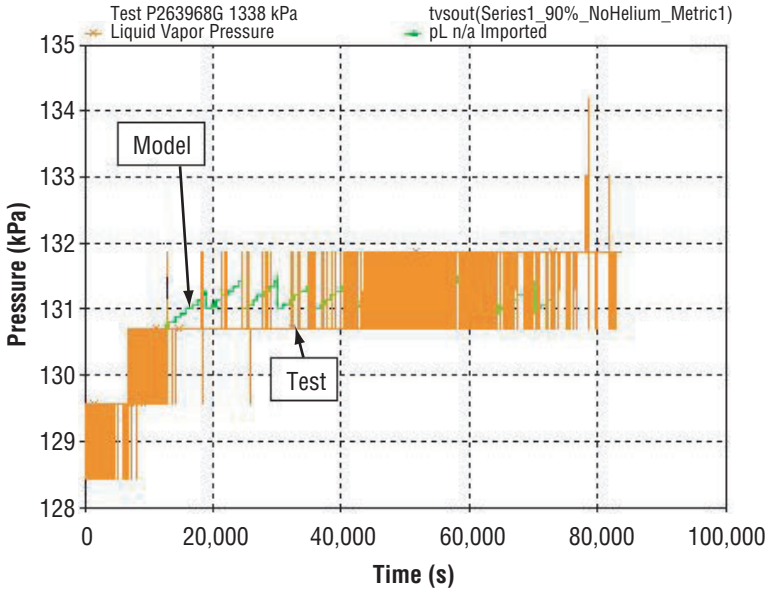

Figure 60. Bulk liquid saturation pressure modeling comparison with 1996 test P263968G—mixing and venting with 90-percent fill.

Test Conditions

- 90% Fill, GH_2 Ullage
- Tank Heat Leak: 20.2 W
- P4 Upper Limit: 137.9 kPa
- P4 Lower Limit: 131.0 kPa
- Vent Flow Rate: 0.0034 kg/s

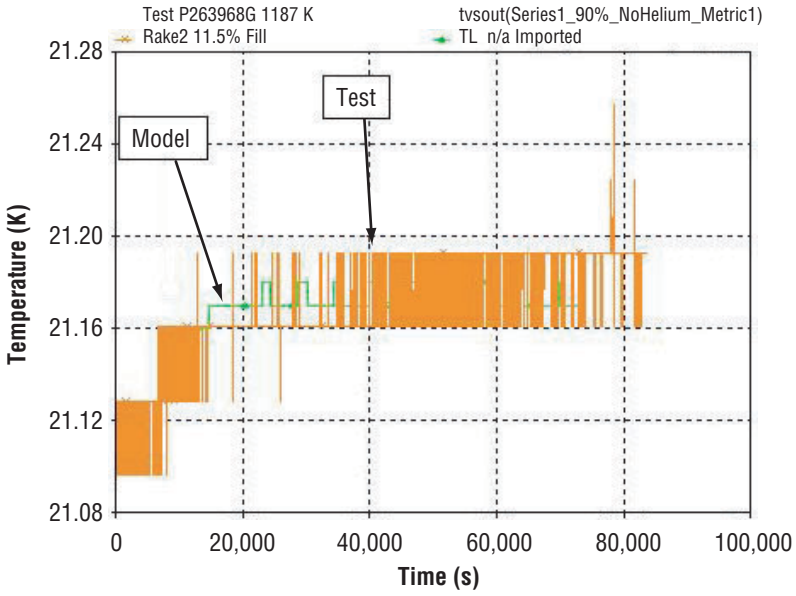

Figure 61. Bulk liquid saturation temperature modeling comparison with 1996 test P263968G—mixing and venting with 90-percent fill.

9.1.3 Test Segment P263968K—Mixing and Venting, 50-Percent Fill Level

Model and measured comparisons for mixing and venting operations in test segment P263968K, with a 50-percent fill level and 18.7-W heat leak, are presented in figures 62–65. The ullage pressure comparison, presented in figure 62, illustrates relatively good correlation until the tank draining begins shortly after 80,000 s in preparation for the next test series. As expected, the measured vent-mixer cycle rate was slower than with the 90-percent fill level; i.e., the measured TVS cycle durations were approximately 1 and 2 hr at 90 and 50 percent, respectively. However, as with the 90-percent fill level testing, the cycle rate with the model is slower than in the testing. One cycle occurred per 2.4 hr (0.417 cycles/hr) in the testing, whereas one cycle per 3.3 hr (0.3 cycles/hr) occurred in the modeling. Therefore, the modeled cycle rate is ≈28 percent below that measured and, again, is attributed to stratification effects.

The ullage temperature correlation is presented in figure 63, which indicates good agreement; i.e., the averaged model temperatures are within 1 K or ≈4 percent of the averaged measured temperatures. The bulk liquid saturation pressure and temperature correlations, presented in figures 64 and 65, respectively, indicate good agreement. Compared to the test data, the averaged modeled saturation pressures and temperatures are within 1.5 kPa and 0.06 K, respectively, except for slightly more deviation on the first cycle.

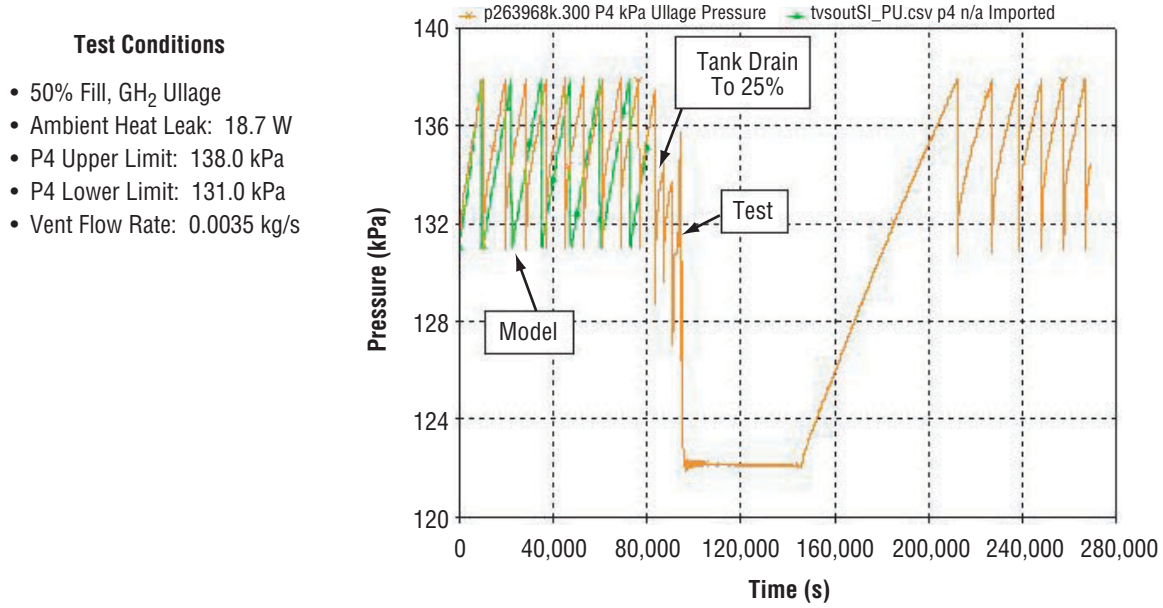

Figure 62. Ullage pressure modeling comparison with 1996 test P263968K—mixing and venting with 50-percent fill.

Test Conditions

- 50% Fill, GH_2 Ullage
- Ambient Heat Leak: 18.7 W
- P4 Upper Limit: 138.0 kPa
- P4 Lower Limit: 131.0 kPa
- Vent Flow Rate: 0.0035 kg/s

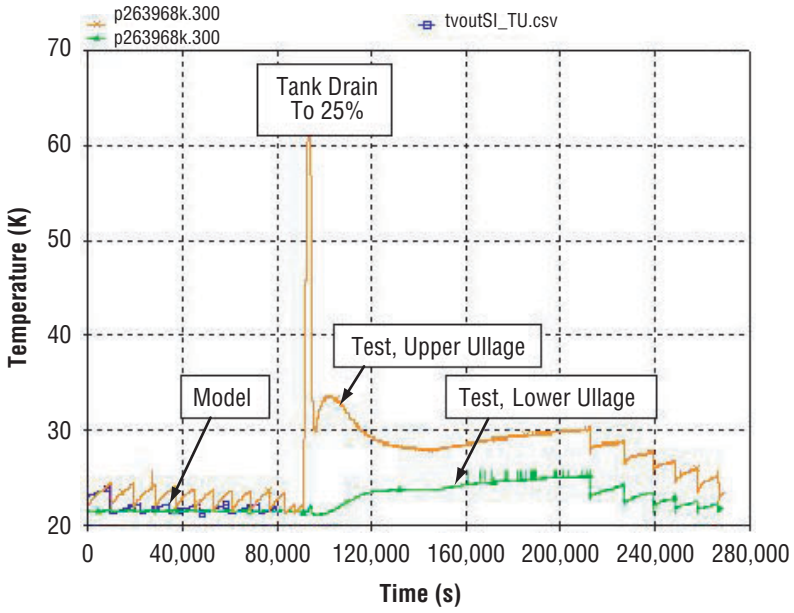

Figure 63. Ullage temperature modeling comparison with 1996 test P263968K—mixing and venting with 50-percent fill.

Test Conditions

- 50% Fill, GH_2 Ullage
- Ambient Heat Leak: 18.7 W
- P4 Upper Limit: 138.0 kPa
- P4 Lower Limit: 131.0 kPa
- Vent Flow Rate: 0.0035 kg/s

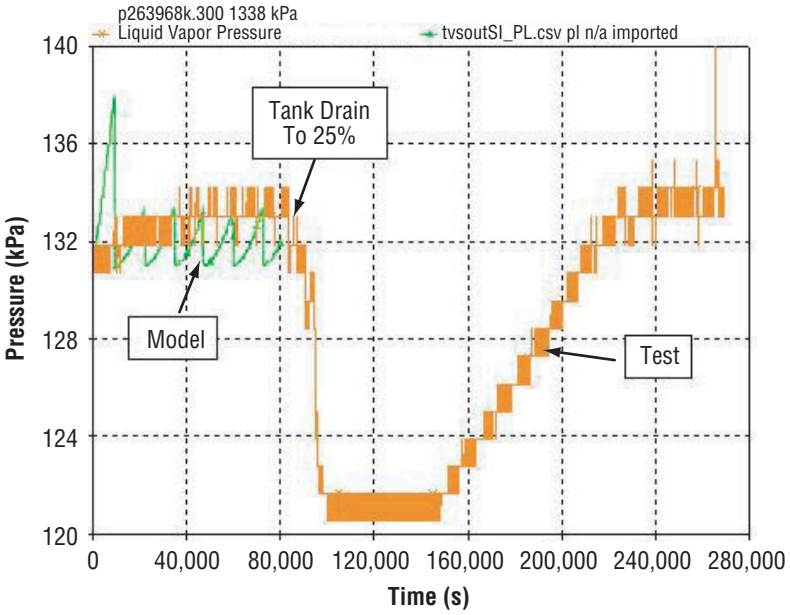

Figure 64. Bulk liquid saturation pressure modeling comparison with 1996 test P263968K—mixing and venting with 50-percent fill.

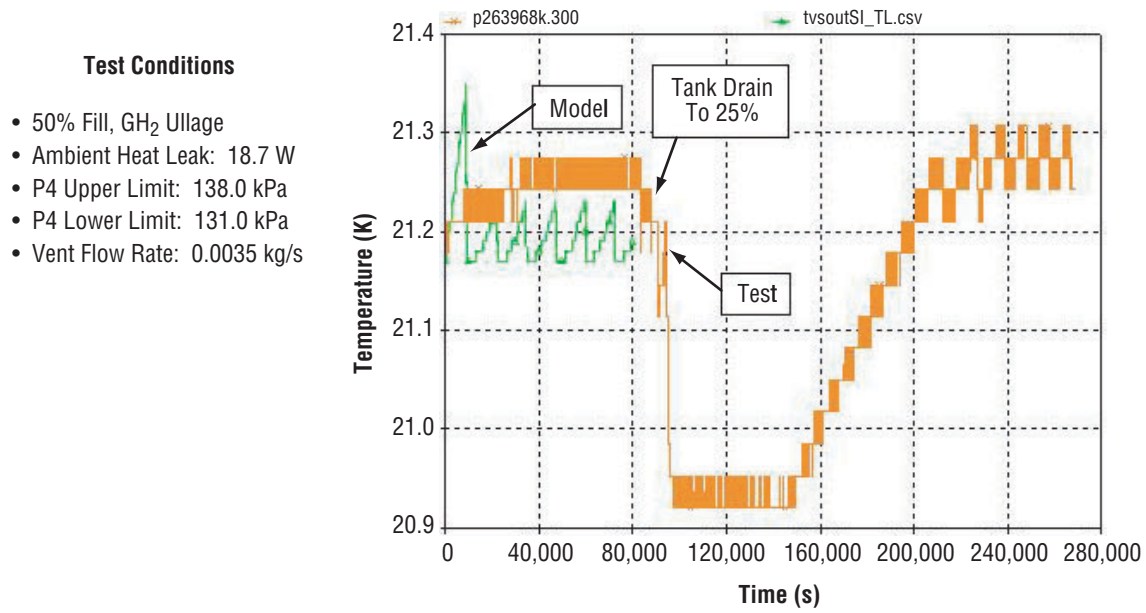

Figure 65. Bulk liquid saturation temperature modeling comparison with 1996 test P263968K—mixing and venting with 50-percent fill.

9.1.4 Test Segments P263968K and P263968L—Self-Pressurization, Mixing and Venting, 25-Percent Fill Level

Model correlations with test data for self-pressurization, mixing, and venting with a 25-percent fill level and an 18.8-W heat leak were performed using a combination of test segments P263968K and P263968L. Figure 66 presents the self-pressurization period after tank lockup at 122 kPa and indicates computed and measured pressure rise rates of 4.32 and 0.86 kPa/hr, respectively. When the mixing cycle began (fig. 67), the modeling results indicate generally good agreement with the test data. The increased ullage volume resulted in extending the measured cycle duration to 2.8 hr compared with 2.4 hr with 50-percent fill. However, the model cycle duration of 3.8 hr was again longer than that measured; i.e., the measured cycle rate (0.35 cycles/hr) was ≈26 percent higher than that computed (0.26 cycles/hr). As with the data previously discussed, the modeled and measured pressure reduction rates correlate very well, whereas the measured pressure rise rates between mixing cycles are higher than those computed.

The ullage temperature correlation is presented in figure 68, which indicates that the average measured temperatures are generally not more than 0.5 K above the model temperatures until ≈80,000 s, when the measured temperature began to drift upward until the J-T valve briefly remained open longer than usual for one cycle at ≈117,000 s. The average measured and calculated bulk liquid saturation pressures (fig. 69) correlated closely; i.e., were within 0.75 kPa. The average bulk liquid saturation temperatures (fig. 70) correlated within 0.04 K.

Test Conditions

- 25% Fill, GH_2 Ullage
- Tank Heat Leak: 18.8 W
- P4 Upper Limit: 138.0 kPa
- P4 Lower Limit: 131.0 kPa
- Vent Flow Rate: 0.0036 kg/s

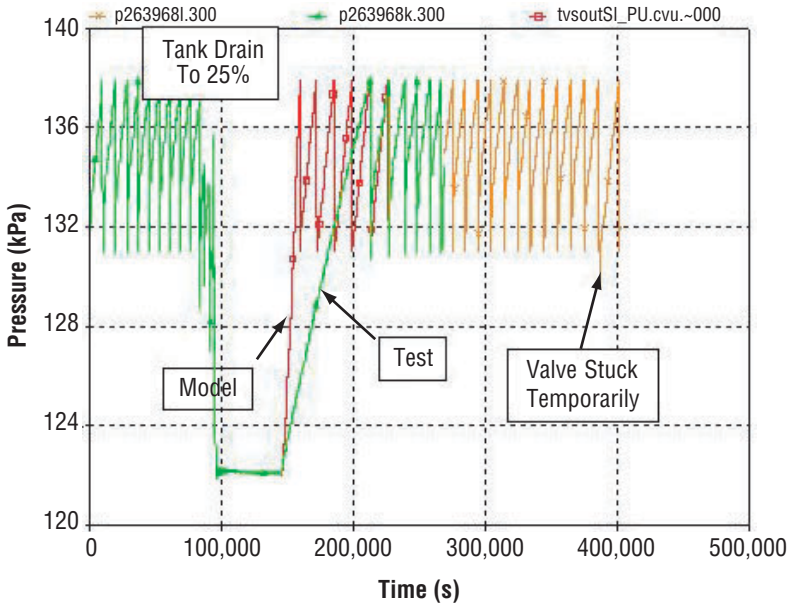

Figure 66. Ullage pressure modeling comparison with 1996 tests P263968K and P263968L—mixing and venting with 25-percent fill.

Test Conditions

- 25% Fill, GH_2 Ullage
- Tank Heat Leak: 18.8 W
- P4 Upper Limit: 138.0 kPa
- P4 Lower Limit: 131.0 kPa
- Vent Flow Rate: 0.0036 kg/s

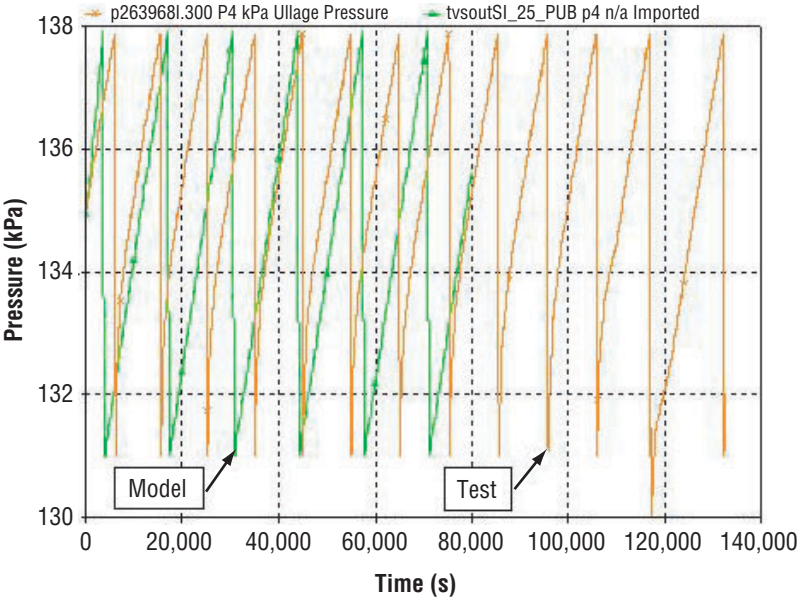

Figure 67. Ullage pressure modeling comparison with 1996 test P263968L—mixing and venting with 25-percent fill.

Test Conditions

- 25% Fill, GH_2 Ullage
- Tank Heat Leak: 18.8 W
- P4 Upper Limit: 138.0 kPa
- P4 Lower Limit: 131.0 kPa
- Vent Flow Rate: 0.0036 kg/s

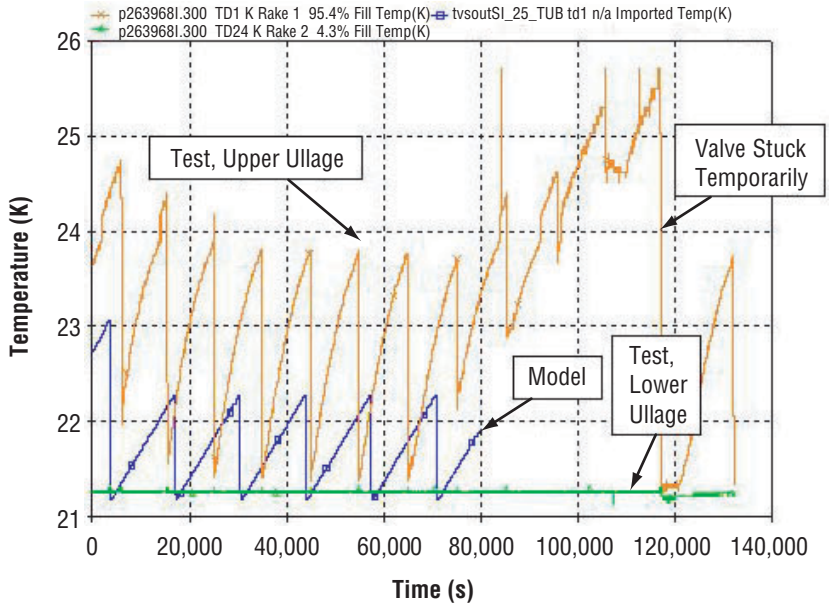

Figure 68. Ullage temperature modeling comparison with 1996 test P263968L—mixing and venting with 25-percent fill.

Test Conditions

- 25% Fill, GH_2 Ullage
- Tank Heat Leak: 18.8 W
- P4 Upper Limit: 138.0 kPa
- P4 Lower Limit: 131.0 kPa
- Vent Flow Rate: 0.0036 kg/s

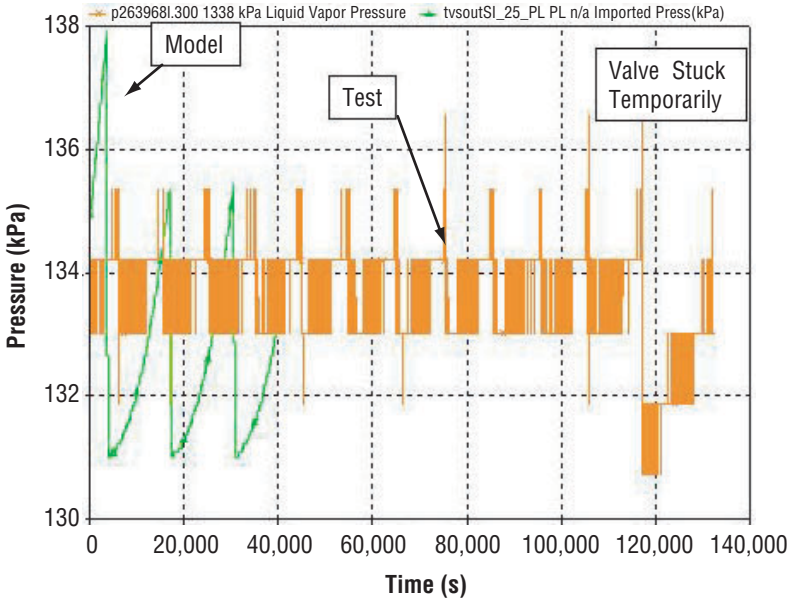

Figure 69. Bulk liquid saturation pressure modeling comparison with 1996 test P263968L—mixing and venting with 25-percent fill.

Test Conditions

- 25% Fill, GH_2 Ullage
- Tank Heat Leak: 18.8 W
- P4 Upper Limit: 138.0 kPa
- P4 Lower Limit: 131.0 kPa
- Vent Flow Rate: 0.0036 kg/s

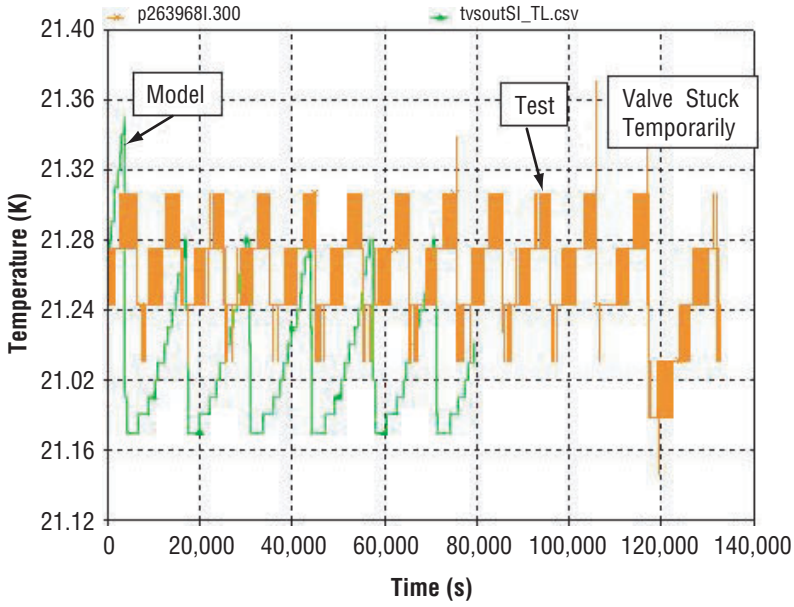

Figure 70. Bulk liquid saturation temperature modeling comparison with 1996 test P263968L—mixing and venting with 25-percent fill.

9.2 Series 2, High Heat Leak Tests

Analytical correlations for segments from all four of the series 2 tests segments were performed Segments from three tests (P263981D, P263981T, P263981X) are discussed below, and to avoid repetition, data for P263981E is presented in appendix C. The third test was performed with GHe injected in the ullage (test segment P263981X) with a 50-percent fill level. The other two test segments—P263981D and P263981T—were performed with GH_2 only in the ullage with 90- and 50-percent fill levels, respectively. In the GH_2 ullage cases, the upper and lower tank pressure control limits were 137.9 kPa (20 psia) and 131 kPa (19 psia), respectively, and the vent flow rates ranged from 0.0036 to 0.0034 kg/s. As with previous correlations, the modeled periods were initialized using measured conditions.

9.2.1 Test Segment P263981D—Self-Pressurization and Mixing, 90-Percent Fill Level

Correlations for self-pressurization and mixing were performed using test segment P263981D, with a 90-percent fill level and 54.1-W tank heat leak. As illustrated in figure 71, tank lockup occurred at 10,380 s and self-pressurization proceeded until the mixing cycles began and continued throughout the remainder of the test segment without venting. The model is in good agreement with the test data in the early stages of self-pressurization after tank lockup at 111.5 kPa (16.2 psia). However, similar to the lower heat leak case, the analytical pressure data begins to deviate after ≈1.14 hr (14,500 s) and rises more rapidly than the measured values. The computed and measured ullage pressures reached the upper pressure limit of 137.9 kPa (20 psia) after ≈2.7 hr (20,000 s) and 5.5 hr (30,000 s), respectively. However, once the mixing cycles begin, both the pressure rise and reduction rates correlated very well. The measured and computed cycle rates were 1.83 and 1.76 cycles/hr, respectively; i.e., the measured rate was <4 percent higher. The ullage temperature correlations presented in figure 72 are consistent with the ullage pressure comparison data. During the self-pressurization period after tank lockup the modeled

Test Conditions

- 90% Fill, GH_2 Ullage
- No Venting
- Ambient Heat Leak: 54.1 W
- P4 Upper Limit: 137.9 kPa
- P4 Lower Limit: 131.0 kPa

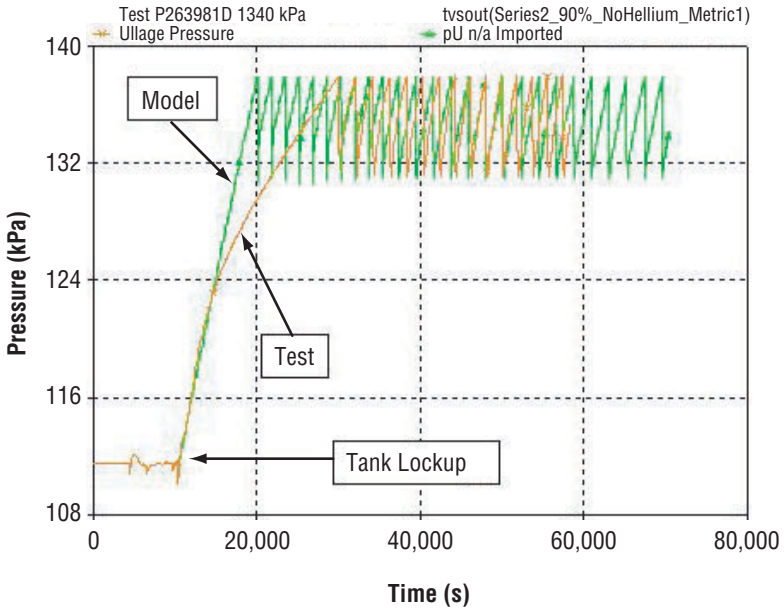

Figure 71. Ullage pressure modeling comparison with 1998 test P263981D—self-pressurization and mixing with 90-percent fill.

Test Conditions

- 1998 Test P263981D, 90% Fill, GH_2 Ullage, Tank Pressurization

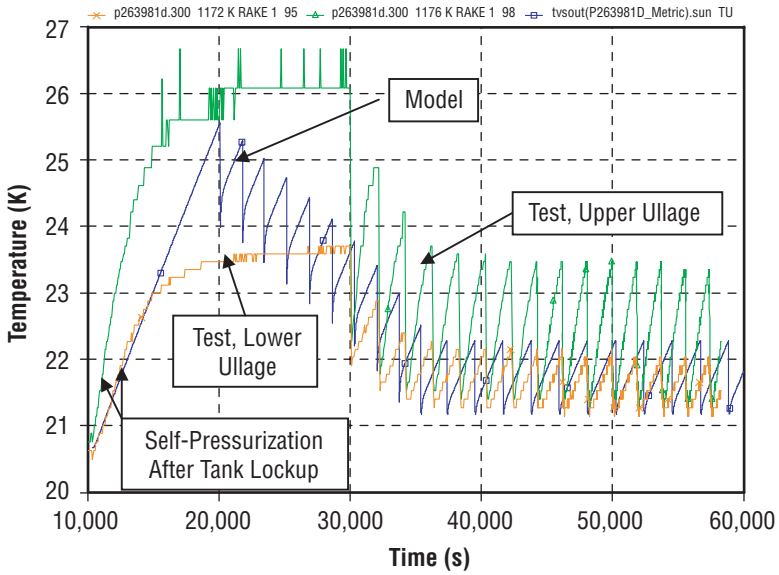

Figure 72. Ullage temperature modeling comparison with 1998 test P263981D—self-pressurization and mixing with 90-percent fill.

Test Conditions

- 90% Fill, GH_2 Ullage
- Ambient Heat Leak: 54.1 W
- P4 Upper Limit: 137.9 kPa
- P4 Lower Limit: 131.0 kPa
- Vent Flow Rate: 0.0048 kg/s

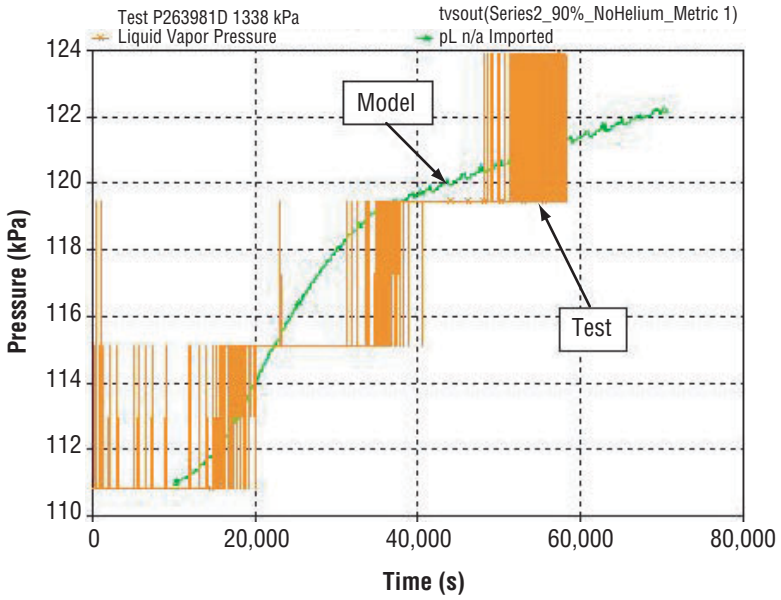

Figure 73. Bulk liquid saturation pressure modeling comparison with 1998 test P263981D—self-pressurization and mixing with 90-percent fill.

Test Conditions

- 90% Fill, GH_2 Ullage
- Ambient Heat Leak: 54.1 W
- P4 Upper Limit: 137.9 kPa
- P4 Lower Limit: 131.0 kPa
- Vent Flow Rate: 0.0048 kg/s

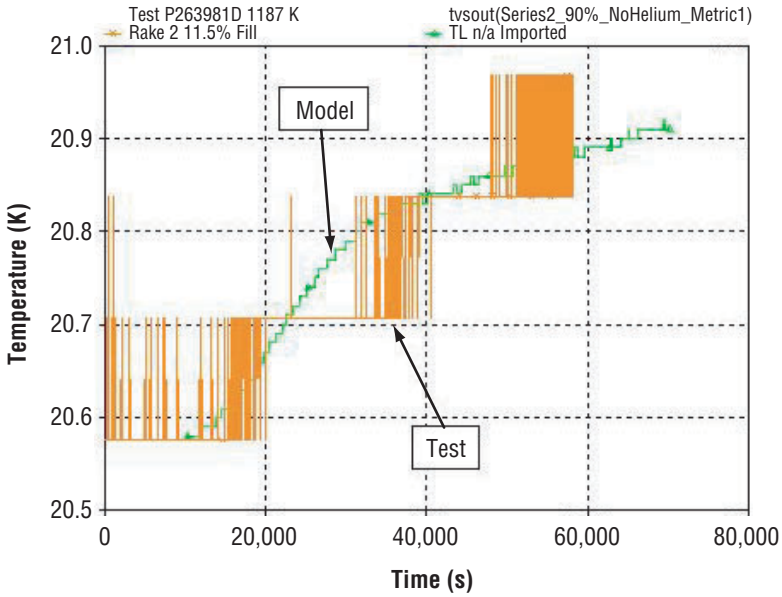

Figure 74. Bulk liquid saturation temperature modeling comparison with 1998 test P263981D—self-pressurization and mixing with 90-percent fill.

ullage temperatures initially followed the measured data in the lower portion of the ullage. However, after ≈1.14 hr (14,500 s) the analytical temperatures begin to rise more rapidly than measured in the lower ullage, but remain below temperatures measured in the upper ullage. The modeled temperatures begin to decrease when mixing begins at 2.7 hr (200,000 s) and very closely follow the measured lower ullage temperatures after the test data indicate that the mixing cycles have begun at 5.5 hr (30,000 s). The average measured and calculated bulk liquid saturation pressures (fig. 73) correlated closely; i.e., were within 2 kPa. The averaged bulk liquid saturation temperatures (fig. 74) correlated within 0.075 K.

9.2.2 Test Segment P263981T—Self-Pressurization and Venting, 50-Percent Fill Level

Correlations for self-pressurization, mixing, and venting were performed using test segment P263981T, with a 50-percent fill level and 51-W tank heat leak. As illustrated in figure 75, tank lockup at 111.5 kPa (16.2 psia) occurred at 127,110 s and self-pressurization proceeded until the mixing cycles began. The model pressure rise rate exceeded that measured. The modeled data indicated that the first mixing cycle began ≈2.8 hr (137,000 s) after lockup whereas mixing occurred ≈13.9 hr (177,000 s) after lockup in the test. Also, the venting began on the fifth cycle in the test, whereas it began on the first model cycle. Therefore, the trend was the same as observed in previous testing and the model again indicated conservative mixing and vent cycle start times.

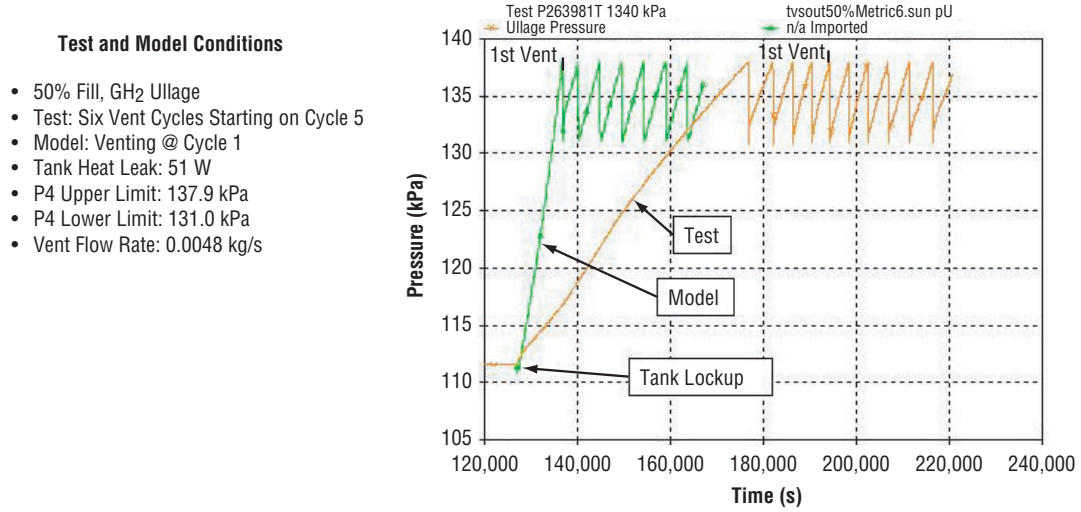

Figure 75. Unshifted ullage pressure modeling comparison with 1998 test P263981T—self-pressurization, mixing, and venting with 50-percent fill.

In order to correlate the mixing/vent cycle characteristics, the model start time with venting, was shifted by 60,350 s (to 187,460 s) to better align with the test data (fig. 71). At the beginning, both the pressure rise and reduction rates correlated reasonably well and the measured cycle rate was about 14 percent higher than computed. Once venting began in the test data, the model and test cycle rates became identical at 1.2 cycles/hr. The corresponding ullage temperature comparison (fig. 77) indicates good correlation in the upper ullage. Once venting began in the test (at 195,000 s), the measured and shifted modeled temperatures both averaged ≈22 K. Similarly, the liquid saturation pressure correlation (fig. 78) indicates close correlation after venting began in the test. Similarly, the liquid saturation temperature correlation (fig. 79) indicated modeled temperatures averaged ≈0.2 K lower than the measured values.

Test and Model Conditions

- 50% Fill, GH_2 Ullage
- Test: Six Vent Cycles Starting on Cycle 5
- Model: Venting @ Cycle 1
- Tank Heat Leak: 51 W
- P4 Upper Limit: 137.9 kPa
- P4 Lower Limit: 131.0 kPa
- Vent Flow Rate: 0.0048 kg/s

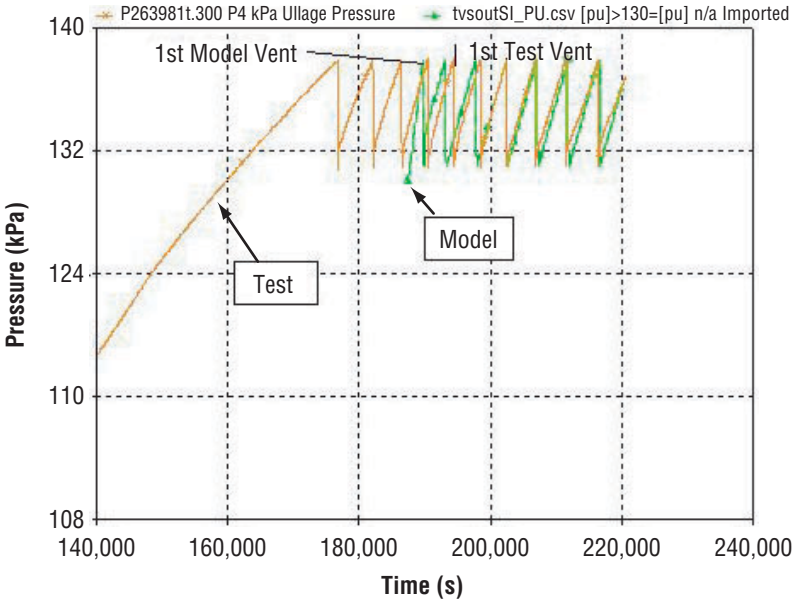

Figure 76. Shifted ullage pressure modeling comparison with 1998 test P263981T—self-pressurization, mixing, and venting with 50-percent fill.

Test and Model Conditions

- 50% Fill, GH_2 Ullage
- Test: Vent Cycles Starting @ Pressurization Cycle 5
- Model: Start Time Shifted, Venting Begins @ Cycle 1
- Tank Heat Leak: 51 W
- P4 Upper Limit: 137.9 kPa
- P4 Lower Limit: 131.0 kPa
- Vent Flow Rate: 0.0048 kg/s

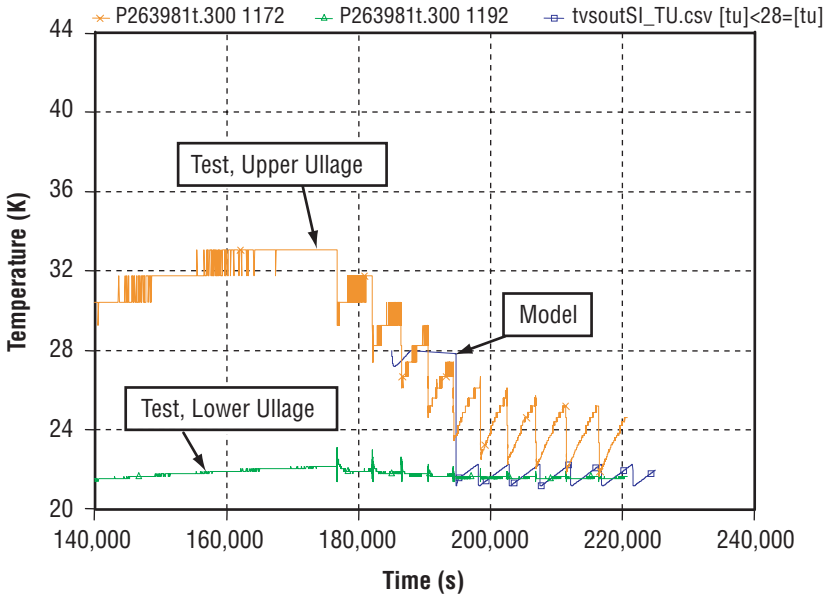

Figure 77. Shifted ullage temperature modeling comparison with 1998 test P263981T—self-pressurization, mixing, and venting with 50-percent fill.

Test and Model Conditions

- 50% Fill, GH_2 Ullage
- Test: Vent Cycles Starting @ Pressurization Cycle 5
- Model: Start Time Shifted, Venting Begins @ Cycle 1
- Tank Heat Leak: 51 W
- P4 Upper Limit: 137.9 kPa
- P4 Lower Limit: 131.0 kPa
- Vent Flow Rate: 0.0048 kg/s

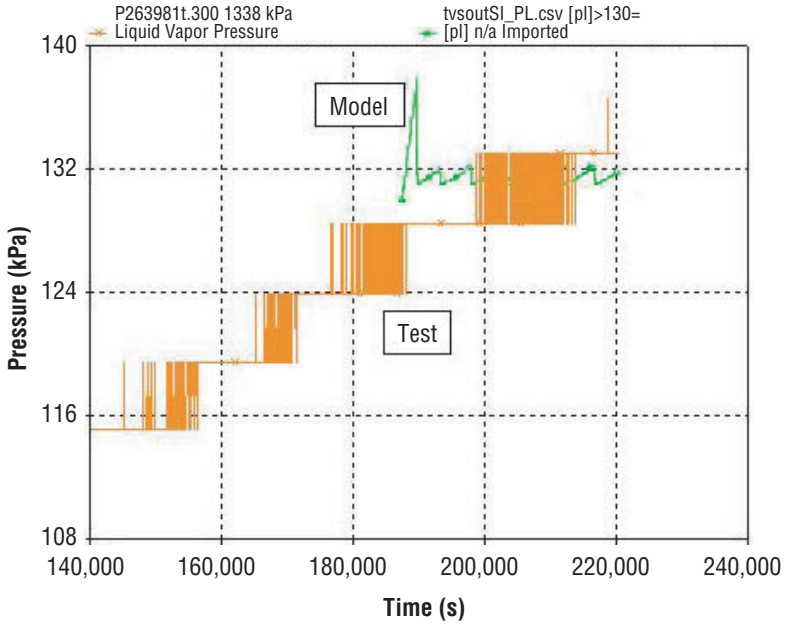

Figure 78. Shifted bulk liquid saturation pressure modeling comparison with 1998 test P263981T—self-pressurization, mixing, and venting with 50-percent fill.

Test and Model Conditions

- 50% Fill, GH_2 Ullage
- Test: Vent Cycles Starting @ Pressurization Cycle 5
- Model: Start Time Shifted, Venting Begins @ Cycle 1
- Tank Heat Leak: 51 W
- P4 Upper Limit: 137.9 kPa
- P4 Lower Limit: 131.0 kPa
- Vent Flow Rate: 0.0048 kg/s

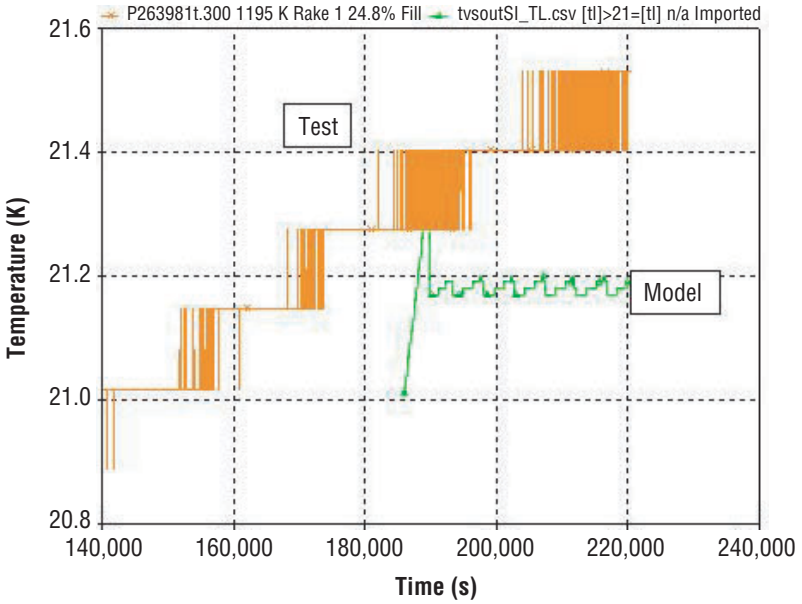

Figure 79. Shifted bulk liquid saturation temperature modeling comparison with 1998 test P263981T—self-pressurization, mixing, and venting with 50-percent fill.

9.2.3 Test Segment P263981X—Self-Pressurization and Venting, 50-Percent Fill Level, GHe and GH_2 Ullage

Correlations for self-pressurization, mixing, and venting were performed using test segment P263981X, with a 50-percent fill level, 51-W tank heat leak, and with GHe injected into the ullage at the beginning of tank lockup. As mentioned earlier, the injected GHe initially elevated the ullage pressure to above the upper control limit of 213 kPa and then the ullage was vented to the lower control limit of 206.84 kPa, whereupon the tank was locked up and the testing began. After the tank self-pressurized to 213 kPa, the mixer started and decreased the ullage pressure to ≈211 kPa, where the pressure leveled off and began to rise. The vent was manually cycled on and the ullage pressure then decreased to the lower limit, 206.8 kPa. The sequence was repeated for two more cycles before the testing was terminated. As described in section 8.3.4, it is believed that the helium acted as a barrier to the mass transfer and to condensation on the liquid surface, thereby constraining the effectiveness of the mixing-only phase and necessitating use of the J-T venting to further cool the ullage and reduce the pressure to the lower setpoint pressure. The analytical and test ullage pressure modeling comparison with the test data is presented in figure 80. The model start time was shifted to match the first vent cycle (6,200 s), but was initiated with measured conditions at the start of tank lockup. The GH_2 and GHe partial pressures used in the model were 165.5 (24 psia) and 41.4 kPa (6 psia), respectively. The model cycle rate was slightly faster than the test data reflected, primarily because the model did not reflect the leveling-off effect observed in the mixer-only testing. Also, since the analytical bulk liquid conditions never indicated saturation, venting did not occur with the model.

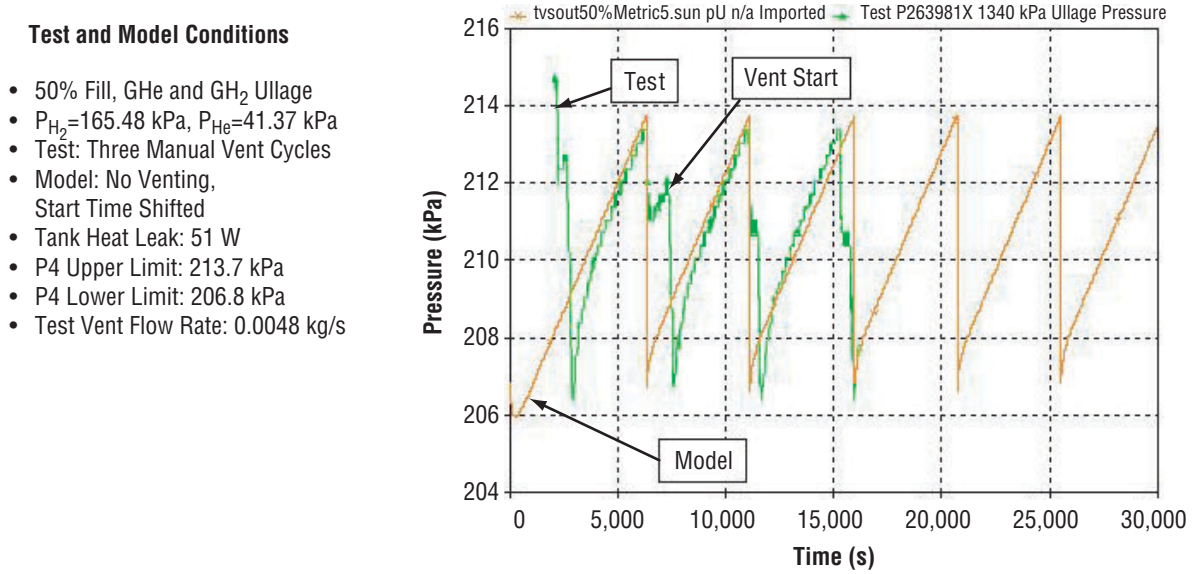

Figure 80. Shifted ullage pressure modeling comparison with test P263981X—tank pressurization, mixing, and venting with 50-percent fill, GHe and GH_2 ullage.

The shifted ullage temperature modeling comparison with the test data is presented in figure 81. The averaged model and test ullage temperatures were about 22.6 and 23 K, respectively; i.e., were within 0.4 K. The shifted bulk liquid saturation pressure and temperature correlations are presented in figures 82 and 83, respectively. The model indicated that the saturation pressure and temperature continued to rise throughout the test segment, whereas the measured saturation conditions remained relatively constant. Longer duration testing definitely is required to better define and analytically correlate the effects of helium pressurant on TVS operation and long-term trends.

Test and Model Conditions

- 50% Fill, GHe and GH_2 Ullage
- P_{H_2}=165.48 kPa, P_{He}=41.37 kPa
- Test: Three Manual Vent Cycles
- Model: No Venting, Start Time Shifted
- Tank Heat Leak: 51 W
- P4 Upper Limit: 213.7 kPa
- P4 Lower Limit: 206.8 kPa
- Test Vent Flow Rate: 0.0048 kg/s

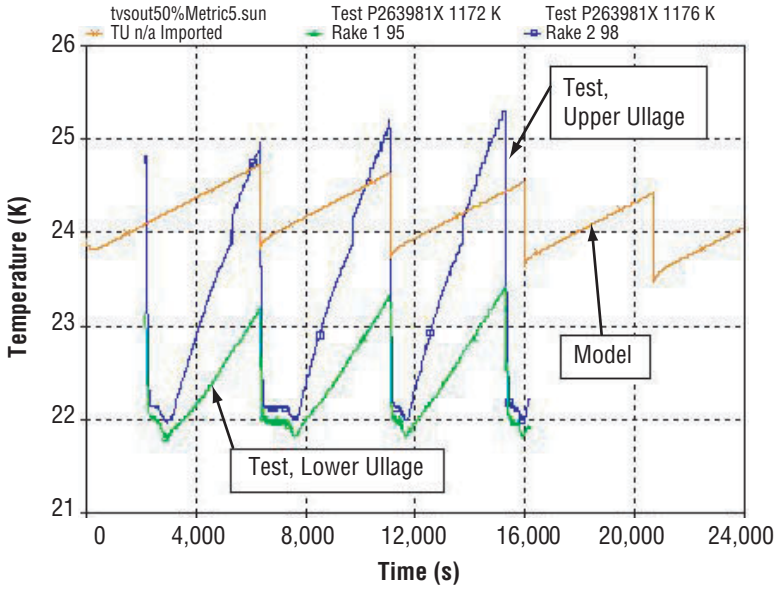

Figure 81. Shifted ullage temperature modeling comparison with 1998 test P263981X—tank pressurization, mixing, and venting with 50-percent fill, GHe and GH_2 ullage.

Test and Model Conditions

- 50% Fill, GHe and GH_2 Ullage
- P_{H_2}=165.48 KPa, P_{He}=41.37 kPa
- Test: Three Manual Vent Cycles
- Model: No Venting, Start Time Shifted
- Tank Heat Leak: 51 W
- P4 Upper Limit: 213.7 kPa
- P4 Lower Limit: 206.8 kPa
- Test Vent Flow Rate: 0.0048 kg/s

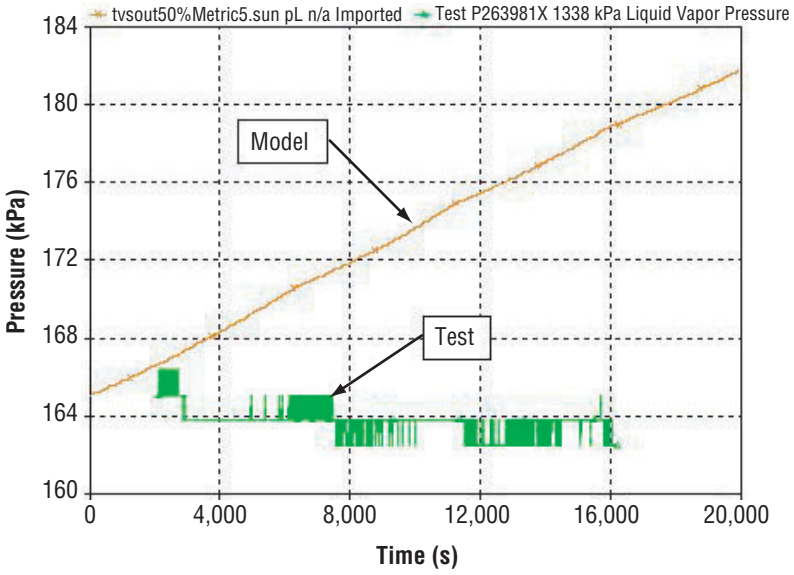

Figure 82. Shifted bulk liquid saturation pressure modeling comparison with 1998 test P263981X—tank pressurization, mixing, and venting with 50-percent fill, GHe and GH_2 ullage.

Test and Model Conditions

- 50% Fill, GHe and GH_2 Ullage
- P_{H_2}=165.48 kPa, P_{He}=41.37 kPa
- Test: Three Manual Vent Cycles
- Model: No Venting, Start Time Shifted
- Tank Heat Leak: 51 W
- P4 Upper Limit: 213.7 kPa
- P4 Lower Limit: 206.8 kPa
- Test Vent Flow Rate: 0.0048 kg/s

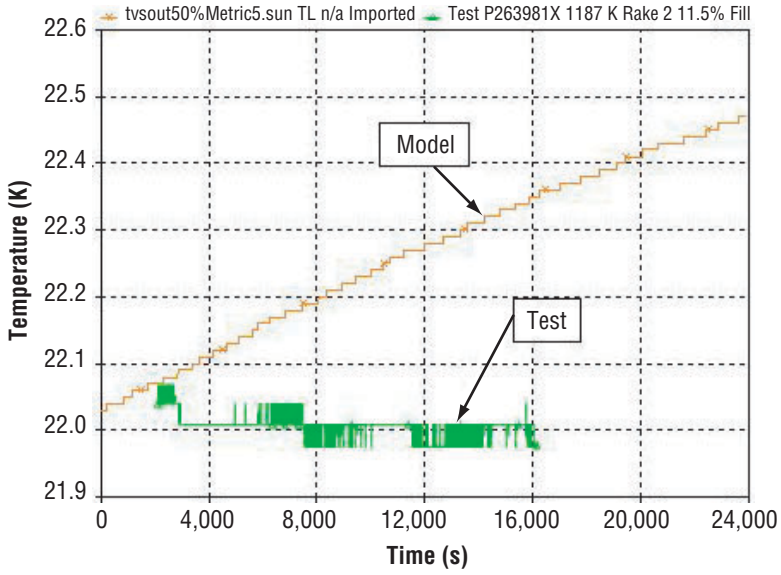

Figure 83. Shifted bulk liquid saturation temperature modeling comparison with 1998 test P263981X—tank pressurization, mixing, and venting with 50-percent fill, GHe and GH_2 ullage.

10. SUMMARY AND RECOMMENDATIONS

The program objective was to design, develop, and demonstrate with ground testing a system that can maintain LH_2 tank pressure control in zero gravity without liquid resettling while minimizing boiloff losses. A spray bar TVS concept by The Boeing Company (formerly Rockwell Aerospace) was selected to demonstrate ullage pressure control within a ±3.45 kPa (±0.5 psi) control band within MSFC's 18-m^3 MHTB LH_2 tank. The longitudinal spray bar was designed to thermally destratify both liquid and ullage, independent of liquid-vapor positions in zero gravity. The basic design requirements were that the TVS accommodate tank heat leaks of up to 55 W, liquid levels of 10 to 95 percent, and operation without dependence on a capillary device.

The spray bar design definition and hardware selection activities resulted in the following:

- A 2.67-m- (105-in-) long spray bar concentric tube heat exchanger assembly with a heat exchange area of 0.27 m^2 between the vented and recirculated fluid. Forty-five 0.17-cm- (0.067-in-) diameter orifices equally spaced in each of four longitudinal tubes enable spray injection in four directions and optimum ullage pressure decay.

- Initiate venting at or near a tank pressure of 137.8 kPa (20 psia) to optimize heat absorption, and vent to a J-T valve with an orifice diameter of 1.96 mm (0.077 in) and flow rate capability of 0.0021 kg/s (0.0047 lb/s).

- Barber-Nichols pump which produces 113.5 L/min (30 gal/min) with a head rise of 6.89 kPa/m^2 at 4,158 rpm.

Component and subsystem testing performed included: LH_2 spray injection testing within a 55.9-cm- (22-in-) diameter dewar to verify ullage pressure collapse analytical modeling, recirculation pump testing with methanol to define pump head and flow coefficients, full-scale spray bar flow tests with water to measure pressure losses and verify uniform flow distributions, heat exchanger cold side pressure drop testing with LN_2, and pump flowmeter water calibration testing using actual line inlet and outlet geometries.

A transient analytical model was formulated to characterize TVS performance within the MHTB. Individual thermal-fluid models of the heat exchanger, spray manifold and injection tubes, recirculation pump, and tank were developed and verified before being integrated into the transient TVS model. The heat exchanger model is a multinode finite difference model that simulates two-phase flow in a quasi-steady-state mode. A one-dimensional, incompressible fluid dynamic model characterizes flow within and exiting the spray manifold and injection tubes. The recirculation pump performance model is based on the pump head versus flow rate data provided by the manufacturer combined with standard analytical equations for a centrifugal pump. The tank model consists of four control volumes: (1) Ullage, (2) tank wall, (3) liquid on the tank wall, and (4) bulk liquid.

The MSFC vacuum facility and associated controls performed very well, producing over 420 hr of testing. During the orbital simulation periods with cold walls, the vacuum was successfully maintained at 10^{-6} torr or less. Without the chamber cold walls operating, vacuum levels were 10^{-5} torr or less. During the steady-state heat leak or boiloff testing, the facility ullage pressure control system maintained LH_2 tank pressure within ±0.00689 kPa (±0.001 psi) of the prescribed setpoint. During TVS testing when the J-T venting was routed into an adjacent 4.6-m- (15-ft-) diameter vacuum chamber, the supporting chamber maintained pressure levels below 75 torr (1.4 psia). Also, the MHTB environmental shroud successfully maintained multilayer insulation exterior boundaries at the prescribed level of 305 K throughout the testing.

Boiloff testing established the tank heat leak prior to TVS testing at the 90-, 50-, and 25-percent fill levels. One TVS test series was with a low heat leak (19–20 W), and another test series with a high heat leak (51–54 W). Both the low and high heat leak test data confirmed the spray bar to be effective in destratifying both the ullage and liquid for all conditions. Generally, the mixing durations were shorter when venting occurred due to the heat extraction effect. The mixing durations clearly increased with decreasing fill levels with the mixing cycle durations ranging from 43 to 535 s, depending on the test condition. For example, at the 90-percent fill level, the mixer operation duration per cycle increased from 134 s at the beginning to 535 s as saturation was approached prior to the initiation of venting. The time between mixing cycles ranged from 25 to 173 min for all fill levels and conditions tested.

The automated TVS control system successfully maintained tank pressure within the selected control band of ±3.45 kPa (±0.5 psia) throughout the testing with a GH_2 ullage. Tank mixing alone maintained pressure control until the saturation pressure increased to the lower limit of the TVS control band. At the 90-percent fill level with a 20 W heat leak, for example, 2.5 days elapsed before J-T venting was necessitated. The low heat leak saturation pressure rise rates were ≈0.3 kPa/hr (0.044 psi/hr) at the 90- and 50-percent fill levels and ≈0.50 kPa/hr (0.073 psi/hr) at the 25-percent fill. Mixing and venting began simultaneously at the 25-percent fill level. Therefore, there apparently is a minimum liquid level below which tank mixing alone is insufficient to reduce tank pressure beginning with the first mixing cycle. TVS heat extraction rates were computed based on the TVS instrumentation data. When comparing the computed or derived heat extraction values to the measured tank heat leak for the same test, the extraction rates were 7 to 21 percent lower than the corresponding tank heat. In reality, the thermal energy removed by the TVS equaled the heat leak into the tank. The differences between the measured heat leak and heat extraction calculation are most likely due to the sensitivity of the extremely small vent flow rates (0.0035 to 0.0048 kg/s) derived from the measured data. Also, erratic J-T valve operation compromised test results on two occasions; i.e., it stuck open for a few seconds on one test and remained open on another, necessitating test termination. A more reliable valve is recommended for future testing.

To support future mission scenarios or options involving orbital propellant storage and transfer, an additional test at the 25-percent fill level was conducted to evaluate the ability of the TVS to reduce the saturation conditions of the bulk LH_2. In this case, the J-T valve was allowed to remain open and the mixer operated continuously, which successfully reduced the saturation conditions from 133 to 70 kPa (19.3 psia to 10 psia) in 118 min. About 25.5 kg (56 lb) of vented LH_2 were required to achieve the saturation pressure reduction.

Limited testing with the 50-percent fill level, 51-W heat leak condition was conducted to evaluate TVS performance with a noncondensable gas, helium, in the ullage. Even though the ullage pressures were above saturation, mixing alone did not sufficiently reduce ullage pressure. It was concluded that helium constrained the energy exchange between the GH_2 and LH_2, reducing the condensation effects of both the sprayed droplets and convection at the bulk liquid-vapor interface. The trend was toward more effective mixing with each succeeding cycle, and it is possible that the pressure "leveling off" effect would have eventually disappeared with more mixing cycles. Further testing is required to ascertain the long-term effects of helium on TVS performance, but it is evident that the TVS control system logic would have to be modified to accommodate the presence of helium.

Using the MHTB TVS analytical model, correlations with the measured ullage pressure and temperature, and with the bulk liquid saturation pressure and temperature were developed for eight representative test segments. Correlations for the extended self-pressurization periods after each tank lockup indicated that the model pressure rise rates exceeded those measured by factors of ≈2 at the 90-percent fill level, and a factor of 5 at the 50- and 25-percent levels. It is believed the analytical modeling, which assumes that the liquid and ullage are each represented by single nodes, did not simulate the complex energy exchange that actually occurred at the liquid-vapor interface. Indications are that the model assumed thermal energy addition to the ullage at a constant rate; whereas in reality, a low-temperature mass transfer across the liquid-vapor interface began after 1–2 hr to suppress the ullage pressure rise rate.

Once the mixing and venting cycles began, the analytical and measured data more closely matched. With the low heat leak condition, it was noted that the measured pressure rise rates were slightly steeper than analytically modeled, whereas the pressure reduction rates were practically identical. The low heat leak-modeled TVS cycle rates ranged from 11- to 33-percent lower than the measured cycle rates. However, the cycle rate correlations improved with the higher heat leak condition, and the measured rates were 4 to 14 percent higher than the modeled rates for the mixing "without venting" cases, and almost identical in the "with venting" cases. As expected, the cycle rates did decrease with increasing ullage volume level. The correlations for ullage pressure and temperature, and the bulk liquid saturation pressure and temperature, indicated relatively good agreement for the entire range of conditions tested.

When helium was present in the ullage, the model indicated that mixing alone reduced the ullage pressure to the lower setpoint (no venting) since the bulk liquid was below saturation. In reality, manual use of the J-T venting became necessary to achieve the lower setpoint. Therefore, the effectiveness of the mixing-only phase was compromised by the helium presence. Furthermore, the modeled saturation pressure and temperature continued to rise throughout the test segment, whereas the measured saturation conditions remained relatively constant. Longer duration testing definitely is required to better define and analytically correlate the effects of helium pressurant on TVS operation and long-term trends.

APPENDIX A—MULTIPURPOSE HYDROGEN TEST BED TANKING TABLE

A tanking table (table 8) has been calculated based on the design geometry of the MHTB test tank. This table provides volume, ullage, and mass estimates based on the fluid level as referenced to the tank bottom. The tank fluid level is measured with a capacitance probe mounted such that its active length begins 10 cm above the tank bottom and continues for 2.878 m (113.3125 in) or to a height 2.978 m (117.25 in) above the tank bottom. Therefore, all capacitance probe height data must be corrected by adding 10 cm (3.9375 in) to the recorded height value to obtain the actual liquid height inside the tank.

Table 8. MHTB tanking table.

Total Tank Volume = 639.34 ft^3 18.10 m^3
LH_2 Density = 4.419 lbm/ft^3 70.786 kg/m^3
Note: Height is measured from the bottom of the tank.

Height (in)	Height (cm)	Volume (ft^3)	Volume (m^3)	Ullage (%)	Liquid (%)	Liquid Mass (lbm)	Liquid Mass (kg)
0.00	0.00	0.00	0.0000	100.00	0.00	0.00	0.0000
0.50	1.27	0.05	0.0015	99.99	0.01	0.24	0.1087
1.00	2.54	0.22	0.0061	99.97	0.03	0.95	0.4324
1.50	3.81	0.48	0.0137	99.92	0.08	2.13	0.9673
2.00	5.08	0.85	0.0242	99.87	0.13	3.77	1.7098
2.50	6.35	1.33	0.0375	99.79	0.21	5.86	2.6560
3.00	7.62	1.90	0.0537	99.70	0.30	8.38	3.8025
3.50	8.89	2.57	0.0727	99.60	0.40	11.34	5.1453
4.00	10.16	3.33	0.0944	99.48	0.52	14.73	6.6809
4.50	11.43	4.19	0.1187	99.34	0.66	18.53	8.4055
5.00	12.70	5.15	0.1457	99.20	0.80	22.74	10.3154
5.50	13.97	6.19	0.1753	99.03	0.97	27.35	12.4068
6.00	15.24	7.32	0.2073	98.85	1.15	32.36	14.6762
6.50	16.51	8.54	0.2419	98.66	1.34	37.74	17.1198
7.00	17.78	9.85	0.2788	98.46	1.54	43.51	19.7338
7.50	19.05	11.23	0.3181	98.24	1.76	49.64	22.5146
8.00	20.32	12.70	0.3597	98.01	1.99	56.13	25.4585
8.50	21.59	14.25	0.4035	97.77	2.23	62.97	28.5618
9.00	22.86	15.88	0.4495	97.52	2.48	70.15	31.8207
9.50	24.13	17.58	0.4977	97.25	2.75	77.67	35.2316
10.00	25.40	19.35	0.5480	96.97	3.03	85.52	38.7907
10.50	26.67	21.20	0.6003	96.68	3.32	93.68	42.4943
11.00	27.94	23.12	0.6546	96.38	3.62	102.16	46.3388
11.50	29.21	25.10	0.7109	96.07	3.93	110.94	50.3204
12.00	30.48	27.16	0.7690	95.75	4.25	120.01	54.4354
12.50	31.75	29.28	0.8290	95.42	4.58	129.37	58.6801
13.00	33.02	31.46	0.8907	95.08	4.92	139.00	63.0509
13.50	34.29	33.70	0.9542	94.73	5.27	148.91	67.5439
14.00	35.56	36.00	1.0193	94.37	5.63	159.08	72.1556
14.50	36.83	38.36	1.0861	94.00	6.00	169.50	76.8821
15.00	38.10	40.77	1.1545	93.62	6.38	180.16	81.7198
15.50	39.37	43.24	1.2243	93.24	6.76	191.06	86.6650

Table 8. MHTB tanking table (Continued).

Height (in)	Height (cm)	Volume (ft^3)	Volume (m^3)	Ullage (%)	Liquid (%)	Liquid Mass (lbm)	Liquid Mass (kg)
16.00	40.64	45.76	1.2957	92.84	7.16	202.19	91.7140
16.50	41.91	48.32	1.3684	92.44	7.56	213.55	96.8630
17.00	43.18	50.94	1.4425	92.03	7.97	225.11	102.1084
17.50	44.45	53.60	1.5179	91.62	8.38	236.88	107.4464
18.00	45.72	56.31	1.5946	91.19	8.81	248.84	112.8734
18.50	46.99	59.06	1.6724	90.76	9.24	261.00	118.3856
19.00	48.26	61.85	1.7515	90.33	9.67	273.33	123.9794
19.50	49.53	64.68	1.8316	89.88	10.12	285.83	129.6510
20.00	50.80	67.55	1.9128	89.43	10.57	298.50	135.3967
20.50	52.07	70.45	1.9949	88.98	11.02	311.32	141.2128
21.00	53.34	73.39	2.0780	88.52	11.48	324.29	147.0957
21.50	54.61	76.35	2.1620	88.06	11.94	337.40	153.0415
22.00	55.88	79.35	2.2469	87.59	12.41	350.64	159.0467
22.50	57.15	82.37	2.3325	87.12	12.88	364.00	165.1074
23.00	58.42	85.42	2.4188	86.64	13.36	377.48	171.2200
23.50	59.69	88.49	2.5059	86.16	13.84	391.06	177.3808
24.00	60.96	91.59	2.5935	85.67	14.33	404.74	183.5861
24.50	62.23	94.71	2.6818	85.19	14.81	418.51	189.8321
25.00	63.50	97.84	2.7705	84.70	15.30	432.36	196.1152
25.50	64.77	100.99	2.8598	84.20	15.80	446.29	202.4317
26.00	66.04	104.16	2.9494	83.71	16.29	460.28	208.7778
26.50	67.31	107.34	3.0394	83.21	16.79	474.32	215.1498
27.00	68.58	110.53	3.1298	82.71	17.29	488.42	221.5441
27.50	69.85	113.73	3.2204	82.21	17.79	502.56	227.9569
28.00	71.12	116.93	3.3112	81.71	18.29	516.73	234.3845
28.50	72.39	120.15	3.4021	81.21	18.79	530.92	240.8233
29.00	73.66	123.36	3.4932	80.70	19.30	545.14	247.2695
29.50	74.93	126.58	3.5843	80.20	19.80	559.36	253.7193
30.00	76.20	129.80	3.6755	79.70	20.30	573.58	260.1718
30.50	77.47	133.02	3.7666	79.19	20.81	587.80	266.6225
31.00	78.74	136.23	3.8577	78.69	21.31	602.02	273.0731
31.50	80.01	139.45	3.9489	78.19	21.81	616.24	279.5237
32.00	81.28	142.67	4.0400	77.68	22.32	630.47	285.9743
32.50	82.55	145.89	4.1311	77.18	22.82	644.69	292.4250
33.00	83.82	149.11	4.2222	76.68	23.32	658.91	298.8756
33.50	85.09	152.33	4.3134	76.17	23.83	673.13	305.3262
34.00	86.36	155.54	4.4045	75.67	24.33	687.35	311.7768
34.50	87.63	158.76	4.4956	75.17	24.83	701.57	318.2275
35.00	88.90	161.98	4.5868	74.66	25.34	715.79	324.6781
35.50	90.17	165.20	4.6779	74.16	25.84	730.01	331.1287

Table 8. MHTB tanking table (Continued).

Height (in)	Height (cm)	Volume (ft^3)	Volume (m^3)	Ullage (%)	Liquid (%)	Liquid Mass (lbm)	Liquid Mass (kg)
36.00	91.44	168.42	4.7690	73.66	26.34	744.24	337.5793
36.50	92.71	171.63	4.8601	73.15	26.85	758.46	344.0300
37.00	93.98	174.85	4.9513	72.65	27.35	772.68	350.4806
37.50	95.25	178.07	5.0424	72.15	27.85	786.90	356.9312
38.00	96.52	181.29	5.1335	71.64	28.36	801.12	363.3818
38.50	97.79	184.51	5.2247	71.14	28.86	815.34	369.8325
39.00	99.06	187.73	5.3158	70.64	29.36	829.56	376.2831
39.50	100.33	190.94	5.4069	70.13	29.87	843.78	382.7337
40.00	101.60	194.16	5.4980	69.63	30.37	858.00	389.1843
40.50	102.87	197.38	5.5892	69.13	30.87	872.23	395.6350
41.00	104.14	200.60	5.6803	68.62	31.38	886.45	402.0856
41.50	105.41	203.82	5.7714	68.12	31.88	900.67	408.5362
42.00	106.68	207.03	5.8626	67.62	32.38	914.89	414.9868
42.50	107.95	210.25	5.9537	67.11	32.89	929.11	421.4375
43.00	109.22	213.47	6.0448	66.61	33.39	943.33	427.8881
43.50	110.49	216.69	6.1359	66.11	33.89	957.55	434.3387
44.00	111.76	219.91	6.2271	65.60	34.40	971.77	440.7893
44.50	113.03	223.13	6.3182	65.10	34.90	986.00	447.2400
45.00	114.30	226.34	6.4093	64.60	35.40	1000.22	453.6906
45.50	115.57	229.56	6.5005	64.09	35.91	1014.44	460.1412
46.00	116.84	232.78	6.5916	63.59	36.41	1028.66	466.5918
46.50	118.11	236.00	6.6827	63.09	36.91	1042.88	473.0425
47.00	119.38	239.22	6.7738	62.58	37.42	1057.10	479.4931
47.50	120.65	242.43	6.8650	62.08	37.92	1071.32	485.9437
48.00	121.92	245.65	6.9561	61.58	38.42	1085.54	492.3943
48.50	123.19	248.87	7.0472	61.07	38.93	1099.76	498.8450
49.00	124.46	252.09	7.1384	60.57	39.43	1113.99	505.2956
49.50	125.73	255.31	7.2295	60.07	39.93	1128.21	511.7462
50.00	127.00	258.53	7.3206	59.56	40.44	1142.43	518.1968
50.50	128.27	261.74	7.4117	59.06	40.94	1156.65	524.6475
51.00	129.54	264.96	7.5029	58.56	41.44	1170.87	531.0981
51.50	130.81	268.18	7.5940	58.05	41.95	1185.09	537.5487
52.00	132.08	271.40	7.6851	57.55	42.45	1199.31	543.9993
52.50	133.35	274.62	7.7763	57.05	42.95	1213.53	550.4500
53.00	134.62	277.83	7.8674	56.54	43.46	1227.76	556.9006
53.50	135.89	281.05	7.9585	56.04	43.96	1241.98	563.3512
54.00	137.16	284.27	8.0496	55.54	44.46	1256.20	569.8018
54.50	138.43	287.49	8.1408	55.03	44.97	1270.42	576.2525
55.00	139.70	290.71	8.2319	54.53	45.47	1284.64	582.7031
55.50	140.97	293.93	8.3230	54.03	45.97	1298.86	589.1537

Table 8. MHTB tanking table (Continued).

Height (in)	Height (cm)	Volume (ft^3)	Volume (m^3)	Ullage (%)	Liquid (%)	Liquid Mass (lbm)	Liquid Mass (kg)
56.00	142.24	297.14	8.4142	53.52	46.48	1313.08	595.6043
56.50	143.51	300.36	8.5053	53.02	46.98	1327.30	602.0550
57.00	144.78	303.58	8.5964	52.52	47.48	1341.53	608.5056
57.50	146.05	306.80	8.6875	52.01	47.99	1355.75	614.9562
58.00	147.32	310.02	8.7787	51.51	48.49	1369.97	621.4068
58.50	148.59	313.23	8.8698	51.01	48.99	1384.19	627.8575
59.00	149.86	316.45	8.9609	50.50	49.50	1398.41	634.3081
59.50	151.13	319.67	9.0521	50.00	50.00	1412.63	640.7587
60.00	152.40	322.89	9.1432	49.50	50.50	1426.85	647.2093
60.50	153.67	326.11	9.2343	48.99	51.01	1441.07	653.6600
61.00	154.94	329.33	9.3254	48.49	51.51	1455.29	660.1106
61.50	156.21	332.54	9.4166	47.99	52.01	1469.52	666.5612
62.00	157.48	335.76	9.5077	47.48	52.52	1483.74	673.0118
62.50	158.75	338.98	9.5988	46.98	53.02	1497.96	679.4625
63.00	160.02	342.20	9.6900	46.48	53.52	1512.18	685.9131
63.50	161.29	345.42	9.7811	45.97	54.03	1526.40	692.3637
64.00	162.56	348.63	9.8722	45.47	54.53	1540.62	698.8143
64.50	163.83	351.85	9.9633	44.97	55.03	1554.84	705.2650
65.00	165.10	355.07	10.0545	44.46	55.54	1569.06	711.7156
65.50	166.37	358.29	10.1456	43.96	56.04	1583.29	718.1662
66.00	167.64	361.51	10.2367	43.46	56.54	1597.51	724.6168
66.50	168.91	364.73	10.3278	42.95	57.05	1611.73	731.0675
67.00	170.18	367.94	10.4190	42.45	57.55	1625.95	737.5181
67.50	171.45	371.16	10.5101	41.95	58.05	1640.17	743.9687
68.00	172.72	374.38	10.6012	41.44	58.56	1654.39	750.4193
68.50	173.99	377.60	10.6924	40.94	59.06	1668.61	756.8700
69.00	175.26	380.82	10.7835	40.44	59.56	1682.83	763.3206
69.50	176.53	384.03	10.8746	39.93	60.07	1697.06	769.7712
70.00	177.80	387.25	10.9657	39.43	60.57	1711.28	776.2218
70.50	179.07	390.47	11.0569	38.93	61.07	1725.50	782.6725
71.00	180.34	393.69	11.1480	38.42	61.58	1739.72	789.1231
71.50	181.61	396.91	11.2391	37.92	62.08	1753.94	795.5737
72.00	182.88	400.13	11.3303	37.42	62.58	1768.16	802.0243
72.50	184.15	403.34	11.4214	36.91	63.09	1782.38	808.4750
73.00	185.42	406.56	11.5125	36.41	63.59	1796.60	814.9256
73.50	186.69	409.78	11.6036	35.91	64.09	1810.82	821.3762
74.00	187.96	413.00	11.6948	35.40	64.60	1825.05	827.8268
74.50	189.23	416.22	11.7859	34.90	65.10	1839.27	834.2775
75.00	190.50	419.43	11.8770	34.40	65.60	1853.49	840.7281
75.50	191.77	422.65	11.9682	33.89	66.11	1867.71	847.1787

Table 8. MHTB tanking table (Continued).

Height (in)	Height (cm)	Volume (ft^3)	Volume (m^3)	Ullage (%)	Liquid (%)	Liquid Mass (lbm)	Liquid Mass (kg)
76.00	193.04	425.87	12.0593	33.39	66.61	1881.93	853.6293
76.50	194.31	429.09	12.1504	32.89	67.11	1896.15	860.0800
77.00	195.58	432.31	12.2415	32.38	67.62	1910.37	866.5306
77.50	196.85	435.53	12.3327	31.88	68.12	1924.59	872.9812
78.00	198.12	438.74	12.4238	31.38	68.62	1938.82	879.4318
78.50	199.39	441.96	12.5149	30.87	69.13	1953.04	885.8824
79.00	200.66	445.18	12.6061	30.37	69.63	1967.26	892.3331
79.50	201.93	448.40	12.6972	29.87	70.13	1981.48	898.7837
80.00	203.20	451.62	12.7883	29.36	70.64	1995.70	905.2343
80.50	204.47	454.83	12.8794	28.86	71.14	2009.92	911.6849
81.00	205.74	458.05	12.9706	28.36	71.64	2024.14	918.1356
81.50	207.01	461.27	13.0617	27.85	72.15	2038.36	924.5862
82.00	208.28	464.49	13.1528	27.35	72.65	2052.58	931.0368
82.50	209.55	467.71	13.2440	26.85	73.15	2066.81	937.4874
83.00	210.82	470.93	13.3351	26.34	73.66	2081.03	943.9381
83.50	212.09	474.14	13.4262	25.84	74.16	2095.25	950.3887
84.00	213.36	477.36	13.5173	25.34	74.66	2109.47	956.8393
84.50	214.63	480.58	13.6085	24.83	75.17	2123.69	963.2899
85.00	215.90	483.80	13.6996	24.33	75.67	2137.91	969.7406
85.50	217.17	487.02	13.7907	23.83	76.17	2152.13	976.1912
86.00	218.44	490.23	13.8819	23.32	76.68	2166.35	982.6418
86.50	219.71	493.45	13.9730	22.82	77.18	2180.58	989.0924
87.00	220.98	496.67	14.0641	22.32	77.68	2194.80	995.5431
87.50	222.25	499.89	14.1552	21.81	78.19	2209.02	1001.9937
88.00	223.52	503.11	14.2464	21.31	78.69	2223.24	1008.4443
88.50	224.79	506.33	14.3375	20.80	79.20	2237.46	1014.8949
89.00	226.06	509.54	14.4286	20.30	79.70	2251.68	1021.3456
89.50	227.33	512.76	14.5198	19.80	80.20	2265.90	1027.7962
90.00	228.60	515.98	14.6108	19.30	80.70	2280.12	1034.2433
90.50	229.87	519.19	14.7019	18.79	81.21	2294.33	1040.6895
91.00	231.14	522.41	14.7929	18.29	81.71	2308.52	1047.1282
91.50	232.41	525.61	14.8837	17.79	82.21	2322.69	1053.5559
92.00	233.68	528.81	14.9743	17.29	82.71	2336.83	1059.9687
92.50	234.95	532.00	15.0646	16.79	83.21	2350.93	1066.3630
93.00	236.22	535.18	15.1546	16.29	83.71	2364.98	1072.7350
93.50	237.49	538.35	15.2443	15.80	84.20	2378.97	1079.0811
94.00	238.76	541.50	15.3335	15.30	84.70	2392.89	1085.3976
94.50	240.03	544.63	15.4223	14.81	85.19	2406.74	1091.6807
95.00	241.30	547.75	15.5105	14.33	85.67	2420.51	1097.9267
95.50	242.57	550.84	15.5982	13.84	86.16	2434.19	1104.1320

Table 8. MHTB tanking table (Continued).

Height (in)	Height (cm)	Volume (ft^3)	Volume (m^3)	Ullage (%)	Liquid (%)	Liquid Mass (lbm)	Liquid Mass (kg)
96.00	243.84	553.92	15.6852	13.36	86.64	2447.78	1110.2928
96.50	245.11	556.97	15.7716	12.88	87.12	2461.25	1116.4054
97.00	246.38	559.99	15.8572	12.41	87.59	2474.61	1122.4661
97.50	247.65	562.99	15.9420	11.94	88.06	2487.85	1128.4713
98.00	248.92	565.95	16.0260	11.48	88.52	2500.96	1134.4171
98.50	250.19	568.89	16.1091	11.02	88.98	2513.93	1140.3000
99.00	251.46	571.79	16.1913	10.57	89.43	2526.75	1146.1161
99.50	252.73	574.66	16.2724	10.12	89.88	2539.42	1151.8618
100.00	254.00	577.49	16.3526	9.67	90.33	2551.92	1157.5334
100.50	255.27	580.28	16.4316	9.24	90.76	2564.26	1163.1272
101.00	256.54	583.03	16.5095	8.81	91.19	2576.41	1168.6394
101.50	257.81	585.73	16.5861	8.38	91.62	2588.37	1174.0664
102.00	259.08	588.40	16.6615	7.97	92.03	2600.14	1179.4044
102.50	260.35	591.01	16.7356	7.56	92.44	2611.71	1184.6498
103.00	261.62	593.58	16.8084	7.16	92.84	2623.06	1189.7988
103.50	262.89	596.10	16.8797	6.76	93.24	2634.19	1194.8478
104.00	264.16	598.57	16.9496	6.38	93.62	2645.09	1199.7930
104.50	265.43	600.98	17.0179	6.00	94.00	2655.76	1204.6307
105.00	266.70	603.34	17.0847	5.63	94.37	2666.18	1209.3572
105.50	267.97	605.64	17.1498	5.27	94.73	2676.34	1213.9689
106.00	269.24	607.88	17.2133	4.92	95.08	2686.25	1218.4619
106.50	270.51	610.06	17.2751	4.58	95.42	2695.88	1222.8327
107.00	271.78	612.18	17.3350	4.25	95.75	2705.24	1227.0774
107.50	273.05	614.23	17.3932	3.93	96.07	2714.31	1231.1924
108.00	274.32	616.22	17.4494	3.62	96.38	2723.09	1235.1740
108.50	275.59	618.14	17.5037	3.32	96.68	2731.57	1239.0185
109.00	276.86	619.99	17.5560	3.03	96.97	2739.73	1242.7221
109.50	278.13	621.76	17.6063	2.75	97.25	2747.58	1246.2812
110.00	279.40	623.46	17.6545	2.48	97.52	2755.10	1249.6921
110.50	280.67	625.09	17.7005	2.23	97.77	2762.28	1252.9510
111.00	281.94	626.64	17.7444	1.99	98.01	2769.13	1256.0543
111.50	283.21	628.11	17.7860	1.76	98.24	2775.62	1258.9981
112.00	284.48	629.49	17.8253	1.54	98.46	2781.75	1261.7790
112.50	285.75	630.80	17.8622	1.34	98.66	2787.51	1264.3930
113.00	287.02	632.02	17.8967	1.15	98.85	2792.90	1266.8366
113.50	288.29	633.15	17.9288	0.97	99.03	2797.90	1269.1060
114.00	289.56	634.19	17.9583	0.80	99.20	2802.51	1271.1974
114.50	290.83	635.15	17.9853	0.66	99.34	2806.72	1273.1073
115.00	292.10	636.01	18.0097	0.52	99.48	2810.52	1274.8319
115.50	293.37	636.77	18.0313	0.40	99.60	2813.91	1276.3675

Table 8. MHTB tanking table (Continued).

Height (in)	Height (cm)	Volume (ft^3)	Volume (m^3)	Ullage (%)	Liquid (%)	Liquid Mass (lbm)	Liquid Mass (kg)
116.00	294.64	637.44	18.0503	0.30	99.70	2816.87	1277.7103
116.50	295.91	638.01	18.0665	0.21	99.79	2819.40	1278.8567
117.00	297.18	638.49	18.0799	0.13	99.87	2821.48	1279.8030
117.50	298.45	638.86	18.0904	0.08	99.92	2823.12	1280.5455
118.00	299.72	639.12	18.0979	0.03	99.97	2824.30	1281.0804
118.50	300.99	639.28	18.1025	0.01	99.99	2825.01	1281.4041
119.00	302.26	639.34	18.1040	0.00	100.00	2825.25	1281.5128

APPENDIX B—MULTIPURPOSE HYDROGEN TEST BED TEST ARTICLE INSTRUMENTATION

Appendix B contains the instrumentation database document that describes the MHTB instrumentation used in the spray bar performance testing. Some of the information repeats that presented in the main body of this Technical Memorandum and some is applicable only to previously performed thermal insulation testing. However, in the interest of completeness, the entire document is presented.

Multipurpose Hydrogen Test Bed (MHTB)
Instrumentation Data Base

James Martin/EP25

This document details the instrumentation use on the Multipurpose Hydrogen Test Bed hardware. This includes instrumentation used on the tank interior/exterior, tank insulation/penetrations, tank support system and environmental shroud. This document is dedicated primarily to instrumentation which was installed during fabrication and assembly of test hardware, however, some facility instrumentation is noted if it is mounted in close proximity to the test hardware.

The breakdown of test article instrumentation is outlined by the following categories:

1) MHTB Program Over View and Hardware Description
2) MHTB Tank General Instrumentation Layout
3) MHTB Thermal Control System Instrumentation
4) MHTB Support Leg Penetration Instrumentation
5) MHTB Vent Penetration Instrumentation
6) MHTB Fill / Drain Penetration Instrumentation
7) MHTB Pressurization Penetration Instrumentation
8) MHTB MLI Interstitial Pressure Probe Instrumentation
9) MHTB Manhole Cover and Pump Out Penetration Instrumentation
10) MHTB Internal Rake and Fluid Instrumentation
11) MHTB Environmental Shroud Instrumentation
12) MHTB Zero-g Thermodynamic Vent System Instrumentation

Related Documents

1) MHTB Test Requirements Document (EP25 (93-25))
2) MHTB Thermal Control Subsystem (TCS) Test Plan (EP25 (94-04))
3) MHTB Pre-Installation Operations Document (EP25(94-13))
4) MHTB Thermodynamic Vent System (TVS) Test Plan (EP25(94-12))
5) MHTB Thermodynamic Vent System Installation Procedure

1) MHTB Program Over View and Hardware Description

The MSFC has established a technology/advanced development program to address the area of Cryogenic Fluid Management (CFM) for orbital applications, an area common to practically all future space programs. As part of this activity a test bed, termed the multipurpose hydrogen test bed (MHTB), was devised such that a variety of CFM subsystems could be integrated and evaluated in a ground based test environment. To minimize the reliance on scaling analyses in extrapolating overall performance data, the test bed is representative in both size and shape to that of a full scale space transfer vehicle liquid hydrogen tank. Current plans baseline testing of two key technology needs in representative spacecraft thermal and vacuum environments. The first involves evaluation of a foam multilayer insulation (FMLI) thermal control concept. This concept incorporates a spray on foam insulation (SOFI) attached to the surface of the test bed tank and is in turn covered with a 45 layer variable density multilayer insulation (MLI) blanket. This blanket is constructed of double aluminized mylar (DAM) sheets separated by Dacron netting. The second, an active tank pressure control system, is referred to as a zero-g thermodynamic vent system (TVS). This hardware will be installed after completion of the TCS test phase and consists of a tank internal spray bar/heat exchanger and tank external recirculation pump, Joule Thompson valve and back pressure orifice. More information regarding exact details of each test program can be found in the respective subsystem test plans.

The MHTB tank is constructed of aluminum 5083 and has a cylindrical shape with both a height and diameter of 3.05 m (10 ft) and elliptical domes as shown in figure 84. The tank has an internal volume of 18.09 m^3 (639 ft^3) with a surface area to volume ratio of 1.92 l/m (0.58 l/ft). The tank was designed and constructed per the ASME code (section VIII, Division 1) for a working differential pressure of 344 kPa (50 psig). The tank's total weight is 1270 kg (2800 lbm). The tank is equipped with a variety of penetrations, supporting hardware, and technology subsystems illustrated in figure 84.

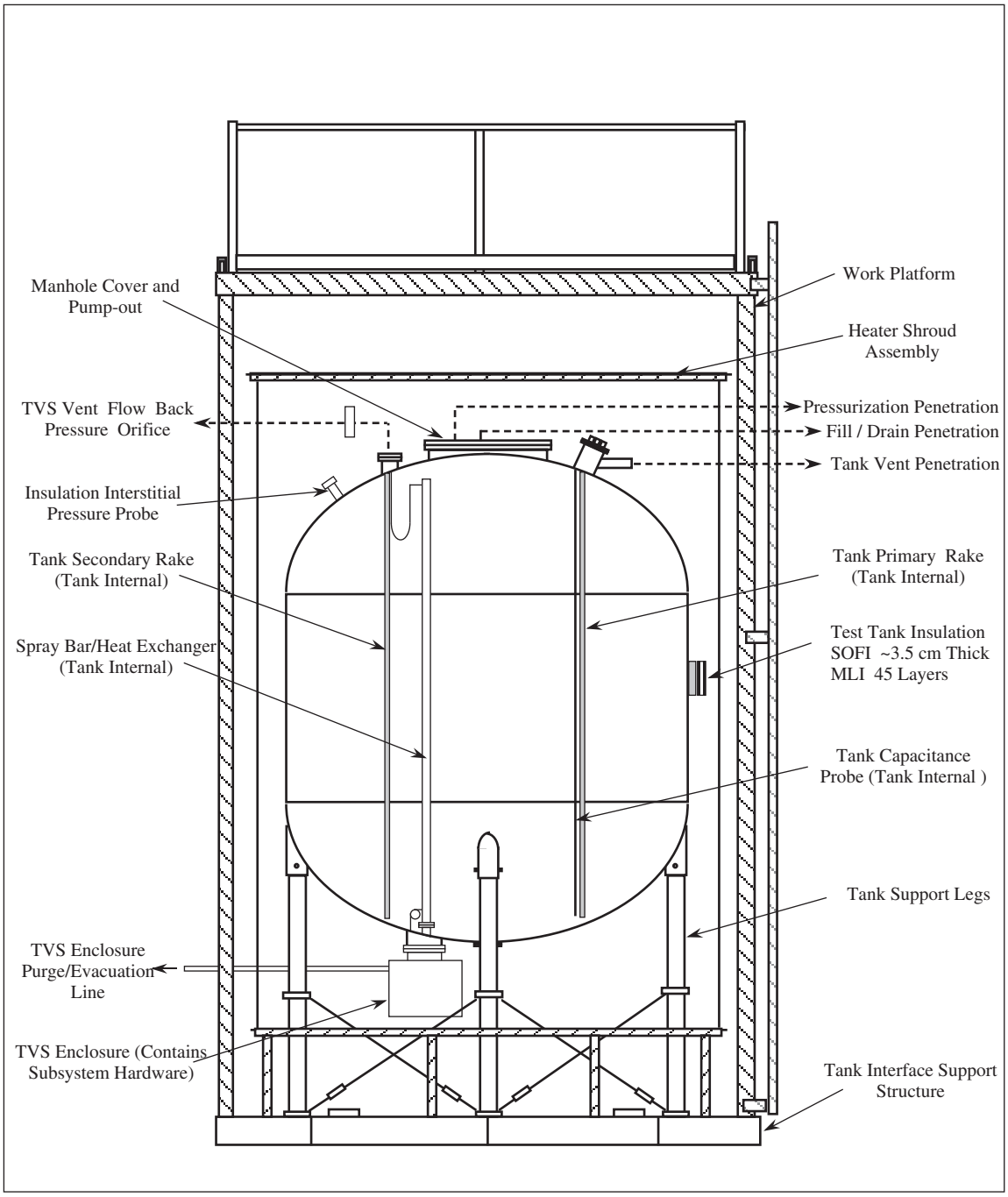

Figure 84. General MHTB tank schematic.

2) General MHTB Tank Instrumentation Layout

The general layout of instrumentation on the test bed is illustrated in figures 85–87. These figures represent the top, front and bottom views of the test tank without insulation to avoid confusion. However, the seams between major MLI blanket assemblies are indicated by dotted lines. A detailed description of instrumentation numbers and profiles shown on these figures is discussed in later document sections and Appendix A. Most of the instrumentation is composed of silicon diodes and thermocouples for measurement of thermal gradients (several pressure transducers are present). Typically, silicon diodes (Lakeshore type DT-470-11A) temperature transducers are placed in areas of lowest temperatures because they possess a higher accuracy at these temperatures when compared to thermocouples. Typical low temperature areas include the tank aluminum shell and SOFI material covering the tank. Thermocouples (Type E) are used in regions of higher temperature, such as within the MLI or on surfaces somewhat distant from the test tank contact point, where their accuracy becomes somewhat improved. The bulk of the instrumentation leads for components residing on the upper bulkhead and barrel section were routed toward the tank vent flange, while those on the lower bulkhead were routed out leg #1. There were some exceptions to this rule. Some of the penetration instrumentation was easier to route out along the respective penetration rather than snaking it to the vent or leg #1 area.

The tank orientation with respect to the vacuum chamber is such that the 0^{o} reference is directed from the test tank center through the secondary instrumentation rake penetration toward the chamber door. Positive angle measurement from this reference is taken in a clockwise location from a vacuum chamber perspective looking down on top of the test article. The complete MHTB instrumentation data base is included in Appendix A of this document.

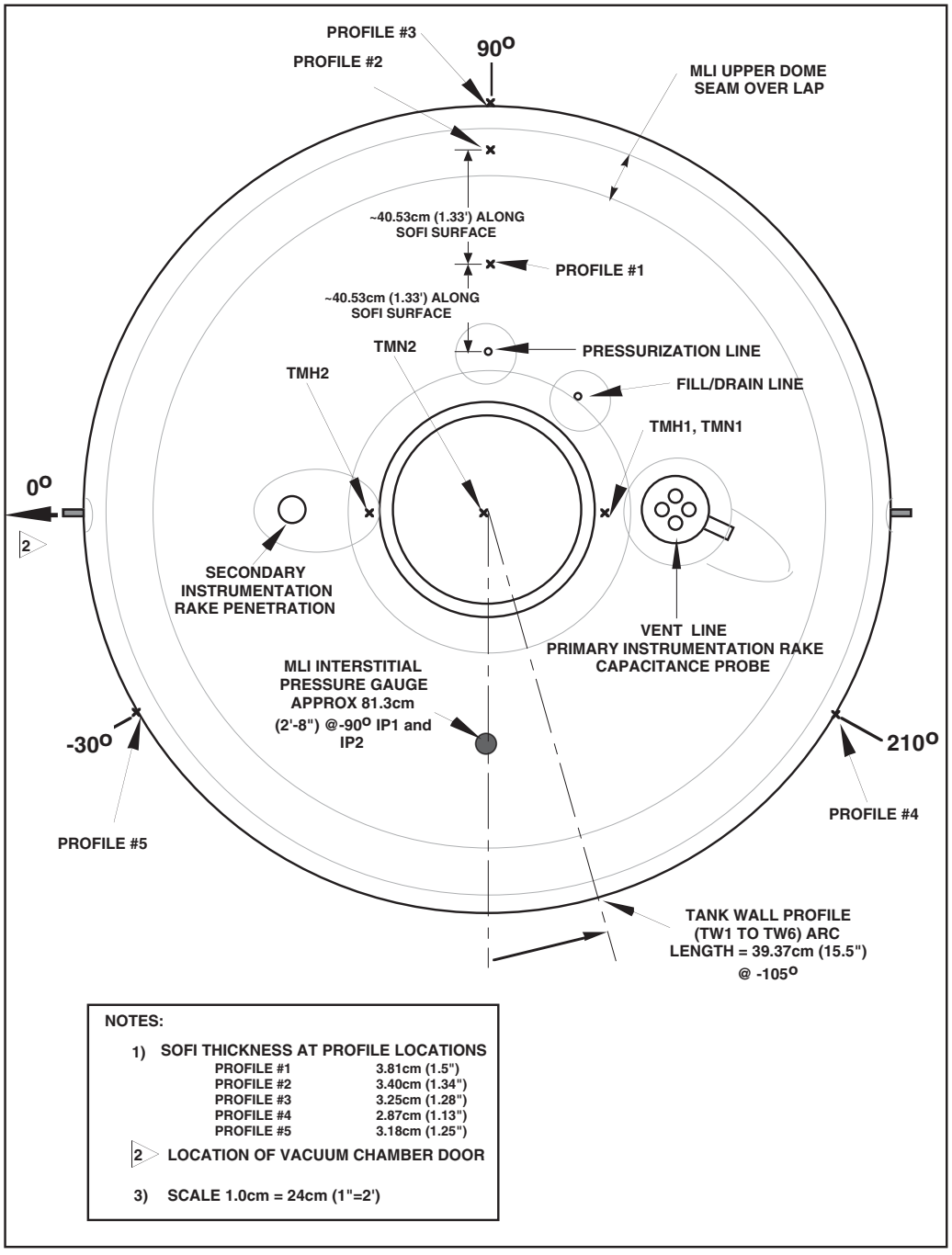

Figure 85. MHTB tank instrumentation top view.

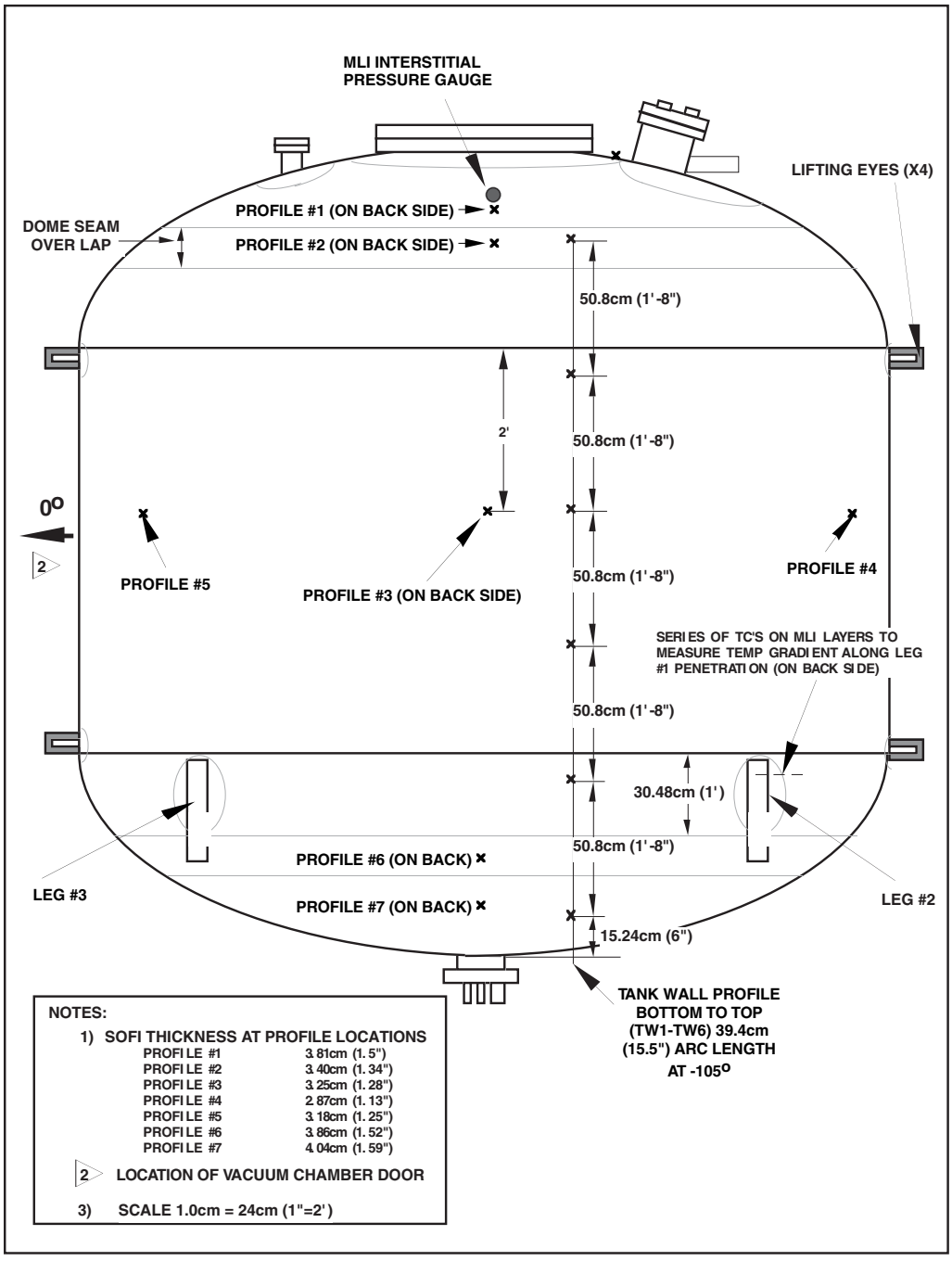

Figure 86. MHTB tank instrumentation side view.

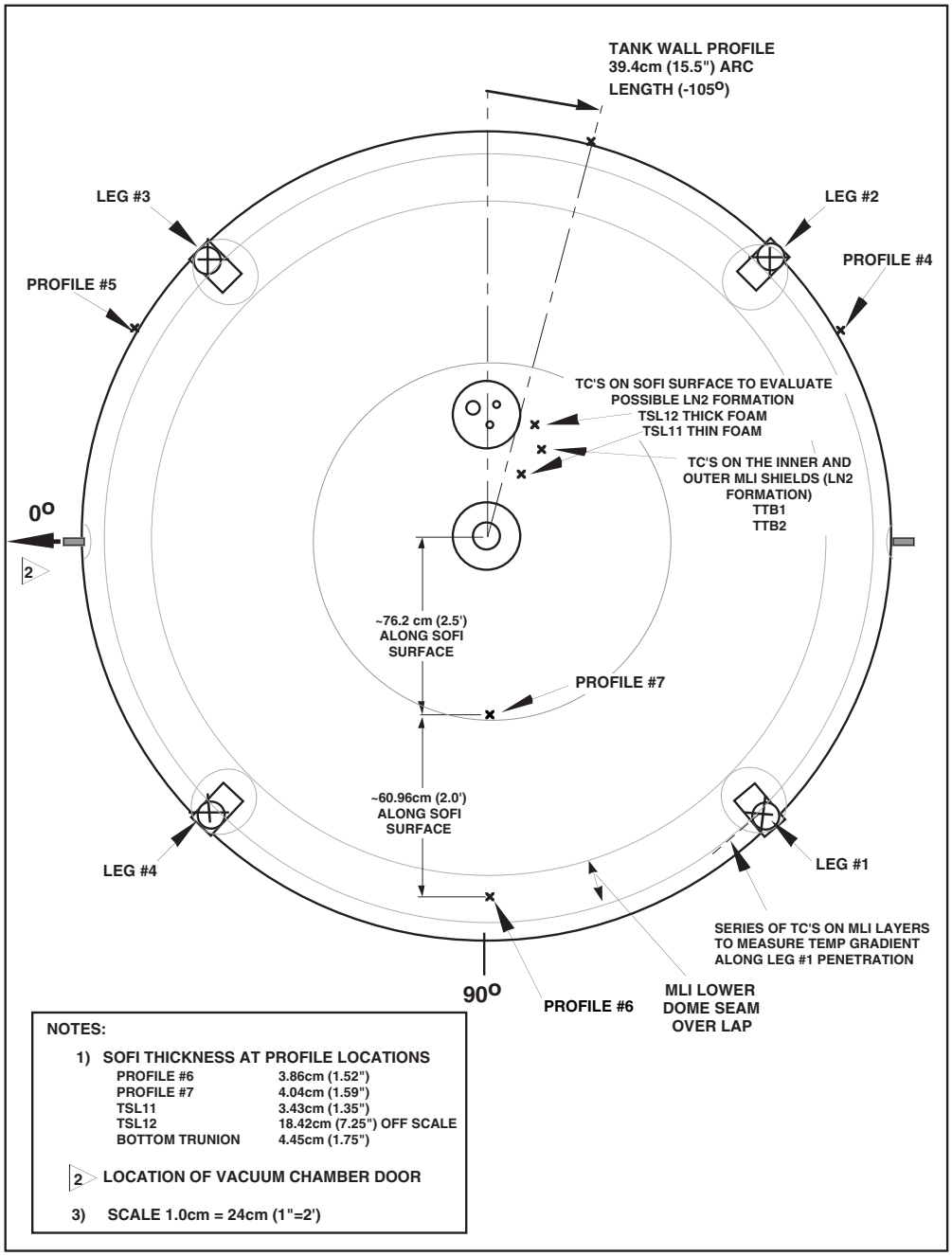

Figure 87. MHTB tank instrumentation bottom view.

3) MHTB Thermal Control System Instrumentation

A total of seven instrumentation profiles are incorporated into the test tank FMLI insulation with each profile composed of one silicon diode and four thermocouples. Figure 88 illustrates the typical location of each piece of instrumentation within the insulation layers. The diode (TSF#) was attached to the foam surface using a cryogenic epoxy (Lakeshore Stycast) while the thermocouples (TM#, TMI#, TMM# and TMO#) were attached to the MLI shields by using a piece of aluminized tape. In an effort to limit heat leak along the thermocouple leads toward the bead attachment point, approximately 5.08cm (2") of lead wire was spiraled around the bead (and placed under the tape). Additionally, each thermocouple lead was routed out (toward the exit point) along the same MLI shield to which it was attached. The thermocouples TM# were attached to the outer surface of the inner most MLI shield. The thermocouples TMI# were attached to the outer surface of the 10 MLI shield (interface between low and medium density MLI spacing). The thermocouples TMM# were attached to the outer surface of the 25 MLI shield (interface between medium and high density MLI spacing). The thermocouples TMO# were attached to the outer surface of the outer most MLI shield (shield 45 of the high density MLI spacing). The aluminized tape used to attach the thermocouples was manufactured by Lamart Corporation and was type #326L. This tape is electrically conductive on the exterior surface and has the same approximate surface emissivity as the DAM. The tape was purchased from:

Can-Do Incorporated
P.O. Box 4366
Nashville, Tn 37204
Tele. (615) 383-1775

At each instrumentation profile the SOFI thickness was measured using a Kaman eddy current device. Figures 85–87 indicate the SOFI thickness measured at each profile location. These thicknesses will be used in determining the thermal performance of the foam insulation. Data concerning each piece of instrumentation attached to the tank insulation is included in Appendix A.

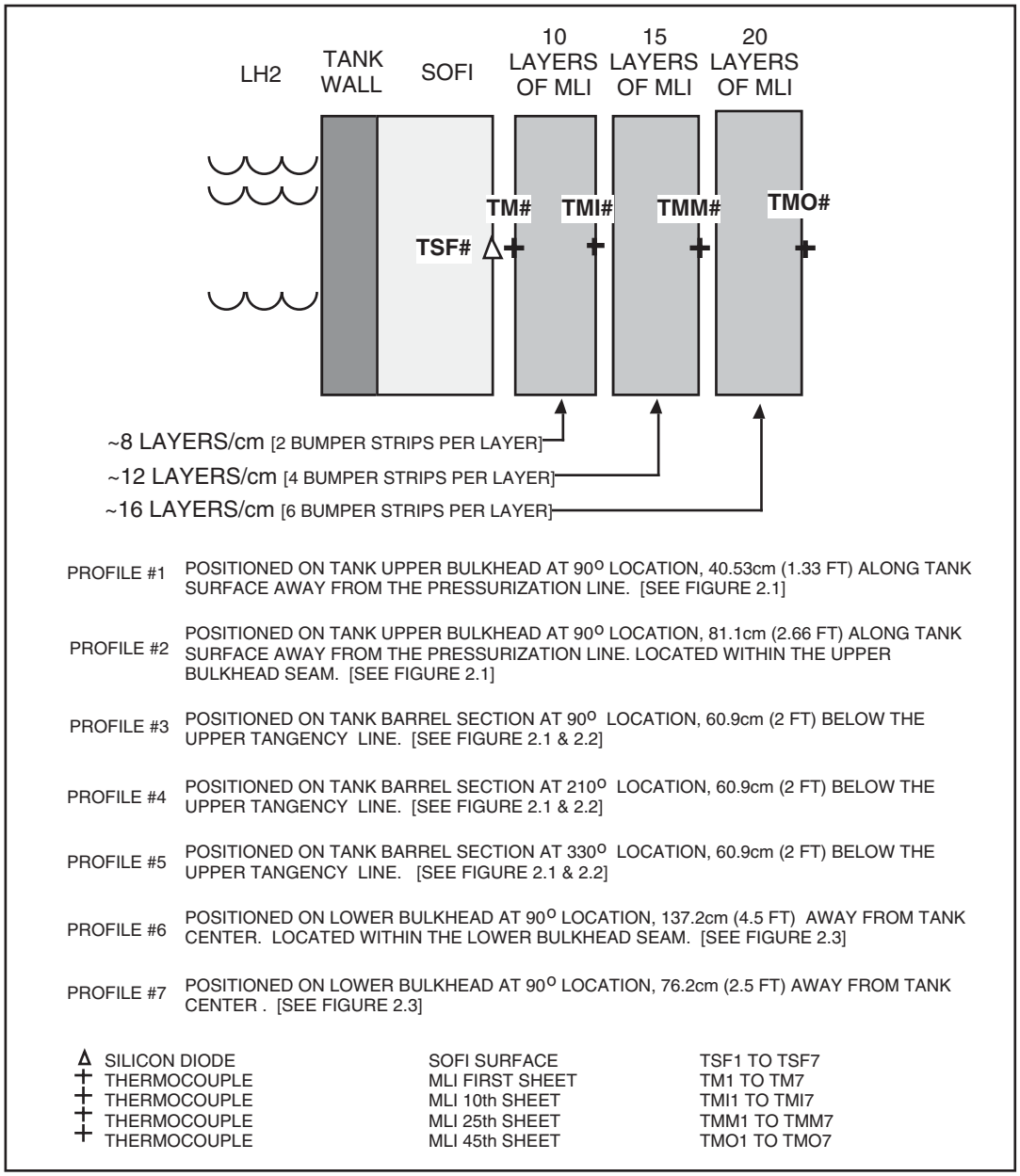

Figure 88. Typical insulation instrumentation profile.

4) MHTB Support Leg Penetration Instrumentation

The MHTB is supported by four legs as shown in figures 86 and 87. Each leg is comprised of two composite sections joined in the center by a stainless steel union. Each leg end is also equipped with stainless steel end caps which mount to the test tank and interface support structure. Two of the four tank legs are instrumented one of which, leg #1, is heavily instrumented as shown in figure 89. Silicon diodes (TSL1 and TSL2) and thermocouples (TSL5 through TSL10) are attached to the composite material (diodes closest to the tank) for determination of heat input along the support. Diodes TSL3 and TSL4 have been placed on leg #3. Each leg is equipped with a heat guard to reduce the amount of heat input. Legs #1 and #3 are instrumented with diodes (HG1 and HG3, respectively) to measure the heat guard boundary temperature. The SOFI surface (TSL17, TSL18 and TSL19) and MLI (TL13 through TL19) are also instrumented for determination of the insulation temperature profile. There are also thermocouples (TSL14 on leg #1 and TSL15 on leg #3) attached to the innermost layer of crumpled MLI (against foam) which occupies the hollow interior of the legs. These measurements will be used to determine if condensation of the insulation gaseous nitrogen (GN_2) purge gas occurs within the legs. A foam plug approximately 10.16cm (4") thick was poured into the top section of each leg's interior (above the MLI) to prevent potential condensation. The outer surface of each leg was also closed out with pour foam starting at the tank SOFI and extending out over the composite to a distance of approximately 15.24 cm (6"). Average foam thickness was based on the applied foam circumference measurements and determined to be 3.81 cm (1.5") for legs 1, 3 and 4 and 4.445 cm (1.75") for leg #2. The leg stainless steel center joint and interface support structure attachment point were instrumented with thermocouples for legs #1 (TLB1 and ISS1) and #3 (TLB3 and ISS3). Appendix A contains, in a data base format, additional information concerning the tank leg instrumentation.

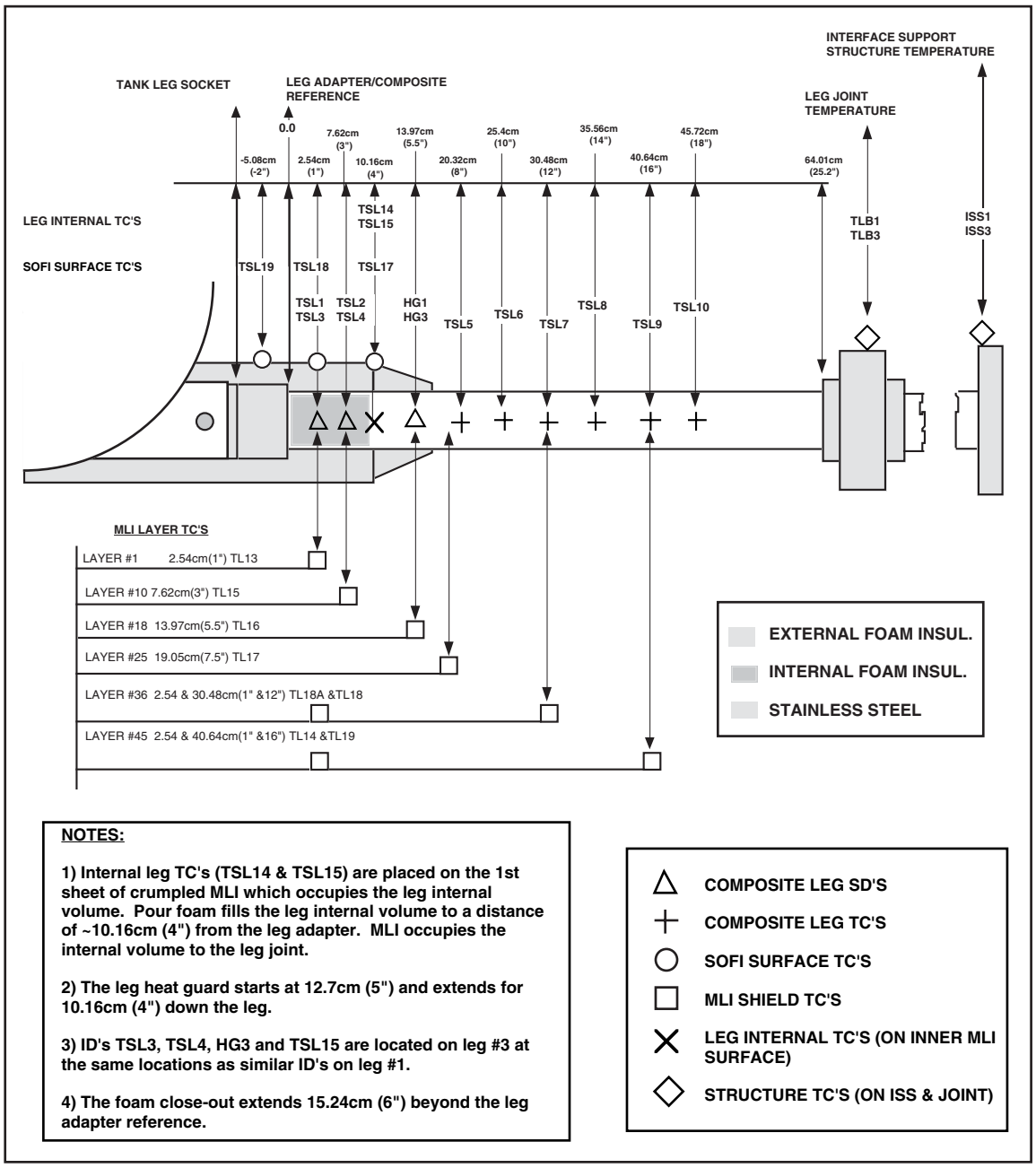

Figure 89. Leg No. 1 instrumentation locations.

5) MHTB Vent Penetration Instrumentation

The MHTB tank internal volume is vented through a 5.08 cm (2") diameter tube connected to a 20.32 cm (8") tank penetration (Conflat type flange) as illustrated in figure 90. The vent tube transitions to a vacuum jacketed pipe assembly approximately 30.48 cm (12") from the tank penetration. The penetration and tube are closed out with foam extending out over the vacuum jacketed pipe section approximately 40.64 cm (16") from the tank penetration. Average thickness of this foam based on the measured circumference is 6.98 cm (2.75"). Three silicon diodes are place along the length of the tube for determination of heat input (TVL1 and TVL2) and evaluation of the heat guard (HG7) operation. The vent tube foam surface is instrumented with two thermocouples (TVL6 and TVL7) to assist in evaluation of heat input through the foam. The vent penetration top flange contains a tank ullage pressure measurement port and 1.27 cm (0.5") diameter sampling tube which is equipped with two thermocouples (TUP1 and TUP2). The surface temperature of the top flange is measured by a silicon diode (TVL3). Internal to the tank, the vent flange supports a capacitance probe (CAP1) and an instrumentation rake. Two diodes (TVL4 and TVL5) are supported by the rake at the 99.4% tank fill location. These diodes are positioned just below the vent penetration (inside the test tank) and provide a measurement of the out flowing gas temperature. Details regarding the instrumentation rakes will be described in a later section. Appendix A contains, in a data base format, additional information regarding this instrumentation.

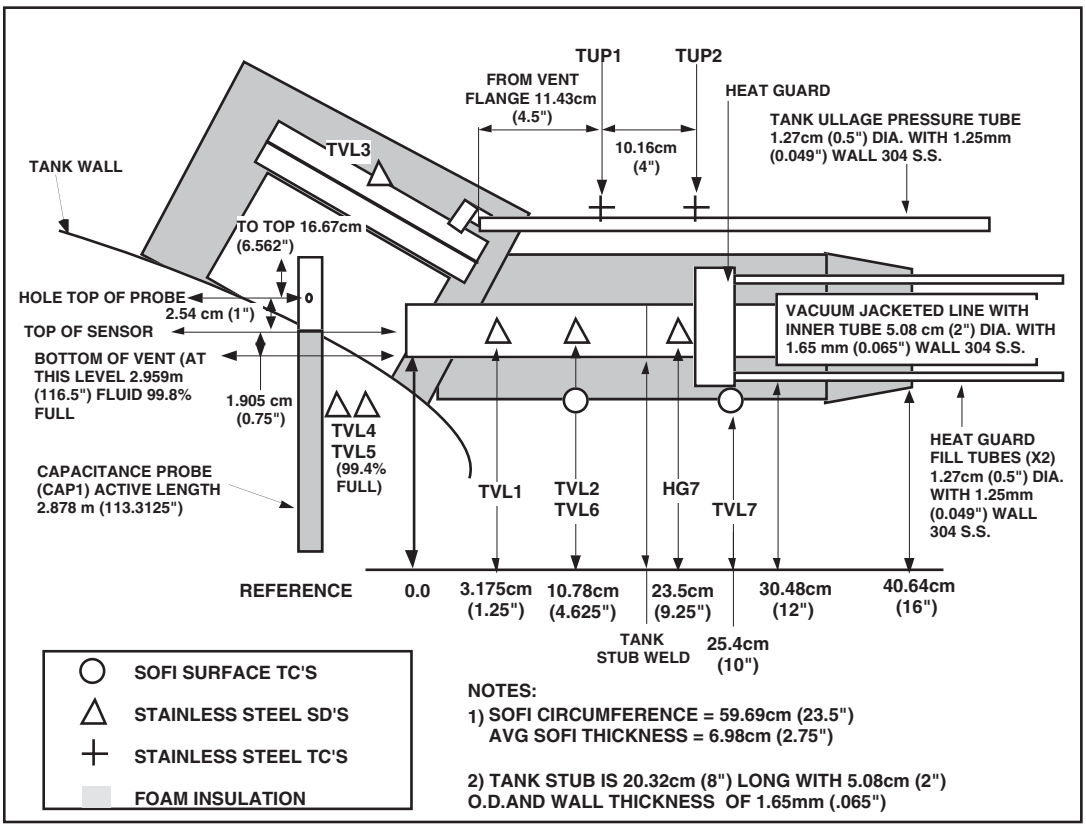

Figure 90. MHTB tank vent penetration instrumentation.

6) MHTB Fill/Drain Penetration Instrumentation

The MHTB LH_2 fluid service is provided through a 2.54 cm (1") diameter fill/drain tube attached to the test tank with an aluminum to stainless steel transition joint as illustrated in figure 91. The fill/drain tube transitions to a vacuum jacketed pipe assembly 16.51cm (6.5") from the tank penetration. A foam close-out is applied to the line and extends out over the vacuum jacketed pipe section approximately 35.56 cm (14") from the tank penetration. The average foam thickness around the fill/drain line is 6.604cm (2.6") based on the measured circumference. The tube is instrument with three silicon diodes placed along its length to determine heat input (TFD1 and TFD2) and operation of the heat guard (HG6). The outer surface of the foam is also instrumented with two thermocouples (TFD3 and TFD4) to assist in evaluation of heat input through the foam. Appendix A contains, in a data base format, additional information regarding this instrumentation.

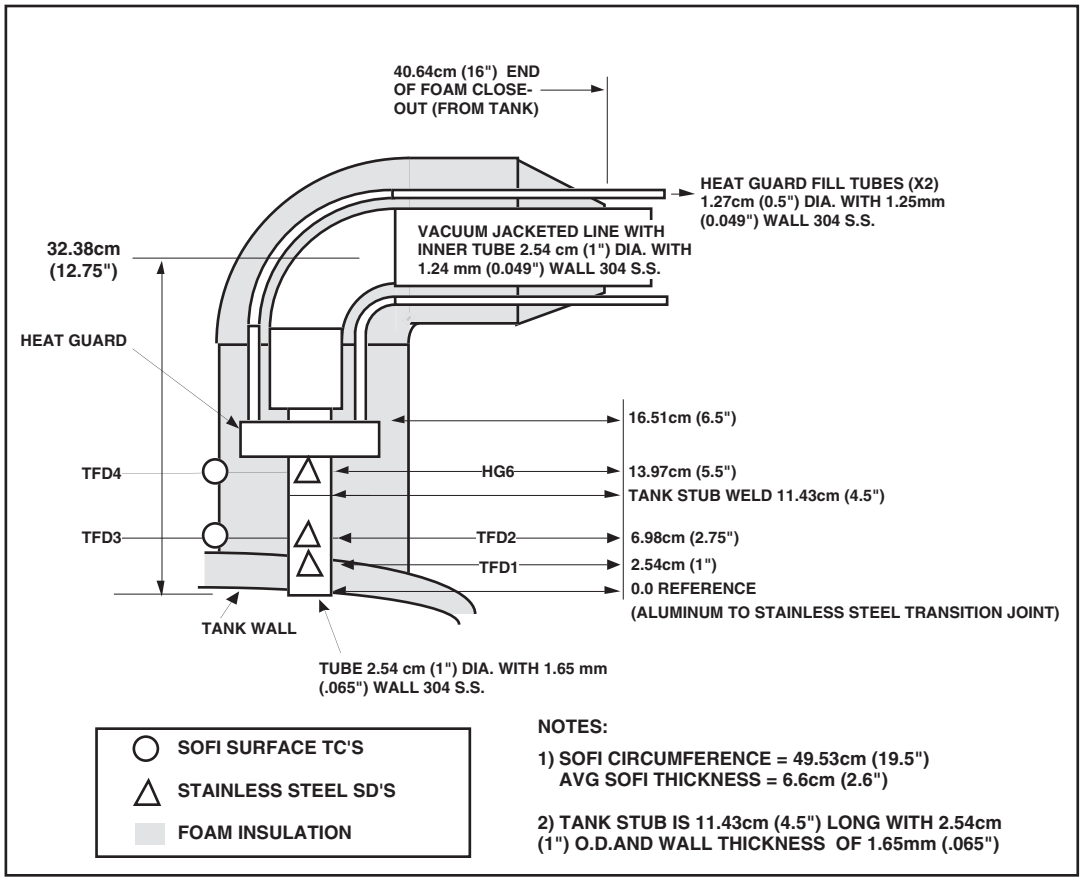

Figure 91. MHTB tank fill/drain penetration instrumentation.

7) MHTB Pressurization Penetration Instrumentation

The MHTB tank internal volume is pressurized using a 2.54 cm (1") diameter tube attached to the tank with an aluminum to stainless steel transition joint as illustrated in figure 92. The pressurization tube transitions to a double walled jacketed pipe assembly (used for gas conditioning purposes) 32.385 cm (12.75") from the tank wall. A foam close-out extends out over the jacketed pipe section approximately 40.64 cm (16") from the tank penetration. The average foam thickness around the pressurization line is 3.556 cm (1.4") based on the measured circumference. Three silicon diodes are place along the length of the tube, between the tank and heat guard, for determination of heat input (TPL1 and TPL2) and evaluation of the heat guard (HG5) operation. The line is also equipped with two thermocouples, (TPS1) used to measure the temperature of the pressurant gas flow within the line, and (TPS2) used to measures the pressurization line outer jacket temperature. The outer surface of the foam close-out is also instrumented with two thermocouples (TPL3 and TPL4) to assist in evaluation of heat input through the foam. Appendix A contains, in a data base format, additional information regarding this instrumentation.

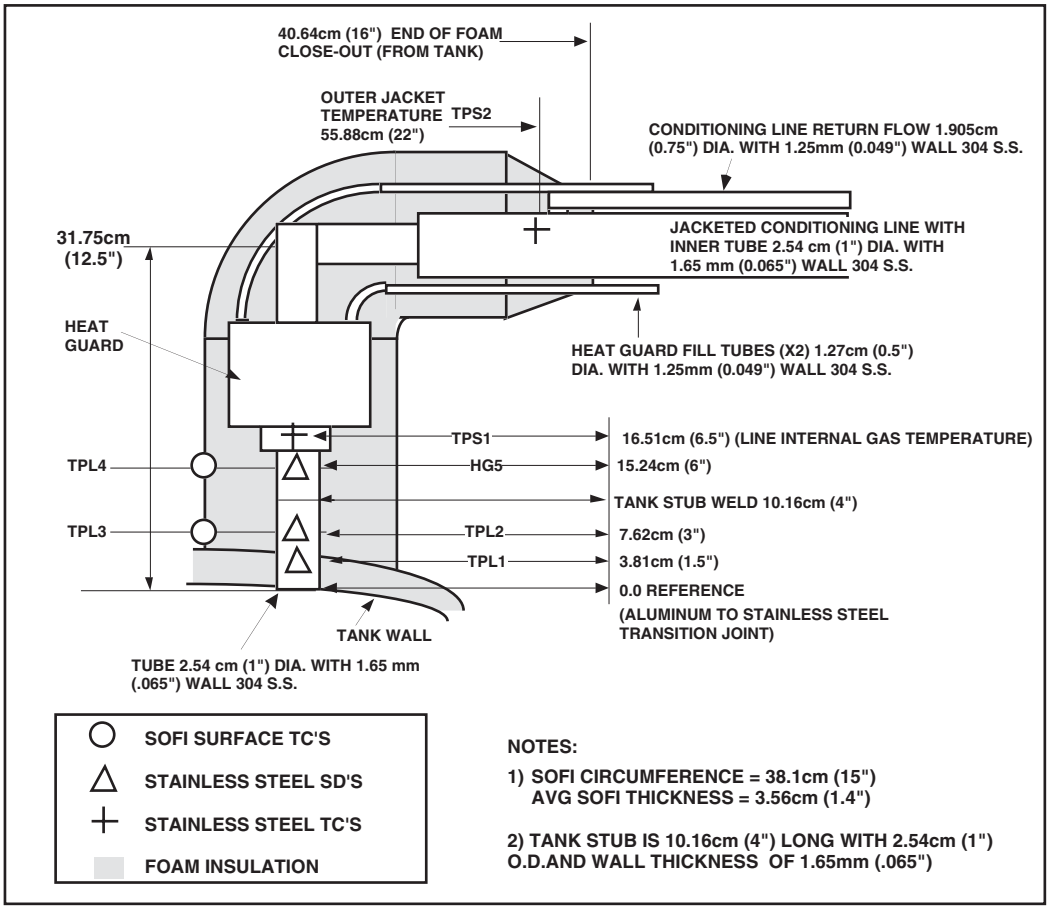

Figure 92. MHTB tank pressurization penetration instrumentation.

8) MHTB MLI Interstitial Pressure Probe Instrumentation

The gas pressure at the foam/MLI interface is measured with two pressure sensors mounted on top of a 5.08 cm (2") diameter thin wall probe that has a length of 22.86 cm (9") as illustrated in figure 93. This probe rests on the tank SOFI surface and is supported by the MLI which is taped out layer by layer to the surrounding MLI and to the probe body so as to prevent leakage of trapped MLI gases. The probe is also equipped with a 6.35mm (0.25") diameter sampling port for obtaining both dew point levels (using a hydrometer) and gas species samples (using a residual gas analyzer) from within the MLI. The two pressure transducers, a Gran Philips 275 (IP1) and a cold cathode (IP2), cover a complete pressure range from 760 to 10^{-7} torr. The Gran Philips gauge is remote mounted (for easier access) on top of the heater shroud and connected to the probe body using a flex hose. The probe body tube is equipped with three thermocouples placed along its length (IPP1, IPP2 and IPP3) to determine heat input through the probe. This probe, if necessary, shall be supported off of the tank heater shroud structure using stainless steel wire and springs to absorb transportation loads. The dew point measurement within the MLI is taken with a facility supplied Endress Hauser Model #2200 Hydrometer (DEW1). The sensing head for this unit is located in the MLI gas sample tube. Appendix A contains, in a data base format, additional information regarding this instrumentation.

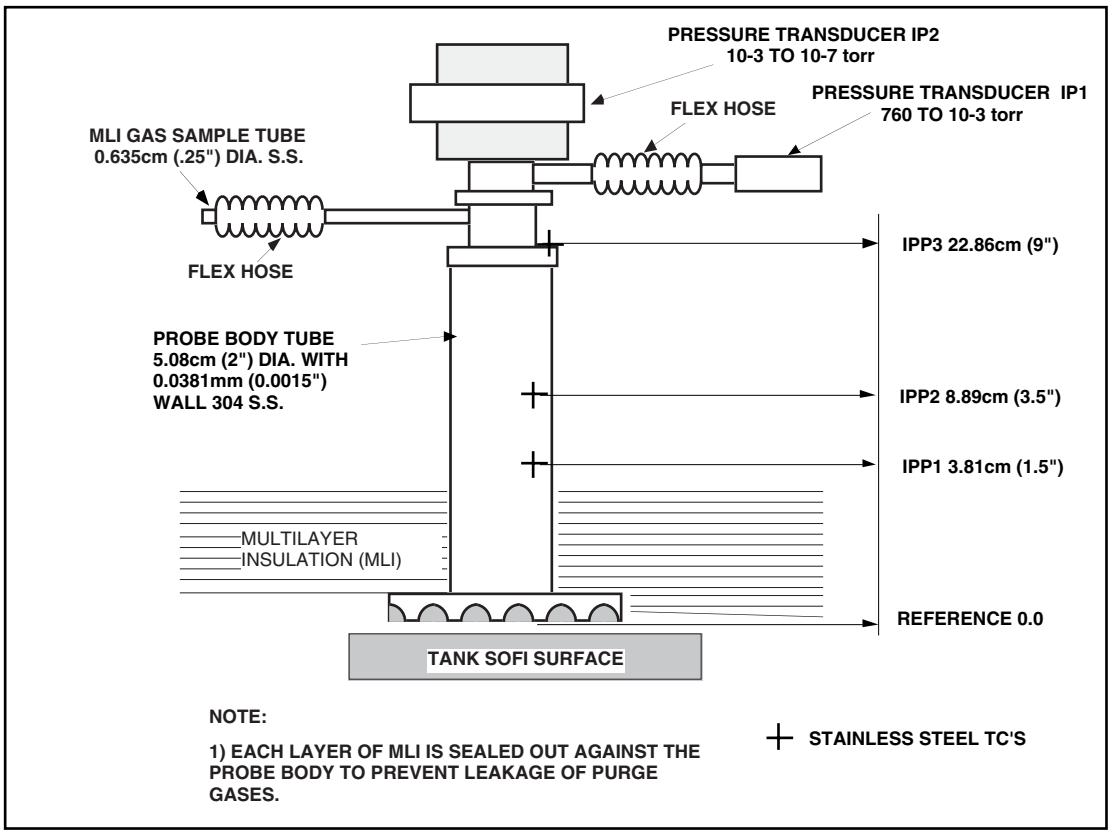

Figure 93. MHTB MLI probe instrumentation.

9) MHTB Manhole Cover & Pump Out Penetration Instrumentation

The MHTB tank is equipped with two manhole covers (inner and outer) to control potential leakage resulting in the degradation of insulation performance. Figure 94 illustrates the manhole cover set-up. The inner cover is equipped with two silicon diodes (TMN3 and TMN4) adhesively bonded to its inner surface with cryogenic epoxy (Lakeshore Stycast). The outer manhole cover exterior surface is equipped with a silicon diode (TMN2) bonded to its center with a single diode (TMN1) and two thermocouples (TMH1 and TMH2) bonded to its flange area. These temperature measurements will be used to assess the total thermal capacitance carried by the massive tank manhole system. The gas volume trapped between the inner and outer manhole covers is connected to a stainless steel evacuation line (flex hose) which is used to intercept potential leakage from the inner cover if it should occur. This flex line is equipped with two thermocouples (TCP1 and TCP2) attached to determine heat input. The spatial distance between the thermocouples is 5.08 cm (2"), however, the flex hose has a 3 to 1 contraction ratio yielding a material length of 15.24 cm (6"). The entire surface of the outer manhole cover is covered with foam insulation at an approximate thickness of 3.175cm (1.25"). The evacuation line is routed along the vent line and as such, is buried beneath the vent line foam insulation. Appendix A contains, in a data base format, additional information regarding this instrumentation.

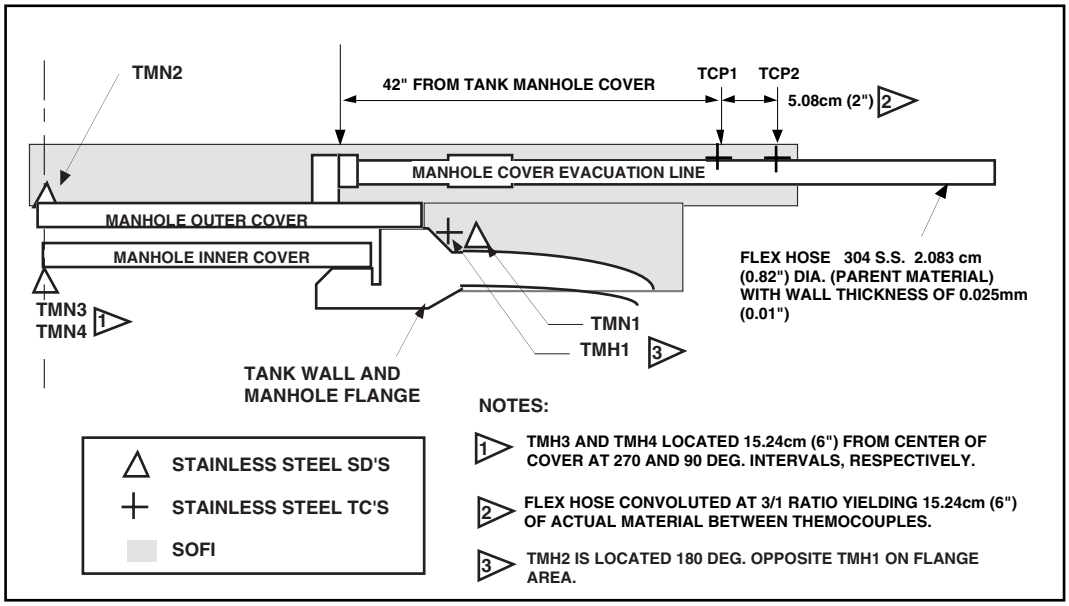

Figure 94. MHTB manhole cover and pump-out port instrumentation.

10) MHTB Internal Rake and Fluid Instrumentation

The MHTB tank is equipped internally with two instrumentation rakes and a capacitance probe which are supported from the top of the tank and extend downward. The rakes are constructed from a Fiberglass Epoxy channel section and are equipped with silicon diodes attached at given intervals using nylon rod offsets and cryogenic epoxy as illustrated in figure 95. The purpose of the rakes is to provide measurement of the temperature gradient within both the tank ullage and liquid masses in addition to providing a rough check of the liquid level to verify the capacitance probe operation. The primary rake (TD1 through TD12) positioned at 180 degrees is connected to the vent flange, while the secondary rake (TD13 through TD24) is positioned at 0 degrees as illustrated in figure 85 and 96. The capacitance probe (CAP1) provides continuous liquid level measurement and is mounted to the vent flange at the 180 degree position beside the primary rake. All tank internal instrumentation is passed through the 20.32cm (8") vent flange using four 37 pin Deutsch connectors. The exception is the capacitance probe which is equipped with its own co-axial feed through mounted in a 1.27cm (0.5") conflat type connector and attached to the center of the 20.32cm (8") vent flange. Appendix A contains, in a data base format, additional information regarding this instrumentation. Appendix B contains an MHTB tanking table with information regarding fill height, percent liquid/ullage volume and LH_2 mass.

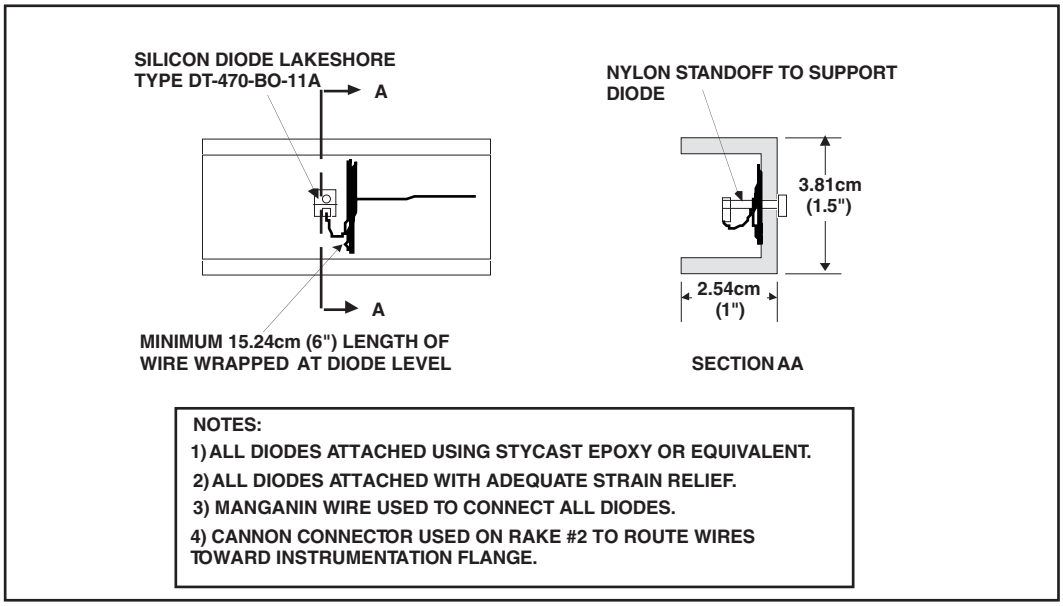

Figure 95. MHTB instrumentation rake silicon diode attachment.

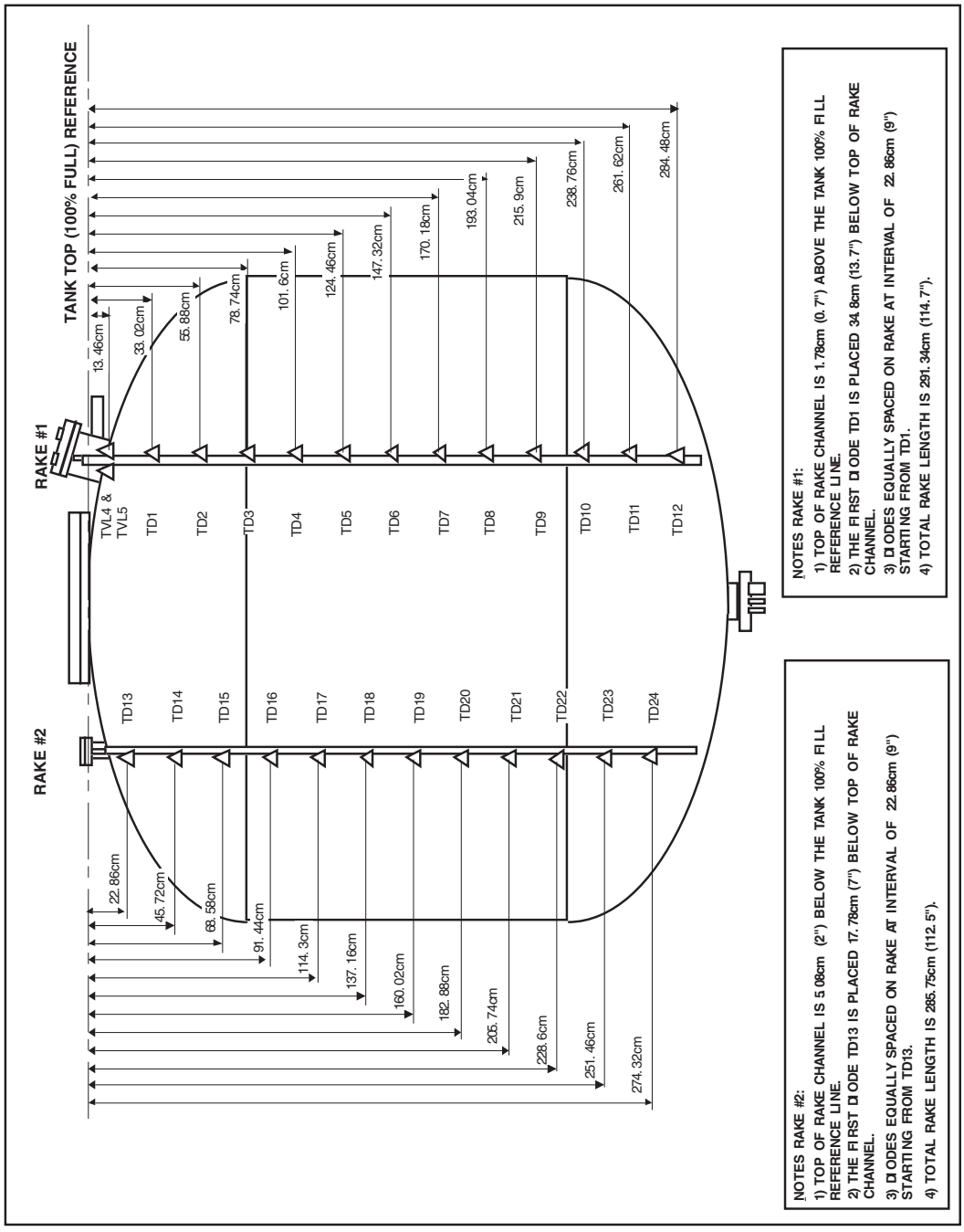

Figure 96. MHTB tank rake instrumentation layout.

11) MHTB Environmental Shroud Instrumentation

The MHTB tank and insulation systems are contained within a shroud structure that completely surrounds them and provides a warm boundary condition for which performance can be measured during testing. This structure is made completely of aluminum and is supported by the interface support structure as shown in figure 84. The shroud is composed of 17 individual panels each equipped with thermocouples attached to the inner surface of the shroud and placed beneath the electrical heating strip. These thermocouples are used with a closed loop control system to regulate each shroud panel's temperature. A minimum of two thermocouples are applied to each panel providing a primary and a backup in case of failure. Two panels #5 and #11 are equipped with additional thermocouples to provide data concerning shroud temperature gradients. Panel #11 has six thermocouples while panel #5 is heavily instrumented with 13 thermocouples since it was used during evaluation of the techniques used to assemble the shroud panels (documented in EP25(94-03)). The top shroud panels #1 through #4 are illustrated in figure 97. The typical side wall panel (5 through 12) instrumentation layout is provided in figure 98. The lower shroud panel layout (13 through 17) is illustrated in figure 99.

A series of 5 thermocouples are also placed within the annular region created between the vertical shroud panel #6 and the test tank insulation, at the 90 degree location. These thermocouples (HS18 through HS22) are spaced vertically along the panel at an interval of 60.96cm (24") with the thermocouple bead positioned approximately half way into the annular region. This instrumentation is used for measuring purge gas temperatures within the annulus. Vacuum chamber free air space temperatures are measured with facility provided thermocouples (CFA1, CFA2 and CFA3) mounted vertically at the 90 location and external to the test article shroud. These thermocouples are placed at 1.525m (5') intervals above the chamber floor. Purge gas dew point within the environmental shroud is measured with a facility supplied Endress Hauser Model #2200 Hydrometer (DEW2). The sensing head for this unit is located internal to the shroud and mounted on the lower shroud panel. Appendix A contains, in a data base format, additional information regarding this instrumentation.

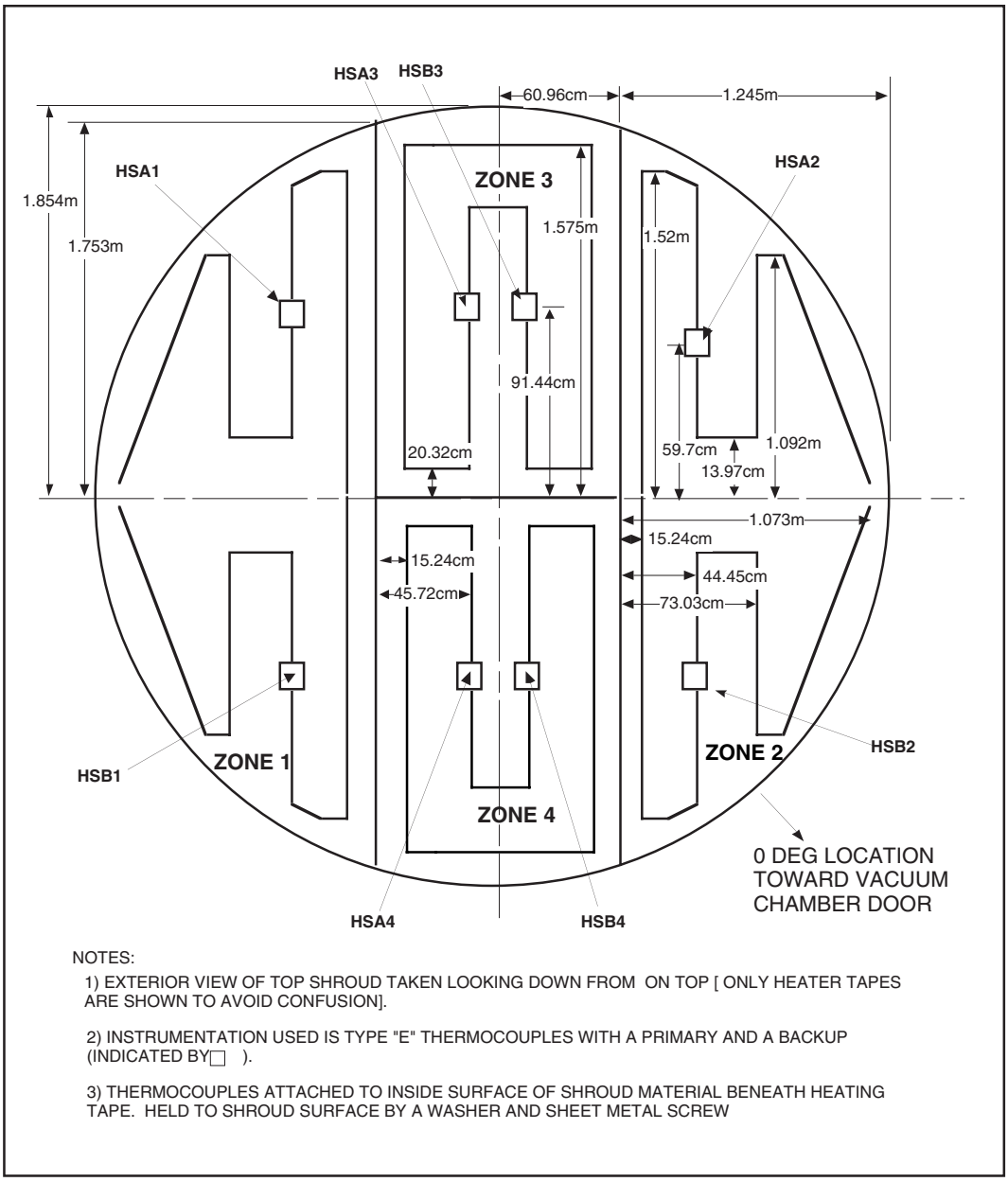

Figure 97. MHTB typical top environmental shroud panels.

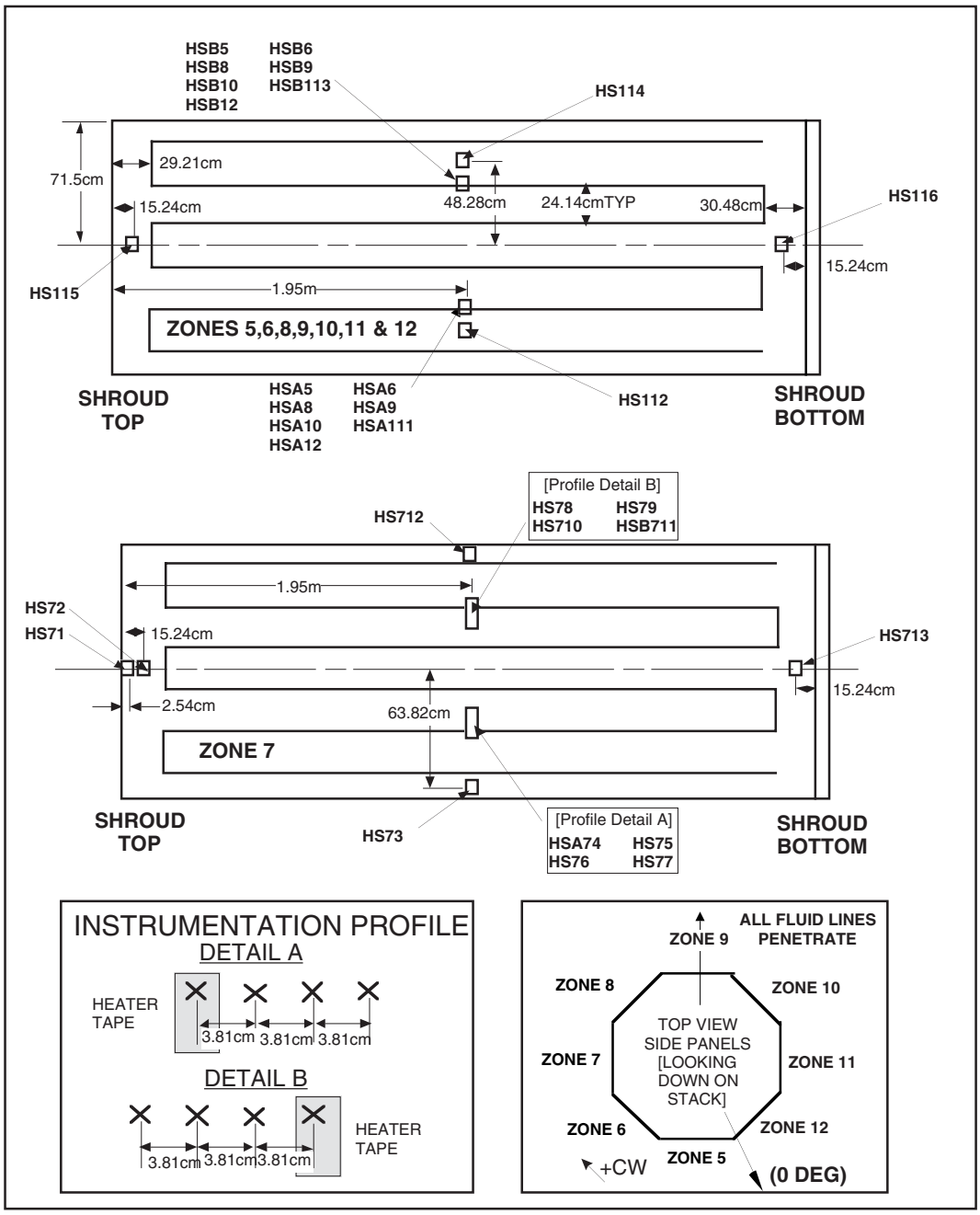

Figure 98. MHTB typical side wall environmental shroud panels.

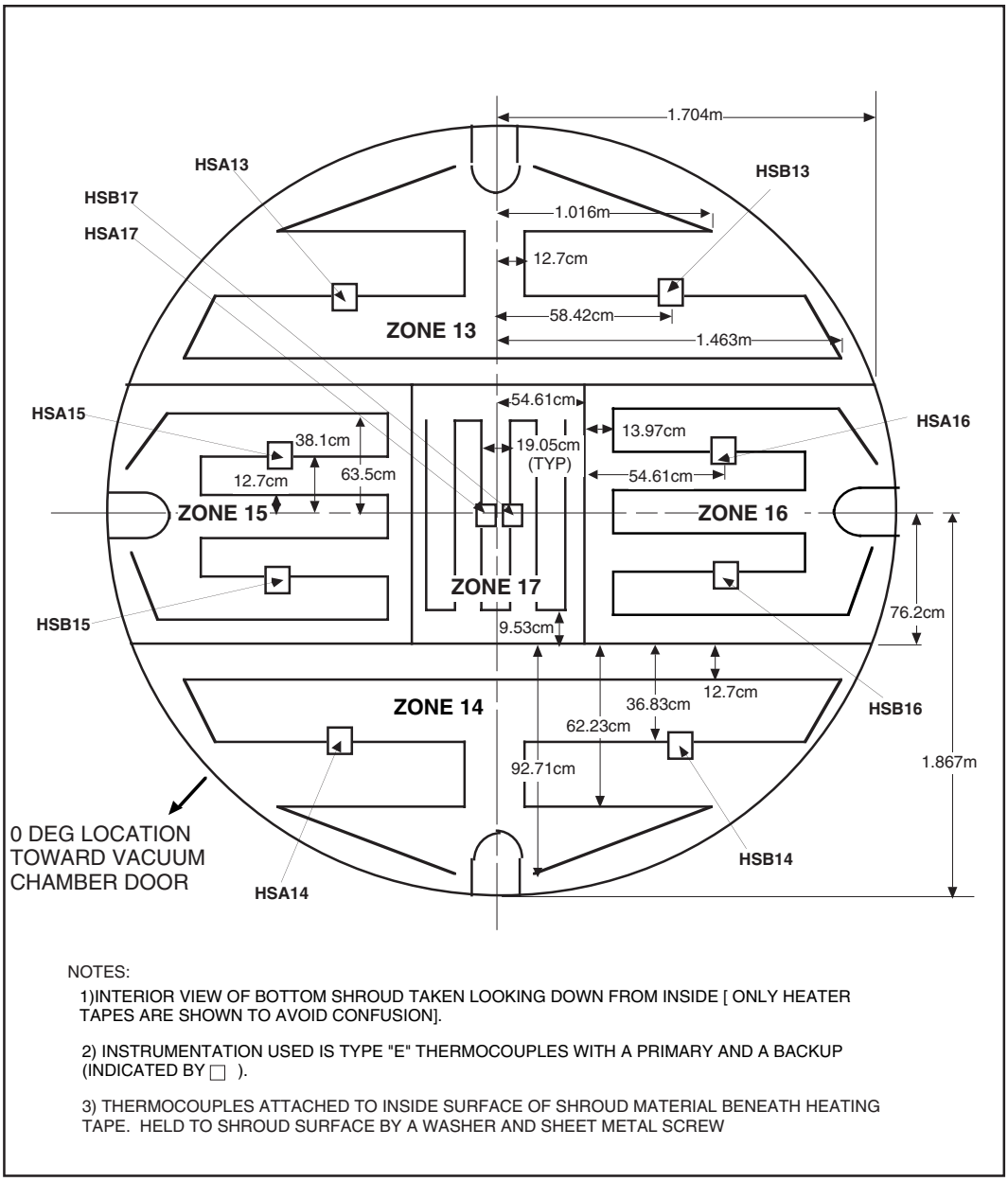

NOTES:

1)INTERIOR VIEW OF BOTTOM SHROUD TAKEN LOOKING DOWN FROM INSIDE [ONLY HEATER TAPES ARE SHOWN TO AVOID CONFUSION].

2) INSTRUMENTATION USED IS TYPE "E" THERMOCOUPLES WITH A PRIMARY AND A BACKUP (INDICATED BY □).

3) THERMOCOUPLES ATTACHED TO INSIDE SURFACE OF SHROUD MATERIAL BENEATH HEATING TAPE. HELD TO SHROUD SURFACE BY A WASHER AND SHEET METAL SCREW

Figure 99. MHTB typical lower environmental shroud panels.

12) MHTB Zero-g Thermodynamic Vent System Instrumentation

The spray bar MHTB test phase requires that hardware related to the zero-g TVS be installed both internal and external to the MHTB test tank. Figure 84 illustrates the general hardware placement on the test tank while instrumentation placement on the hardware is outlined in figure 100. Attached to the lower MHTB tank bulkhead flange (external to the tank) is the vacuum tight TVS enclosure which contains the system control valving and recirculation pump. Instrumentation within the enclosure consists of thermocouples (T411, T412, T415, T416 and T417) pressure transducers (P402, DP400, P403, P404 and P405) and a flow meter (F401). Internal to the test tank is the heat exchanger/spray bar and a back pressure orifice. The spray bar is equipped with two silicon diodes (T413 and T414) and the orifice is instrumented with two diodes (T418 and T419) and two pressure transducers (P406 and P407). External to the MHTB tank, but still within the vacuum chamber, are temperature (diode T420) and pressure (P408) measurements on the TVS vent line to quantify the properties of the exiting gas flow. Instrumentation internal to the MHTB test tank will be routed through the 20.32cm (8") vent flange with the other internal instrumentation. The instrumentation within the TVS enclosure shall be routed through two Deutsch feed throughs and two thermocouple pull throughs. All thermocouples utilize an infinity meter for signal conditioning. The TVS enclosure shall be equipped externally with three thermocouples (T421, T422 and T423) mounted on the top, bottom and side of the enclosure, respectively. The enclosure internal pressure will be measured by two pressure transducers (P409 and P410). Appendix A contains, in a data base format, additional information regarding this instrumentation.

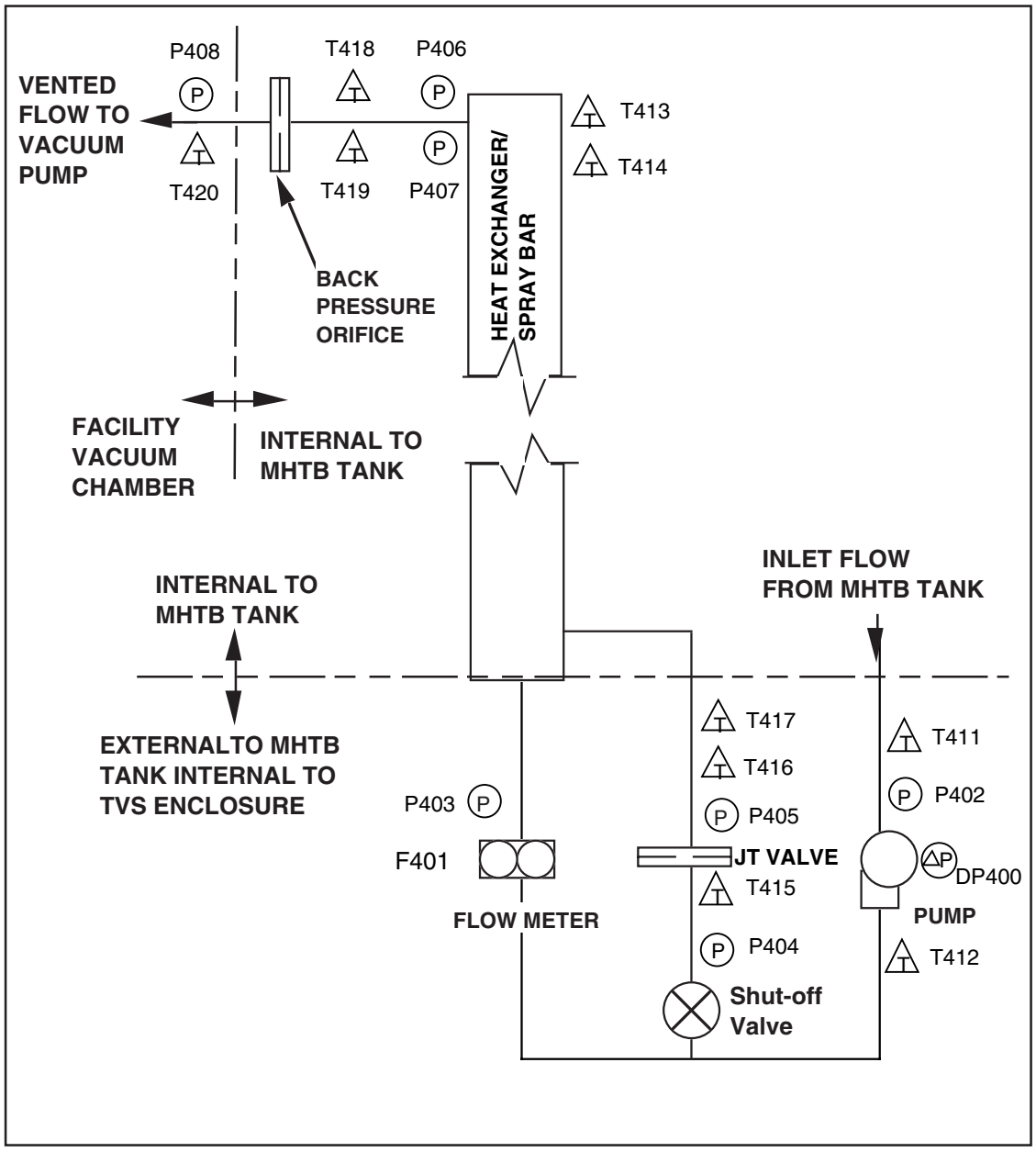

Figure 100. MHTB TVS instrumentation layout.

APPENDIX C—ANALYTICAL CORRELATIONS WITH TEST SEGMENT P263981E

Correlations for the venting and mixing operation were performed using test segment P263981E, with a 90-percent fill level and 54.1-W tank heat leak. The ullage pressure comparison is presented in figure 101. To enable a more realistic comparison of the mixing/venting cycle characteristics, the initial conditions for the analytical model were based on measured conditions at 22,595 s. Venting did not occur with the analytical model since the computed bulk liquid saturation approached, but did not reach, the lower pressure control band limit. During the test, however, the J-T valve opened at 24,108 s. Apparently the bulk liquid did not attain the lower pressure control setpoint during the test, and venting should not have accurred. However, erratic signals from the temperature sensor used to indicate bulk liquid saturation conditions (TD23) caused the J-T vent valve to temporarily open four times. Unfortunately, during the test, the J-T vent valve stuck open on the fourth vent cycle and therefore the correlation period was limited to only about three cycles. The ullage temperature comparison in figure 102 indicates that the average measured and computed ullage temperatures were 21.85 and 21.5 K, respectively; i.e., deviated by <2 percent. The modeled and measured bulk liquid saturation pressure and temperature, presented in figures 103 and 104, respectively, were comparable until the vent valve remained open on the fourth cycle and the measured values began to decrease.

Test and Model Conditions

- 90% Fill, GH_2 Ullage
- Test: Four Vent Cycles
- Model: No Venting
- Tank Heat Leak: 54.1 W
- P4 Upper Limit: 137.9 kPa
- P4 Lower Limit: 131.0 kPa
- Vent Flow Rate: 0.0048 kg/s

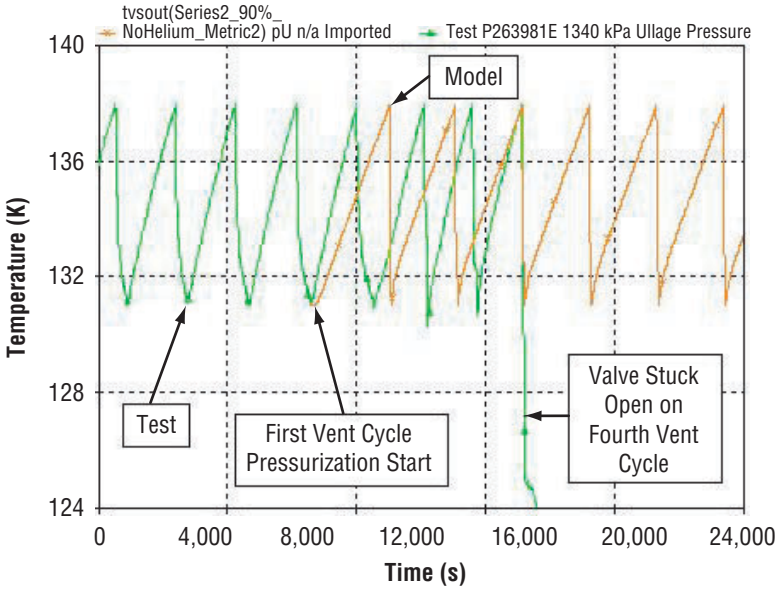

Figure 101. Ullage pressure modeling comparison with 1998 test P263981E—self-pressurization and mixing with 90-percent fill.

Test and Model Conditions

- 90% Fill, GH_2 Ullage
- Test: Four Vent Cycles
- Model: No Venting
- Tank Heat Leak: 54.1 W
- P4 Upper Limit: 137.9 kPa
- P4 Lower Limit: 131.0 kPa
- Vent Flow Rate: 0.0048 kg/s

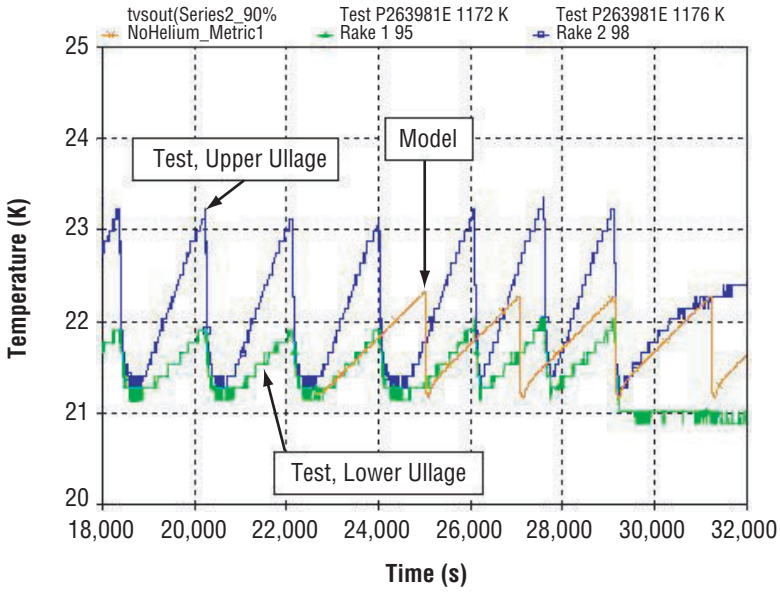

Figure 102. Ullage temperature modeling comparison with 1998 test P263981E—self-pressurization, mixing, and venting with 90-percent fill.

Test and Model Conditions

- 90% Fill, GH_2 Ullage
- Test: Four Vent Cycles
- Model: No Venting
- Tank Heat Leak: 54.1 W
- P4 Upper Limit: 137.9 kPa
- P4 Lower Limit: 131.0 kPa
- Vent Flow Rate: 0.0048 kg/s

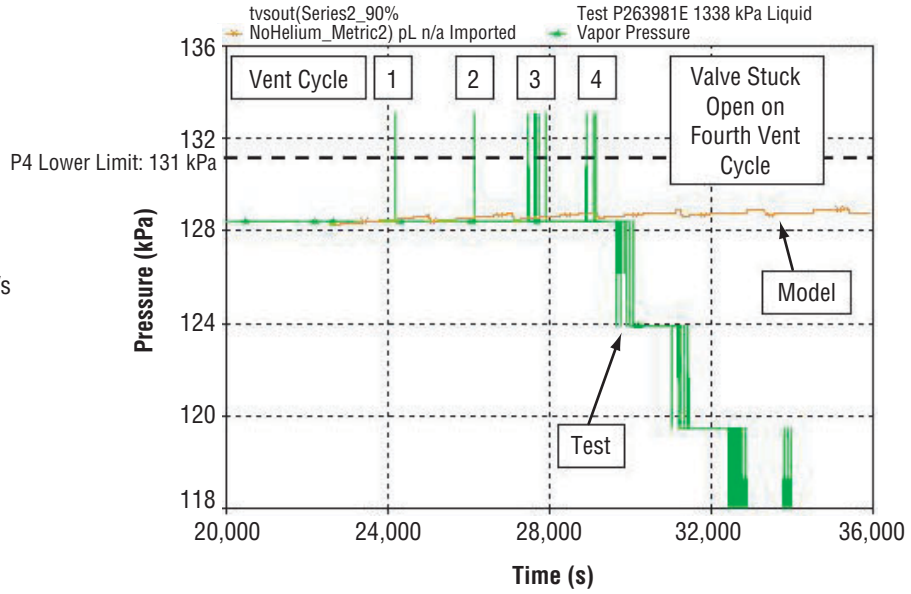

Figure 103. Bulk liquid saturation pressure modeling comparison with 1998 test P263981E—self-pressurization, mixing, and venting with 90-percent fill.

Test and Model Conditions

- 90% Fill, GH_2 Ullage
- Test: Four Vent Cycles
- Model: No Venting
- Tank Heat Leak: 54.1 W
- P4 Upper Limit: 137.9 kPa
- P4 Lower Limit: 131.0 kPa
- Vent Flow Rate: 0.0048 kg/s

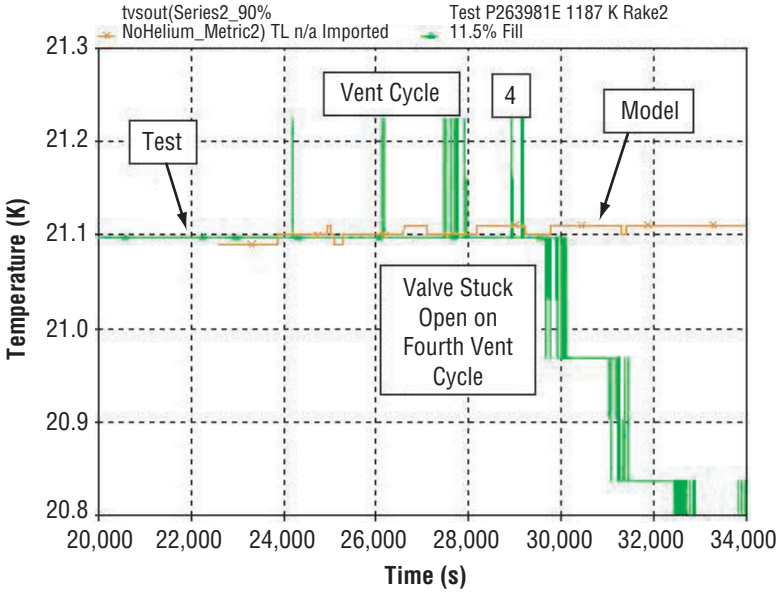

Figure 104. Bulk liquid saturation temperature modeling comparison with 1998 test P263981E—self-pressurization, mixing, and venting with 90-percent fill.

REFERENCES

1. Martin, J.; and Hastings, L.: "Large-Scale Liquid Hydrogen Testing of a Variable Density Multilayer Insulation With a Foam Substrate," *NASA/TM–2001–211089*, Marshall Space Flight Center, AL, June 2001.

2. Cryogenic Fluid Management Technologies for Space Transportation, Zero G Thermodynamic Vent System Final Report, Rockwell Aerospace Report No. SSD 94M0038, Contract NAS8–39202, 1994.

3. Nguyen, H.: Zero-G Thermodynamic Venting System (TVS) Performance Prediction Program, Rockwell Aerospace, Contract NAS8–39202, May 24, 1994.

4. "MPS Propellant Dump and Vacuum Inerting (The Generalized Two-Phase Cryogenic Propellant Dump Model), Program No. MPS–17, 287–104–91–MPS–017, Rockwell International, June 1991.

5. Chen, J.: A Correlation for Boiling Heat Transfer to Saturated Fluids in Convective Flow, ASME Paper No. 63–HT–34, ASME-AIChE Heat Transfer Conference and Exhibit, Boston, MA, August 1963.

6. Generic Fluid Transfer Model, Computer Model Description Document, Rockwell International, December 1987.

7. Ring, E.: *Rocket Propellant and Pressurization Systems*, Prentice-Hall, Inc., Englewood Cliff, NJ, p. 218, 1964.

8. Kreith, H.: *Principles of Heat Transfer*, 4th ed., Harper & Row, New York, pp. 4–6, p.360, 1986.

9. Bailey, J.; and Hedayat, A.: "Thermodynamic Venting System (TVS) Performance Prediction Program Modification and Comparison With Test Data," Sverdrup MSFC Group Report No. MG–02–660, September 2002.

REPORT DOCUMENTATION PAGE

Form Approved
OMB No. 0704-0188

1. AGENCY USE ONLY *(Leave Blank)*	2. REPORT DATE	3. REPORT TYPE AND DATES COVERED
	October 2003	Technical Memorandum

4. TITLE AND SUBTITLE

Spray Bar Zero-Gravity Vent System for On-Orbit Liquid Hydrogen Storage

5. FUNDING NUMBERS

6. AUTHORS

L.J. Hastings,* R.H. Flachbart, J.J. Martin, A. Hedayat, M. Fazah, T. Lak,** H. Nguyen,** and J.W. Bailey***

7. PERFORMING ORGANIZATION NAMES(S) AND ADDRESS(ES)

George C. Marshall Space Flight Center
Marshall Space Flight Center, AL 35812

8. PERFORMING ORGANIZATION REPORT NUMBER

M–1091

9. SPONSORING/MONITORING AGENCY NAME(S) AND ADDRESS(ES)

National Aeronautics and Space Administration
Washington, DC 20546–0001

10. SPONSORING/MONITORING AGENCY REPORT NUMBER

NASA/TM—2003–212926

11. SUPPLEMENTARY NOTES

Prepared by the Vehicle and Systems Development Department, Space Transportation Directorate
*Alpha Technology, Inc. **The Boeing Company ***Sverdrup Technology, Inc.

12a. DISTRIBUTION/AVAILABILITY STATEMENT

Unclassified-Unlimited
Subject Category 16
Availability: (301)621–0390

12b. DISTRIBUTION CODE

13. ABSTRACT *(Maximum 200 words)*

During zero-gravity orbital cryogenic propulsion operations, a thermodynamic vent system (TVS) concept is expected to maintain tank pressure control without propellant resettling. In this case, a longitudinal spray bar mixer system, coupled with a Joule-Thompson (J-T) valve and heat exchanger, was evaluated in a series of TVS tests using the 18-m^3 multipurpose hydrogen test bed. Tests performed at fill levels of 90, 50, and 25 percent, coupled with heat tank leaks of about 20 and 50 W, successfully demonstrated tank pressure control within a 7-kPa band. Based on limited testing, the presence of helium constrained the energy exchange between the gaseous and liquid hydrogen (LH_2) during the mixing cycles. A transient analytical model, formulated to characterize TVS performance, was used to correlate the test data. During self-pressurization cycles following tank lockup, the model predicted faster pressure rise rates than were measured; however, once the system entered the cyclic self-pressurization/mixing/venting operational mode, the modeled and measured data were quite similar. During a special test at the 25-percent fill level, the J-T valve was allowed to remain open and successfully reduced the bulk LH_2 saturation pressure from 133 to 70 kPa in 188 min.

14. SUBJECT TERMS

orbital cryogenic fluid management, orbital cryogenic storage, zero-gravity cryogenic pressure control, thermodynamic vent systems

15. NUMBER OF PAGES

160

16. PRICE CODE

17. SECURITY CLASSIFICATION OF REPORT	18. SECURITY CLASSIFICATION OF THIS PAGE	19. SECURITY CLASSIFICATION OF ABSTRACT	20. LIMITATION OF ABSTRACT
Unclassified	Unclassified	Unclassified	Unlimited